SANDIA REPORT
SAND2019-5972
Printed May 2019

Sandia National Laboratories

PDCI Damping Controller Test Results and Project Summary

David A. Schoenwald, Brian J. Pierre, Felipe Wilches-Bernal, Ryan T. Elliott, Raymond H. Byrne, Jason C. Neely
Sandia National Laboratories

Daniel J. Trudnowski
Montana Technological University

Prepared by
Sandia National Laboratories
Albuquerque, New Mexico
87185 and Livermore,
California 94550

Issued by Sandia National Laboratories, operated for the United States Department of Energy by National Technology & Engineering Solutions of Sandia, LLC.

Available to DOE and DOE contractors from
U.S. Department of Energy
Office of Scientific and Technical Information
P.O. Box 62
Oak Ridge, TN 37831

Telephone: (865) 576-8401
Facsimile: (865) 576-5728
E-Mail: reports@osti.gov
Online ordering: http://www.osti.gov/scitech

Available to the public from
U.S. Department of Commerce
National Technical Information Service
5301 Shawnee Rd
Alexandria, VA 22312

Telephone: (800) 553-6847
Facsimile: (703) 605-6900
E-Mail: orders@ntis.gov
Online order: https://classic.ntis.gov/help/order-methods/

ABSTRACT

This report presents the results from testing of the Pacific DC Intertie (PDCI) wide-area damping controller (DCON) on the actual electric power grid in the western region of North America known as the Western Interconnection (WI). In addition, this report summarizes the key contributions and development strategy of the DCON. Therefore, this report also serves as the final report for the DCON project, which is known as TIP (Technology Innovation Project) no. 289. The purpose of the DCON is to mitigate inter-area oscillations in the WI by active improvement of oscillatory mode damping using phasor measurement unit (PMU) feedback to modulate power flow in the PDCI. This report describes the tests conducted, analysis of the results, and conclusions drawn as to the performance and safety of the DCON in the improvement of damping for inter-area oscillations in the WI. The DCON is the result of a collaboration between Sandia National Laboratories (SNL), Bonneville Power Administration (BPA), Montana Technological University (MTU), and the Department of Energy Office of Electricity (DOE-OE).

ACKNOWLEDGEMENTS

We gratefully acknowledge the support of the BPA Office of Technology Innovation (Project No. 289, Project Managers: Mr. Gordon Matthews and Dr. Jisun Kim, Technical Point of Contact: Dr. Dmitry Kosterev), the DOE Office of Electricity (OE) Transmission Reliability Program (Program Manager: Mr. Phil Overholt), and the DOE-OE Energy Storage Program (Program Manager: Dr. Imre Gyuk). We express our sincere gratitude to BPA staff who have provided us with valuable guidance and advice throughout the project: Mr. Michael Overeem, Mr. Mark Yang, Mr. Jeff Barton, Mr. Greg Stults, Mr. Tony Faris, Mr. Dan Goodrich, Mr. Shawn Patterson, Mr. Alex Chavez, and Dr. Judith Estep. We also express our sincere appreciation for the design guidance of Prof. Matt Donnelly of Montana Technological University.

CONTENTS

LIST OF FIGURES

LIST OF TABLES

This page left blank

EXECUTIVE SUMMARY

Project Background

A collaborative effort between Sandia National Laboratories (SNL), Montana Tech University (MTU), and Bonneville Power Administration (BPA), dating back to 2013, was launched to design, develop, and demonstrate an active damping control system (DCON) to improve damping of inter-area oscillations in the Western Interconnection (WI). The control system accomplishes this goal by using real-time measurements acquired from phasor measurement units (PMUs) to construct a feedback signal that modulates power flow through the Pacific DC Intertie (PDCI).

There are two primary motivations to increase damping of inter-area oscillations. First, if damping is insufficient, oscillations may lead to system-wide tripping events, and in turn to a series of cascading outages. The 1996 system break-up across the west coast of North America can in part be attributed to undamped oscillations. Avoiding these large-scale power outages provides a significant financial incentive in damping inter-area oscillations. Second, power transfer through long transmission corridors in western North America is often constrained due to stability concerns and limited by poorly damped electromechanical oscillations. Thus, additional damping may increase the power transfer capacity. Recent developments in reliable real-time wide-area measurement systems (WAMS) based on PMUs has enabled the potential for large-scale damping control approaches to stabilize critical oscillation modes.

The original idea to modulate PDCI power flow to damp inter-area oscillations was first designed and tested in 1975. The original design utilized the parallel AC real power flow as the feedback signal. Even though this method provided damping to low frequency modes of oscillation, further analysis determined that the local AC power flow feedback signal, had a transfer function zero, which limited the gain of the controller and worsened oscillations at higher frequencies. The DCON is able to avoid this problem because it incorporates GPS time synchronized PMUs to improve damping. This data is now available due to the recent deployment of PMUs throughout the WI, which provide fast, reliable, system-wide measurements.

Currently, the primary approach to mitigate grid oscillations and avoid blackouts in the WI is to operate well below transmission capacity, which is not economical. The DCON uses measurement data, acquired in real time from PMUs, to serve as a feedback signal to inform the controller as to how much power to add (or subtract) to the power flow on the PDCI. This carefully controlled "injection" of power to the PDCI is the action that damps oscillations in the grid. This control strategy provides damping to the primary north-south oscillatory modes in the WI without interacting with speed governor actions. A supervisory system, integrated into the controller, ensures a "do no harm" policy for the grid in which damping is never worsened. By improving the damping of these inter-area oscillations, the DCON has the potential to allow increased power transfers in the WI.

The DCON is the first successful wide-area grid demonstration of real-time feedback control using PMUs in North America. This is a game-changer, enabling the use of widely-distributed networked energy resources that have the potential to transform the existing power grid into the future smart grid. Benefits that the DCON is capable of delivering, once operational, include: (1) Additional reliability to the grid from improved damping of electromechanical oscillations. (2) Additional contingency management of the grid under stressed system conditions. (3) Higher power limits in specific transmission corridors. (4) Reduction and/or postponement in new transmission capacity expansion.

Key Takeaways from this Report

The western North American power system has several lightly-damped inter-area modes due to long transmission paths resulting in oscillatory instability being a concern. Increased power transmission requests, increased penetration of renewable energy systems, low-damping events observed in planning models, and increased observation of actual-system low-damping conditions have spurred engineering and research into the mitigation of such problems. The scope of actions includes implementation of a PMU-based real-time WAMS and the evaluation of large-scale oscillation damping devices/controls.

This report presents the actual-system results of a prototype DC modulation damping controller (denoted hereafter as the DCON) that utilizes WAMS feedback to modulate the PDCI. The basis for the DCON includes several years of research and development culminating with the installation of the DCON at the Celilo facility. The control strategy of the DCON relies on WAMS PMU feedback. The DC modulation is proportional to the frequency difference between 2 geographically separate locations – a northern signal and a signal near the California-Oregon Intertie (COI).

This report describes a series of three tests conducted in 2016, 2017, and 2018. This includes extensive closed-loop tests. The 2018 test series included a walk-away test where the DCON was allowed to operate in an unattended mode for a full month in the summer of 2018. Other tests included inducing transients into the interconnect and observing the performance of the damping controller over many days of operation.

Key conclusions from these tests include:

- The PDCI system is an excellent actuator for damping the widespread and most critical North-South B (NSB) mode. The PDCI response time is sufficiently fast for damping of any mode below 1 Hz. The system also has excellent noise rejection properties. The system showed excellent consistency, repeatability, and linearity for the many tests conducted over the three years of testing.

- The DCON control strategy has excellent robustness properties. For the nearly 100 open-loop measurements conducted over the past several years, all demonstrated that the controller would add damping to any mode in the 0.1 to 1 Hz range. The controllability is especially strong for the NSB mode while the impact on other known modes is minimal. This robustness is preserved during the critical condition when Alberta disconnects from the system which tends to decrease the damping on the NSB mode.

- The maximum prudent gain for the controller is K_0 = 14 MW/mHz (the gain for John Day PMU as the local signal). If the gain exceeds 14 MW/mHz, the gain margin may degrade below 6 dB and results in the DC system response being overly underdamped with a natural frequency near 4 Hz. Reliable performance is achieved with a gain in the 9 to 12 MW/mHz and represents the recommended range. The DCON automatically halves the gain for the Big Eddy PMU local signals to be half that of the John Day signals to preserve this gain margin. The result is less added damping performance. Therefore, John Day is the preferred local PMU.

- The DCON reduces the impact of forced oscillations for all cases except when the forced oscillation is in the 3 to 5 Hz range. In this case, the DCON could slightly amplify the oscillation over the open-loop condition. But, this is likely of little concern because the overall system has very low gain in this higher frequency range. That is, forced oscillations above 1 Hz do not propagate very far from their source as the overall system gain is much lower.

ACRONYMS AND DEFINITIONS

Abbreviation	Definition
AC	Alternating Current
BC	British Columbia, Canada
BCA	Bulk Energy System Cyber Asset
BES	Bulk Energy System
BPA	Bonneville Power Administration
CIP	Critical Infrastructure Protection
COI	California-Oregon Intertie
DAQ	Data Acquisition
DC	Direct Current
DCON	Damping Controller
DOE	Department of Energy
DOE-OE	Department of Energy Office of Electricity
FERC	Federal Energy Regulatory Commission
FISMA	Federal Information Security Management Act
GPS	Global Positioning System
HVDC	High Voltage Direct Current
Hz	Hertz (cycles per second)
I/O	Input-Output
IEEE	Institute of Electrical and Electronics Engineers
kV	Kilo-Volts
KVM	Keyboard Video Monitor
MSF	Multi-Sine Function
MTU	Montana Technological University
MW	Mega-Watts
NERC	North American Electricity Reliability Corporation
NI	National Instruments
PDCI	Pacific Direct Current Intertie
PMU	Phasor Measurement Unit
SNL	Sandia National Laboratories
WAMS	Wide Area Measurement System
WECC	Western Electricity Coordinating Council
WI	Western Interconnection

This page left blank

1. INTRODUCTION

The WI has several lightly-damped inter-area modes due to long transmission paths. Oscillatory instability was a contributing factor to the 1996 system break up [1]. This event, increased power transmission requests, increased penetration of renewable energy systems, low-damping events observed in planning models, and increased observation of actual-system low-damping conditions have spurred engineering and research into the mitigation of such problems. The scope of actions includes implementation of a PMU-based real-time WAMS and the evaluation of large-scale oscillation damping devices/controls. This report presents the actual-system results of a prototype DC modulation damping controller that utilizes WAMS feedback to modulate the PDCI. We term the controller the DCON.

The work described in this report has roots dating back to experiments in the 1970s [2] which demonstrated that PDCI modulation has considerable potential for improving oscillatory stability. The approach used in [2] was based upon local-signal feedback. Although it improved damping of the desired mode, it destabilized a different mode [2]. Analysis presented in [3] explains the reasons why local feedback destabilizes the BC mode.

The control strategy used in the DCON is described in [3] and relies upon WAMS feedback. Effectively, the DC modulation is proportional to the difference in frequency between two geographically separated locations. Using transient-stability simulation and eigenanalysis, it is demonstrated in [3] that this approach has significant advantages over other approaches. Details of the analysis of the extensive simulation studies can be found in [18], [19], [30], [31], [32], [33].

In addition to the model studies, nearly 100 open-loop actual-system modulation tests have been conducted since 2009 [4], [5]. These open-loop tests have confirmed and refined the model-based findings and provided critical information for fine-tuning the control algorithm.

This report describes a series of three tests conducted in 2016, 2017, and 2018. This includes extensive closed-loop tests. These tests included inducing transients into the WI and observing the performance of the damping controller over many days of operation. Test results presented in this report have been the basis of many publications including [6], [12], [13], [15], [17], [19], [20], [29].

A complete listing of project accomplishments including a project overview, project innovations, awards, patent application, journal papers, conference papers, project reports, and project presentations is provided in Appendix D.

This page left blank

2. OVERVIEW OF SYSTEM MODES

This section provides a summary of the key inter-area modes of the WI and their properties. This topic is covered in greater detail in [5] and [7]. Based upon 30 years of actual-system testing and model studies, the frequency, damping, shape, observability, and controllability of the major inter-area modes are well known. The inter-area modes of interest are:

- "NSA Mode" nominally near 0.2 to 0.25 Hz;
- "NSB Mode" nominally near 0.35 to 0.4 Hz;
- "EWA Mode" nominally near 0.4 to 0.5 Hz;
- "BC" mode nominally near 0.6 Hz; and,
- "Montana" mode nominally near 0.8 Hz.

Other modes exist in the system; but, these five have been observed the most. Of the five modes, NSB is the most widespread and troublesome. It is the mode the DCON is designed to address.

The NSA mode has the northern half of the system (Canada and the pacific northwest-US) swinging against the southern half (desert southwest US and southern California). The majority of power swings travel through the western path with the mode-shape dividing line typically near the COI. By far, the dominant observability and controllability point is in Alberta Canada. In fact, a better characterization of this mode is Alberta swinging against the rest of the system. The PDCI has little controllability of this mode. The best controllability points for this mode are generators within the Alberta area.

The NSB Mode has a very widespread shape and is the most troublesome mode within the WI. It has the Alberta area swinging against BC and the northern US which in turn swings against the southern part of the US. The mode's southern dividing line is typically near the COI. The observability/controllability is very widespread with no one location dominant. It is a very widespread mode. The PDCI has excellent controllability of the NSB mode.

Historically, the Alberta interconnection has the strongest influence on the NSA and NSB modes. With Alberta connected, the NSB mode typically has the lowest damping and is the most widespread and troublesome. Its damping is influenced by flows from Canada to California, which are historically high during the summer season. With Alberta disconnected, the two modes meld into a single north-south mode nominally near 0.32 Hz which again has a dividing line near the COI. This mode is typically lightly damped and very widespread. The PDCI has excellent controllability of this melded mode.

The EWA mode has the eastern part of the system, led by the Colorado area, swinging against the southwest. Model studies indicate the mode is controllable from generators in the Colorado area. The "BC" mode primarily has the BC area swinging against the rest of the system. The "Montana" mode has Montana oscillating against the rest of the system. Although these two modes are more localized, they do ripple through the system at a high enough energy to cause concern. The PDCI has little controllability of these modes.

This page left blank

3. DCON DESIGN GOALS

The guiding principles for the design of the control law of modulating PDCI power based upon the relative frequency error are:

- Performance: The DCON shall provide damping to any/all controllable modes that may occur in any AC system configuration. The goal is to focus on the NSB mode.
- Robustness: The DCON must not de-stabilize any component within the AC power system or PDCI.
- The control law must not interact with frequency regulation of the overall system.

A foundation control strategy is described in [3]. Hundreds of simulations, linear analyses, and open-loop actual-system probing tests have shown that the control law fulfills these principles [3], [4], [5], [30], [31], [32], [33]. The concluding results of these past studies and tests are: 1) verification that the control strategy performs as desired; 2) optimal derivative filter settings; 3) requirements on the PDCI dynamics and the communication network delay; 4) desired PMU locations; and 5) selection of a range of control gains.

Figure 3-1 below shows a simplified block diagram of the DCON real-time control loop. The bottom feedback path represents the DCON system. Key elements include:

- The "system" is broken into two components:
  - PDCI. The input to the PDCI is the commanded power modulation from the DCON and the output is the actual AC real power injected into the AC network measured on at the AC transformer on the north side of the PDCI.
  - AC Power System. The input to the "AC Power System" is the AC real power injected into the system from the PDCI (P_{dc}) and the output is the relative PMU voltage angle between two locations.
- The DCON consists of:
  - The relative angle between a "Local" PMU and a "Remote" PMU is measured and calculated for 12 different PMU pairs ($\Delta\theta_1$ thru $\Delta\theta_{12}$).
  - Each relative angle is filtered thru transfer function $H(z)$ which takes the derivative of the relative angle to obtain the relative frequency (Δf_i). The filter parameters are discussed in reference [10].
  - Each relative frequency is scaled by gain K_i.
  - An automated switch selects the desired signal via bump-less transfer using a preset priority. The highest priority signal with available PMUs is selected.
  - Table 3-1 shows the 12 feedback signal pairs with their associated priority and gain. K_0 is the base gain. The priorities were chosen to maximize controller performance as will become evident later in this report. A conclusion of this report is that the priority signals 9 and 10 should be shifted up to priority 5 and 6, respectively. That is, the signals that use John Day as the local measurement should be higher priority. The switch can also be used to set the controller in open loop.
  - An internal probing signal P_{pi} is added to the control signal from the priority switch. This probing signal is used for testing purposes.

- The control signal is then limited to $\pm P_{max}$ and passed out of the DCON to the PDCI control system.

- The PDCI control system interfaces with a 2nd probing signal termed P_{po}. Again, this signal is for test purposes and is applied via the "Probing Signal Generator".

Reference [3] concluded that optimal feedback for the DCON is the relative frequency across the DC system and a sub-optimal solution being relative frequency between north end of the PDCI and Malin. To remain in the BPA territory, the DCON uses the sub-optimal solution.

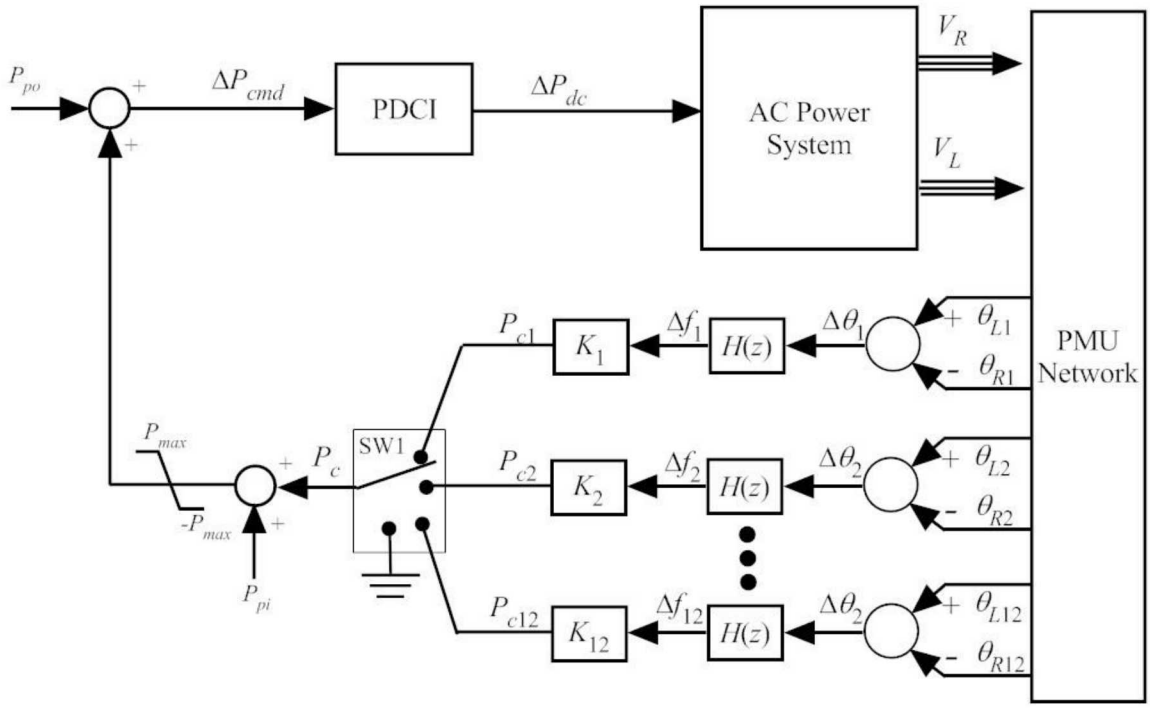

Figure 3-1. DCON block diagram

Table 3-1. Feedback signals and associated gain. K_0 = baseline gain

Priority	PMU		Gain (K)
	Local	Remote	
1	John Day 1 (JD1)	Malin 1 (ML1)	K_0
2	John Day 1 (JD1)	Malin 2 (ML2)	K_0
3	John Day 2 (JD 2)	Malin 1 (ML1)	K_0
4	John Day 2 (JD 2)	Malin 2 (ML2)	K_0
5	Big Eddy 1 (BE1)	Malin 1 (ML1)	$0.5*K_0$
6	Big Eddy 1 (BE1)	Malin 2 (ML2)	$0.5*K_0$
7	Big Eddy 2 (BE2)	Malin 1 (ML1)	$0.5*K_0$
8	Big Eddy 2 (BE2)	Malin 2 (ML2)	$0.5*K_0$
9	John Day 1 (JD1)	Capt Jack (CJ)	K_0
10	John Day 2 (JD 2)	Capt Jack (CJ)	K_0
11	Big Eddy 1 (BE1)	Capt Jack (CJ)	K_0
12	Big Eddy 2 (BE2)	Capt Jack (CJ)	K_0

4. OVERVIEW OF TESTS

A series of open-loop and closed-loop actual-system PDCI control tests were conducted over three years (2016, 2017, and 2018). These tests differ from pasts tests in two ways. First, a significant PDCI upgrade was completed at the end of 2015 [8]. This included replacement and updating of all converter components ranging from power-electronic apparatuses to transformers. A benefit of this up-grade is a faster and more accurate response to power commands such as modulation control. The second unique quality of the tests is that the damping controller prototype is fully developed and installed enabling and both open-loop and closed-loop tests. All past probing tests were open loop and had the ability to analyze the transfer function of the "AC Power System" component in Figure 3-1 but not the "PDCI" dynamics. With these two characteristics in mind, the primary test objectives are to:

- Characterize the PDCI dynamics;
- Verify that the "AC Power System" dynamics in Figure 3-1 are consistent with past tests;
- Quantify damping performance of the NSB mode;
- Analyze impact on other system mode;
- Selection of the control gain to satisfy robustness specifications;
- Demonstration and testing of the controller in closed-loop;
- Quantify impact of DCON of forced oscillations; and
- Testing of DCON supervisory settings.

Three series of DCON tests were conducted, one each in 2016, 2017, and 2018. Appendix A shows the test plans. Tables 4-1, 4-2, and 4-3 describe the 3 test series. Each test consisted of one or more of the following:

- Calibration tests using square-wave pulsing and sinusoids injected via P_{pi}. The objective of these tests is to verify all scaling and timing conditions.
- $\pm$20-MW MSF probes injected via P_{pi} or P_{po}. The MSF is a multi-sine signal with energy content through the bandwidth of the control loop. It is shown in Figure 4-1. The MSF signal used for all test series (2016 thru 2018) is the "MSF-1/30/1/100" signal. It is optimized for PDCI/DCON testing. The MSF tests have two main purposes:
  - In open loop, the goal is to measure the loop transfer function $\frac{P_c}{\Delta P_{cmd}}$.
  - In closed loop, the goal is to excite the full bandwidth of the control loop to verify stable operation and examine the closed-loop performance.
- $\pm$125-MW square-wave pulsing P_{po}. The signal is described in Figure 4-2. It is a 3-cycle 0.4-Hz square wave. The square-wave tests purposes are:
  - Test the dynamic response of the PDCI system both in open-loop and closed-loop configurations.
  - Test the damping performance of the DCON system.
  - Open-loop and closed-loop square-wave pulsing tests are conducted back-to-back in time to facilitate comparison.

- Chief-Jo brake pulse. A 0.5-sec. 1400-MW pulse of the Chief-Jo brake. This test excites the dynamics of the power system especially modes excitable from the Chief-Jo brake. The purpose is to test the damping performance of the DCON. Open-loop and closed-loop tests are conducted back-to-back in time to facilitate comparison.

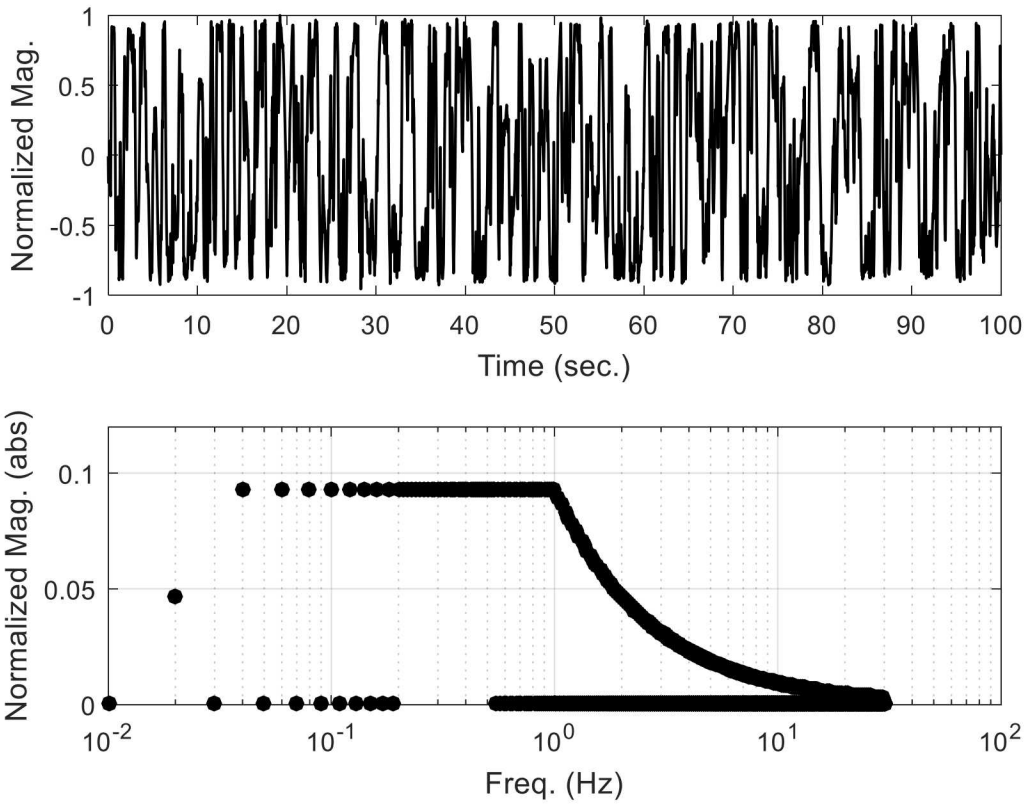

Figure 4-1. MSF-1/30/1/100

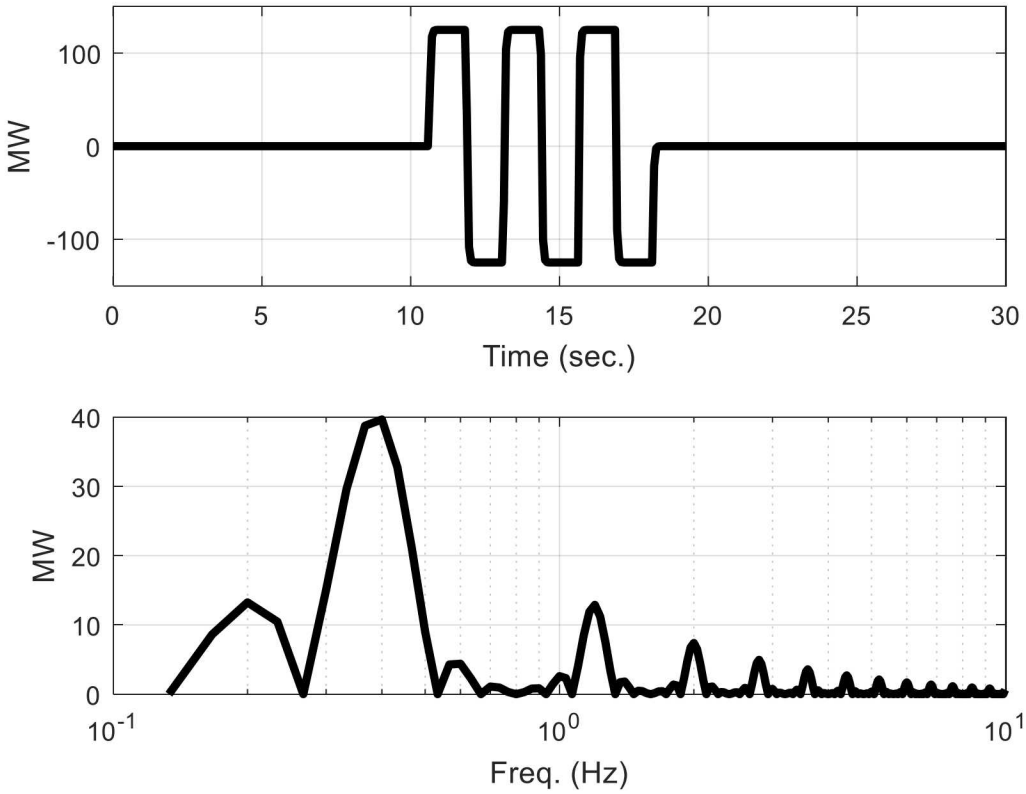

Figure 4-2. Square-wave pulsing signal (Top plot is in the time domain. Bottom plot is the signal spectrum. Signal is 3-cycles of a 2.5-sec period square wave. Peak energy is at 0.4 Hz.)

Table 4-1. 2016 Test Series

Test Name	Date	Time (PT)	DCON Settings			Action	Notes
			Loop	Gain (K_0)	P_{max}		
1609A1	9/13/16	9:10	Open			±20-MW calibration check	Calibration verified.
1609A2		9:15				±20-MW MSF calibration check	
1609A3		9:20				±135-MW 0.1-Hz sine calibration check	
1609A4		9:25				±125-MW 0.3-Hz sine calibration check	
1609A6		9:35				±125 MW 1-Hz sine calibration check	
1609B2	9/13/16	11:30				±20-MW 20-min. MSF probe	Test successful
1609C2	9/13/16	15:28				±20-MW 20-min. MSF probe	Test successful
1609D1	9/28/16	9:10	Open			±135-MW 0.1-Hz sine calibration check	Calibration verified. Tests successful.
1609D2		9:20				±125-MW 0.1-Hz sine calibration check	
1609D3		9:30				±20-MW 10-min. MSF probe	
1609D4		9:45				±125-MW square-wave pulsing	
1609E1	9/28/16	11:10	Closed	6	35	±125-MW 0.1-Hz sine calibration check	Successful closed-loop operation.
1609E2		11:20				±20-MW 20-min. MSF probe	
1609E3		11:45				±125-MW square-wave pulsing	
1609F1	9/28/16	13:11	Open			±135-MW 0.1-Hz sine calibration check	Calibration verified. Tests successful. Tests F4 repeated.
1609F2		13:20				±125-MW 0.1-Hz sine calibration check	
1609F3		13:30				±20-MW 10-min. MSF probe	
1609F4-1		13:45				±125-MW square-wave pulsing	
1609F4-2		13:46				±125-MW square-wave pulsing	
1609G1	9/28/16	15:12	Closed	9	50	±125-MW 0.1-Hz sine calibration check	Successful closed-loop operation.
1609G2		15:20				±20-MW 20-min. MSF probe	
1609G3-1		15:44				±125-MW square-wave pulsing	
1609G3-2		15:47				±125-MW square-wave pulsing	
1609H1	9/29/16	9:10	Closed	6	50	±20-MW 10-min. MSF probe	Successful closed-loop operation.
1609H2		9:24				±125-MW square-wave pulsing	
1609H3		9:29				±125-MW square-wave pulsing	
1609H5		9:39	Open			±125-MW square-wave pulsing	Successful operation.
1609H6		9:44				±125-MW square-wave pulsing	
1609I1	9/29/16	10:10	Closed	9	125	±20-MW 10-min. MSF probe	Successful closed-loop operation.
1609I2		10:24				±125-MW square-wave pulsing	
1609I3		10:34				CJ brake pulse	
1609I5		10:42	Open			CJ brake pulse	Successful operation.
1609I6		10:47				±125-MW square-wave pulsing	
1609J1	9/29/16	11:10	Closed	9	50	±20-MW 10-min. MSF probe	Successful closed-loop operation.
1609J2		11:24				±125-MW square-wave pulsing	
1609J3		11:29				±125-MW square-wave pulsing	
1609J5		11:39	Open			±125-MW square-wave pulsing	Successful operation.
1609J5		11:44				±125-MW square-wave pulsing	
1609K1	9/29/16	13:10	Closed	12	125	±20-MW 10-min. MSF probe	Successful closed-loop operation.
1609K2		13:24				±125-MW square-wave pulsing	
1609K3		13:30				CJ brake pulse	
1609K5		13:40	Open			CJ brake pulse	Successful operation.
1609K6		13:44				±125-MW square-wave pulsing	

Table 4-2. 2017 Test Series

Test Name	Date	Time (PT)	DCON Settings			Action	Notes
			Loop	Gain (K_0)	P_{max}		
1705A1	5/16/17	9:10	Open			Calibration test	Calibration verified. MSF probe successful.
1705A2		9:15				±20-MW 20-min. MSF probe	
1705B1	5/16/17	10:10	Closed	9	125	±20-MW 5-min. MSF probe	Test successful
1705B2		10:20				±125-MW square-wave pulsing	
1705B3		10:25				CJ brake pulse	
1705B5		10:35	Open			CJ brake pulse	
1705B6		10:40				±125-MW square-wave pulsing	
1705C1	5/16/17	11:10	Closed	12	125	±20-MW 5-min. MSF probe	Test successful
1705C2		11:20				±125-MW square-wave pulsing	
1705C3		11:25				CJ brake pulse	
1705C5		11:35	Open			CJ brake pulse	
1705C6		11:41				±125-MW square-wave pulsing	
1705D1	5/16/17	13:10	Open			Calibration test	Calibration verified. MSF probe successful.
1705D2		13:15				±20-MW 20-min. MSF probe	
1705E1	5/16/17	14:10	Closed	18	125	±20-MW 10-min. MSF probe	Test successful
1705E2		14:25				±125-MW square-wave pulsing	
1705E4		14:27	Open			±125-MW square-wave pulsing	
1705F1	5/16/17	15:10	Closed	12	125	±20-MW 0.4-Hz forced oscillation	Tests successful
1705F2		15:13	Open			±20-MW 0.4-Hz forced oscillation	
1705F3		15:20	Open			±30-MW 1-Hz forced oscillation	
1705F4		15:23	Closed	12	125	±30-MW 1-Hz forced oscillation	
1705F5		15:30	Open			±20-MW 3-Hz forced oscillation	
1705F6		15:33	Closed	12	125	±20-MW 3-Hz forced oscillation	
1705F7		15:40	Open			±20-MW 5-Hz forced oscillation	
1705F8		15:45	Closed	12	125	±20-MW 5-Hz forced oscillation	
1705G1	5/16/17	16:10	Closed	12	125	±20-MW 10-min. MSF probe	Used alternative feedback signal. Disabled JD1 and JD2. BE1 is the primary north PMU. Test successful.
1705G2		16:25				±125-MW square-wave pulsing	
1705G6		16:35	Open			±125-MW square-wave pulsing	
1706H1	6/6/17	9:10	Open			Calibration test	Calibration verified. MSF probe successful.
1706H2		9:15				±20-MW 20-min. MSF probe	
1706I0	6/6/17	10:31	Open	10	50	±125-MW square-wave pulsing	Deadband set at 0.25 mHz. Verifyed limits on controller.
1706I2		10:35	Closed	10	50	±125-MW square-wave pulsing	Deadband set at 0.25 mHz. Final walk-away test cancelled to allow BPA more time to conduct simulations.
1706I3		10:40				±20-MW 10-min. MSF probe	
1706I4						CANCELLED	

Table 4-3. 2018 Test Series

Test Name	Date	Time (PT)	DCON Settings			Action	Notes
			Loop	Gain (K_0)	P_{max}		
1805A1	5/23/18	9:12	Open			Calibration test	Calibration verified. MSF probe successful.
1805A2		9:28				±20-MW 20-min. MSF probe	
1805B1	5/23/18	10:10	Closed	9	125	±20-MW 5-min. MSF probe	Deadband set at 0.25 mHz. Test successful
1805B2		10:20				±125-MW square-wave pulsing	
1805B3		10:25				CJ brake pulse	
1805B5		10:32	Open			CJ brake pulse	
1805B6		10:35				±125-MW square-wave pulsing	
1805C1	5/23/18	11:10	Closed	15	125	±20-MW 5-min. MSF probe	Deadband sett at 0.25 mHz. Test successful
1805C2		11:20				±125-MW square-wave pulsing	
1805C3		11:25				CJ brake pulse	
1805C5		11:28	Open			CJ brake pulse	
1805C6		11:40				±125-MW square-wave pulsing	
1805D1	5/23/18	13:06	Open			Calibration test	Calibration verified. MSF probe successful.
1805D2		13:15				±20-MW 20-min. MSF probe	
1805E1	5/23/18	14:10	Closed	21	125	±20-MW 10-min. MSF probe	Deadband set at 0.25 mHz. Test successful
1805E2-1		14:25				±125-MW square-wave pulsing	
1805E2-2		14:27				±125-MW square-wave pulsing	
1805E4		14:29	Open			±125-MW square-wave pulsing	
1805F1	5/23/18	15:11	Open			±20-MW 0.4-Hz forced oscillation	Deadband set at 0.25 mHz. Tests successful
1805F2		15:14	Closed	12	125	±20-MW 0.4-Hz forced oscillation	
1805F3		15:20	Open			±30-MW 1-Hz forced oscillation	
1805F4		15:23	Closed	12	125	±30-MW 1-Hz forced oscillation	
1805F5		15:30	Open			±20-MW 3-Hz forced oscillation	
1805F6		15:33	Closed	12	125	±20-MW 3-Hz forced oscillation	
1805F7		15:40	Open			±20-MW 5-Hz forced oscillation	
1805F8		15:43	Closed	12	125	±20-MW 5-Hz forced oscillation	
1805G1	5/23/18	16:10	Closed	15	125	±20-MW 10-min. MSF probe	Used alternative feedback signal. Disabled JD1 and JD2. BE1 is the primary north PMU. Test successful.
1805G2		16:26				±125-MW square-wave pulsing	
1805G6		16:33	Open			±125-MW square-wave pulsing	
1805H1	5/24/18	10:10	Open			Calibration test	Calibration verified. MSF probe successful. Had to re-start MSF test because dead band was on.
1805H2		10:14				±20-MW 20-min. MSF probe	
1805I0	5/24/18	11:08	Open	12	25	±125-MW square-wave pulsing	Deadband set at 0.25 mHz. Verifyed limits on controller.
1805I2		11:20	Closed	12	25	±125-MW square-wave pulsing	Deadband set at 0.25 mHz.
1805I3		11:25				±20-MW 10-min. MSF probe	
1805I4-1		11:39				±125-MW square-wave pulsing	Channel A verified.
1805I4-2		11:41				±125-MW square-wave pulsing	Channel B verified.
1805I5		11:42	All limit checks verified. Walk away initiated				

5. PDCI DYNAMICS

Figure 5-1 shows the estimated open-loop transfer function from ΔP_{cmd} to P_{dc} in Figure 3-1 based upon 10 different MSF open-loop probing tests. This is the transfer function of the PDCI. The output P_{dc} is the real power measured from the PDCI on the AC side of the converter and is the actual power injected into the AC system. Each test is represented with a distinct color corresponding to the test name in Tables 4-1, 4-2, and 4-3 and the legend in the gain plot. The third plot in Figure 5-1 is the estimated coherency between from ΔP_{cmd} to P_{dc} which indicates excellent noise rejection. The PDCI open-loop step response for five test dates are shown in Figure 5-2. The results in these figures (and the many more collected during the tests) show several ideal properties.

First, as reflected in Figure 5-1 the gain of the PDCI is nearly flat with a bandwidth of nearly 7 Hz which is well past the dynamic bandwidth of electromechanical oscillations. The gain does increase slightly near 5 Hz indicating a slight under-damped response which is consistent with the step responses in Figure 5-2. Because this under-damped response is much faster than the expected modal oscillations, it is of minimal concern.

Second, the response time is very fast. The response time of the PDCI is calculated from the slope of the phase in Figure 5-1; the delay for each test is indicated in the legend for the phase plot. The average delay in the control band (0.1 Hz to 1.0 Hz) is 13.2 msec. This is certainly plenty fast for oscillation damping within the limitations [3], [4].

Thirdly, the system is not corrupted by noise. This is confirmed in the bottom subplot in Figure 5-1 labeled "C_{xy}" which shows the coherency between ΔP_{cmd} and P_{dc}. The coherency is a measure of correlation between two signals; a coherence of zero indicates no correlation and a coherence of unity indicates 100% correlation [9]. This plot demonstrates that 100% of the modulation passes to the AC system.

Lastly, the response is very consistent and linear. This is expected as the dynamics are governed by the PDCI converter controls and electronics which are certainly predicable.

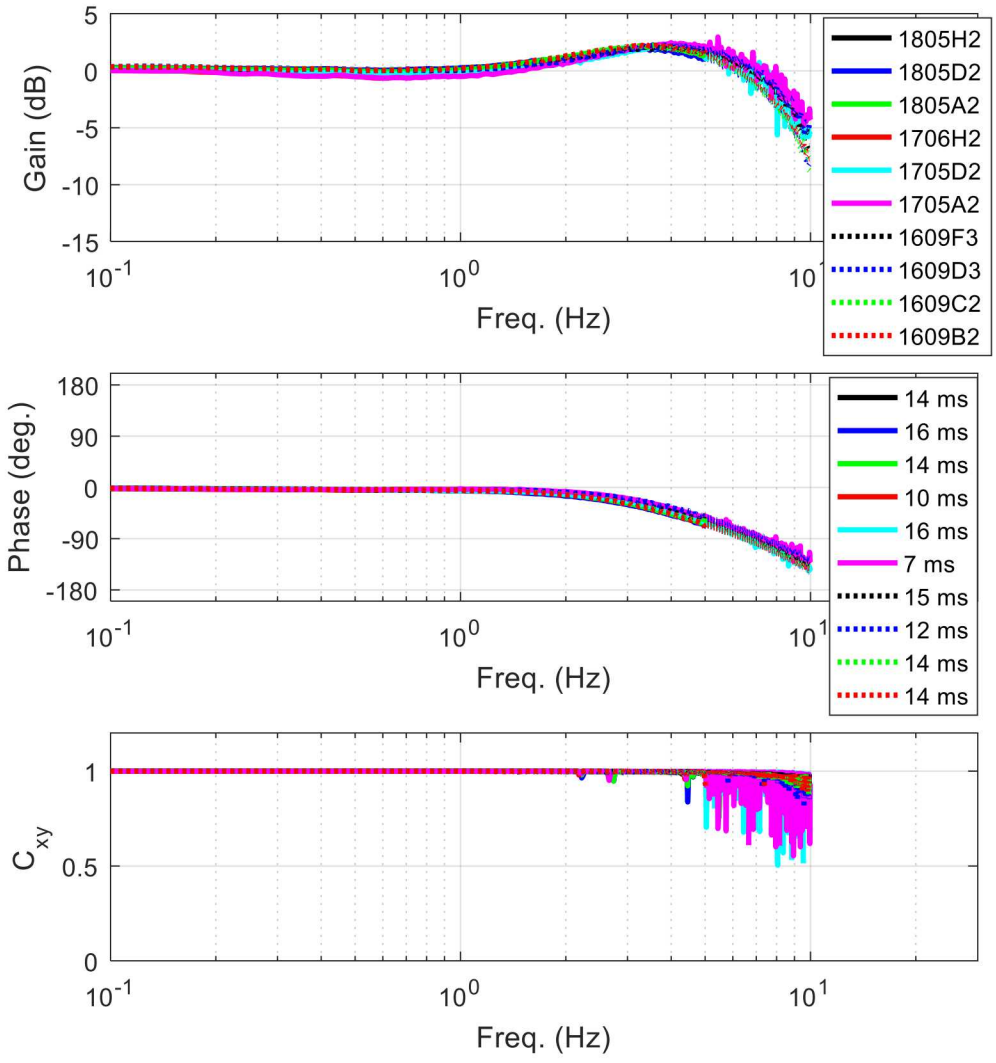

Figure 5-1. Open-loop transfer function $\Delta P_{dc}/\Delta P_{cmd}$ for all (10 total) MSF probing tests (First plot is the gain with the legend showing the name of the test. Second plot shows the phase with the estimated delay; the average delay = 13.2 ms. The third plot shows the coherency.)

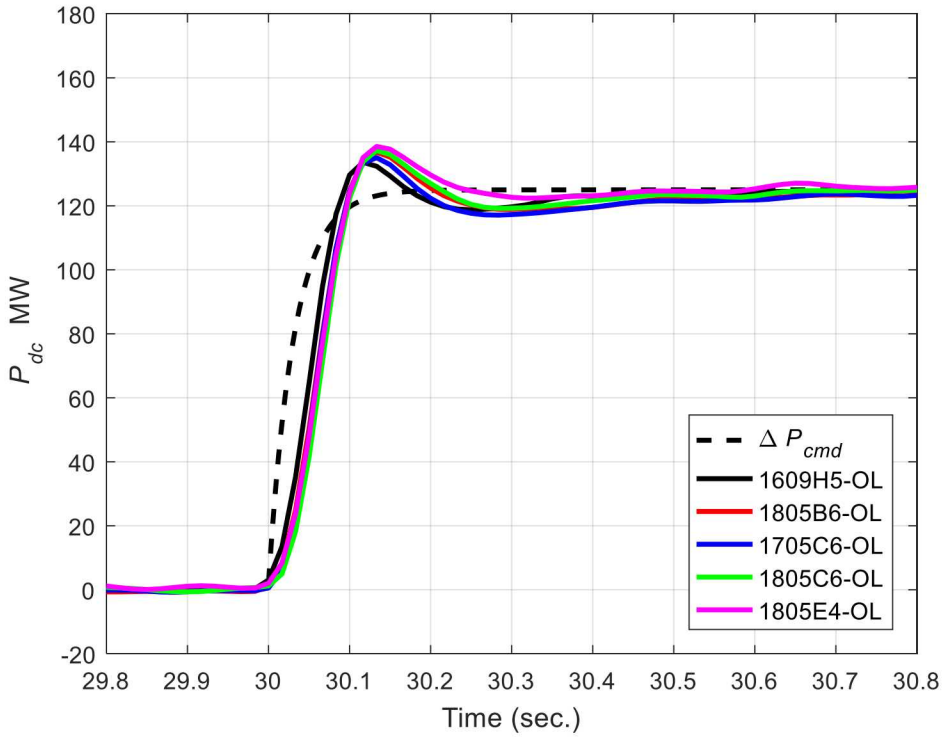

Figure 5-2. PDCI open-loop step response for 5 different test cases (The input is the dotted line.)

This page left blank

6. LOOP TRANSFER FUNCTION

Figure 6-1 shows the estimated open-loop transfer function of the entire loop and the priority one feedback signal for all MSF open-loop probing tests and a control gain K_0 of 9MW/mHz. Note that an extra negative sign is included in the calculation in order to center the phase plot around 0°. It represents the open-loop transfer function from ΔP_{cmd} to $-P_{c1}$ in Figure 3-1. The results are very consistent with the nearly 100 past open-loop probing tests conducted since 2009 [3], [4], [5] and indicate improved damping for all modes controllable during the tests.

Peaks in the gain indicate a system mode below 1 Hz. The plots show three primary peaks near 0.25 Hz (NSA mode), 0.35 Hz (NSB mode), and 0.7 Hz (BC and/or MT modes). As typical of the WI, the modal properties change depending on the particular operating conditions. The 1609 tests show the NSB mode at 0.3 Hz and no discernable NSA mode; this is typical of Alberta being disconnected or very weakly connected. The dynamics above 1 Hz are mainly due to PDCI physics.

Ideally, the phase at a given system modal peak below 1 Hz is near 0°. This indicates the DCON will add damping to that mode. If the phase is outside the $\pm$90° range, the controller will degrade damping. Note that for all NSB peaks, the gain is at a maximum and the phase is very close to 0° range; this indicates the DCON will add the most damping to this mode. The phase is also ideal for the NSA mode peaks; but, the gain is several dB lower indicating the DCON will only add a small amount of damping to this mode. The gain for the BC/MT modes near 0.7 Hz is even lower indicating very little impact for these modes; but, the phase is always within the desired $\pm$90° range.

To preserve controller robustness, a minimum of 6 dB of gain margin is desired. Figure 6-2 shows the open-loop loop transfer-functions for all possible feedback pairs for the 1805H2 test and the gains adjusted for each path to achieve a gain margin of 6 dB (near 3 Hz). The gain for signals using a northern John Day PMU are set to 18 while the gain for feedback signals using a Big Eddy PMU are set to 9. This halving occurred in all tests and is reflected in the guidelines of Table 3-1.

At K_0 = 9 MW/mHz, Figure 6-1 assures a gain margin of 10 dB or more at a crossover frequency of 3 – 4 Hz. This represents good robustness properties. The 4 Hz crossover is well outside the range of electromechanical mode frequencies. A gain margin of 6 dB equates to a conservative K_0 = 14 MW/mHz which is the highest prudent gain in terms of stability with this feedback configuration. The DCON would likely drive the PDCI system to instability near K_0 = 28 MW/mHz.

Reducing the gain of the Big Eddy paths by half will degrade the amount of damping achieved with a Big Eddy PMU. This is seen in the DC – 1-Hz gain plot shown in Figure 6-2. The gain in this frequency range is several dB lower for the Big Eddy paths compared to the John Day paths. This loss of performance is the basis for selecting John Day PMU as the primary feedback path. The priority reflected in Table 3-1 needs to be adjusted by shifting the priority 9 and 10 signals up to priority 5 and 6, respectively. All other tests reflect nearly the exact results shown in Figures 6-1 and 6-2. Plots for all paths are in Appendix A.

It is illustrative to calculate and measure the closed-loop frequency response from the open loop. The calculated closed-loop response is shown in Figure 6-3 for several gain cases on 1805H2; it is calculated from the open-loop response. The growing peak near 3 Hz indicates that as the gain increases the PDCI response becomes more under-damped which is very consistent with the open-loop results described above. Note the decreasing gain near the NSB mode; this indicates the added damping to the mode. The actual closed-loop response for three closed-loop tests are shown in Figure 6-4. The gain settings in Figures 6-3 and 6-4 are the same. The actual measured response is very close to the calculated response indicating the closed-loop system behaves as expected.

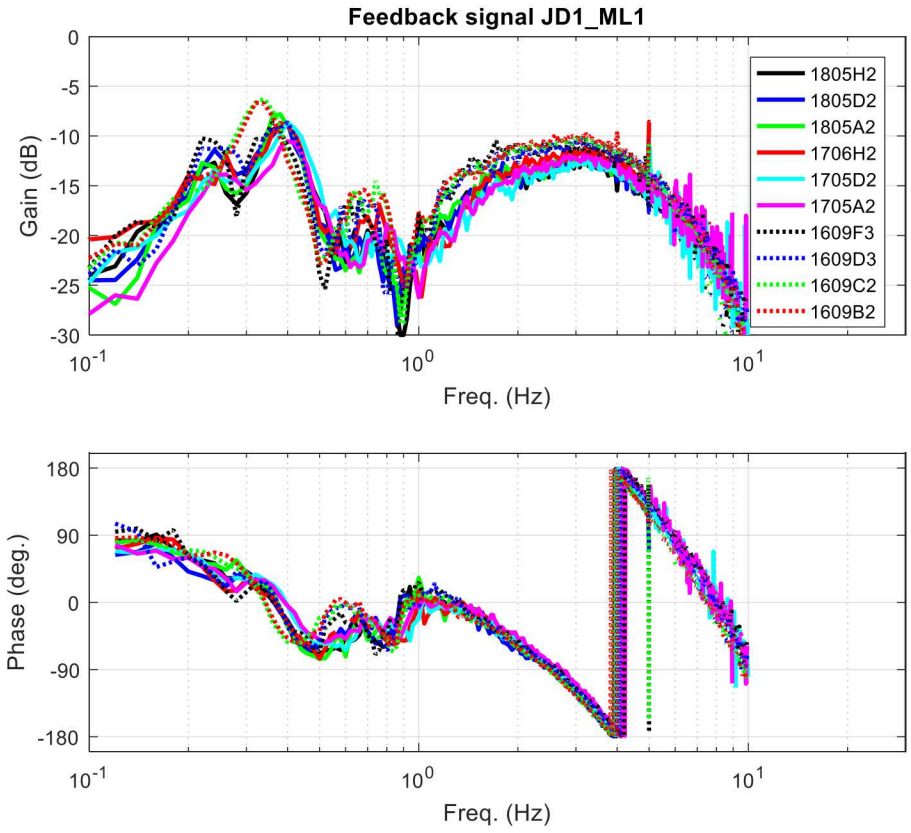

Figure 6-1. Open-loop transfer function $-\Delta P_c/\Delta P_{cmd}$ for the primary feedback pair JD1-ML1 (K_0 = 9 MW/mHz)

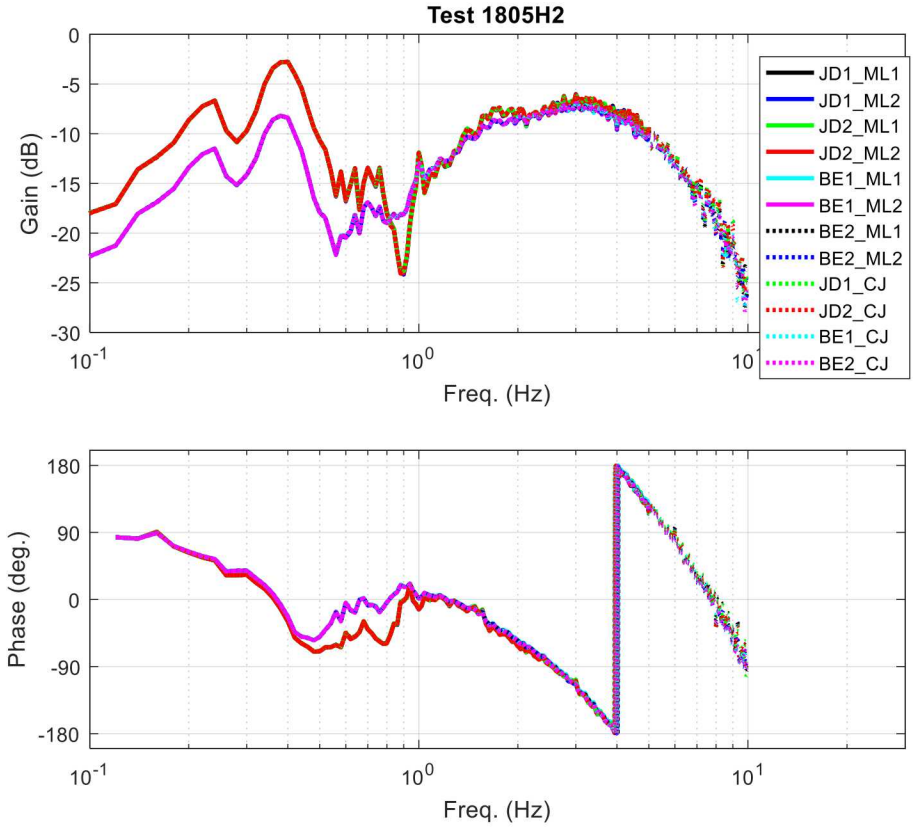

Figure 6-2. Open-loop transfer-functions $-\Delta P_c/\Delta P_{cmd}$. for all 12 feedback pairs for test 1805H2 (K_0 = 18 MW/mHz)

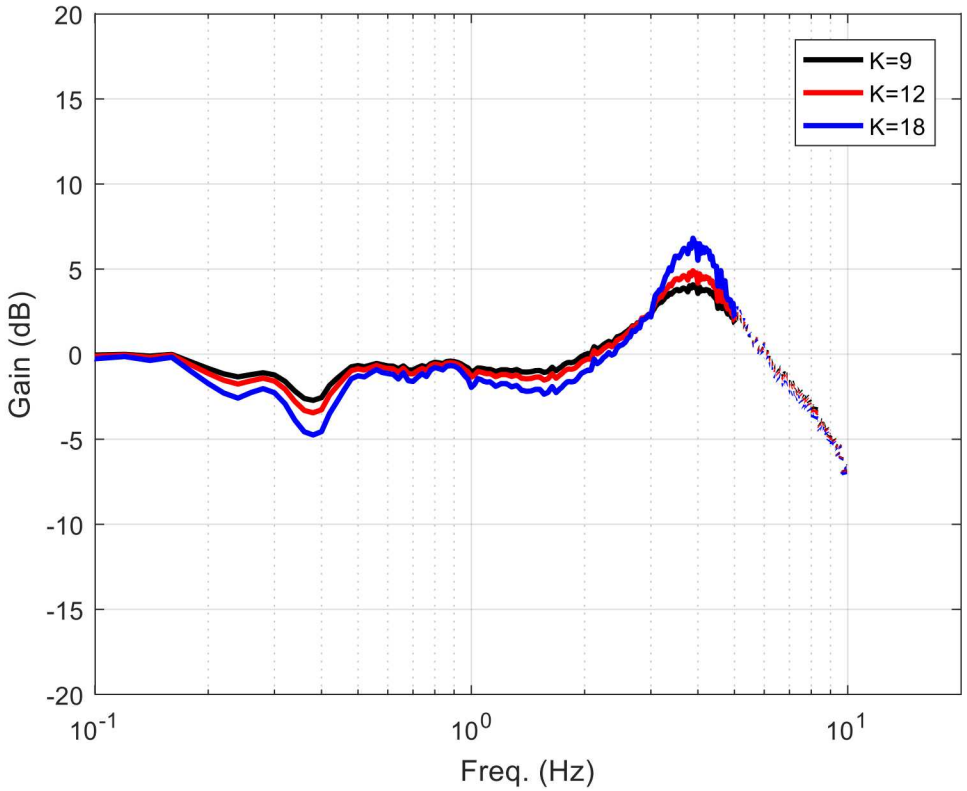

Figure 6-3. Calculated closed-loop transfer-functions $\Delta P_{dc}/P_{pi}$ for several gains for test 1805H2

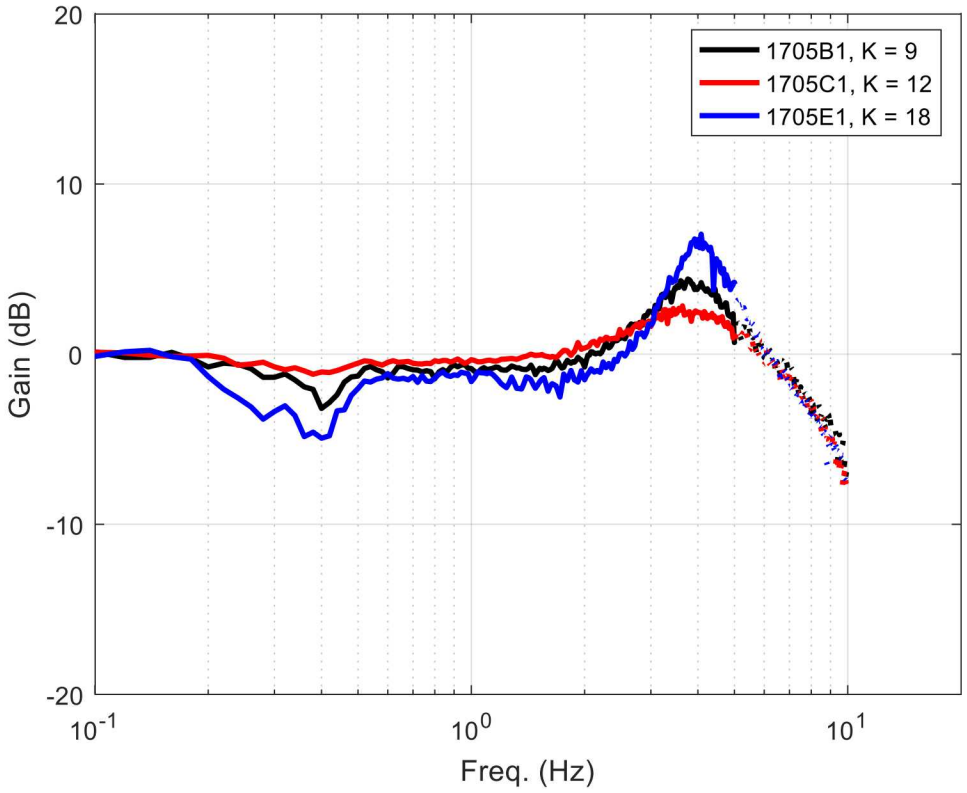

Figure 6-4. Measured closed-loop transfer-functions $\Delta P_{dc}/P_{pi}$ for several gains

This page left blank

7. CLOSED LOOP RESPONSES – IMPACT ON MODES

A variety of closed-loop versus open-loop transient responses were collected to evaluate the effectiveness of the controller in damping the modes. Modeling studies and open-loop tests show that the DCON has significant impact on the NSB mode with less impact on all other modes. In all cases oscillation damping was improved consistent with model studies. Several Chief Jo and square-wave pulsing tests (Figure 4-2) were conducted. In all cases, the open-loop and closed-loop tests were conducted back-to-back in time to facilitate comparison.

Studies have shown that the Chief Jo brake primarily excites the NSB mode and moderately excites the NSA and BC/MT modes [7]. Similarly, square-wave pulsing the PDCI will also primarily excite the NSB mode as indicated in the open-loop frequency responses (e.g., Figure 6-2).

A qualitative perspective is shown in Figure 7-1. This plot compares the system response to a Chief Jo brake pulse for three increasing gain cases (9, 12, and 15 MW/mHz). Note that the magnitude of the DCON input increases as the gain increases. Also, note that the oscillation is significantly damped for all cases. Note that a significant generator trip occurs in the 1805C5 test near the 40 sec. point; this trip is unrelated to the Chief Jo test.

In the following, we discuss the impact on system modes. In each case, a mode "signature signal" is utilized. A "signature signal" is a signal customized to isolate that given mode.

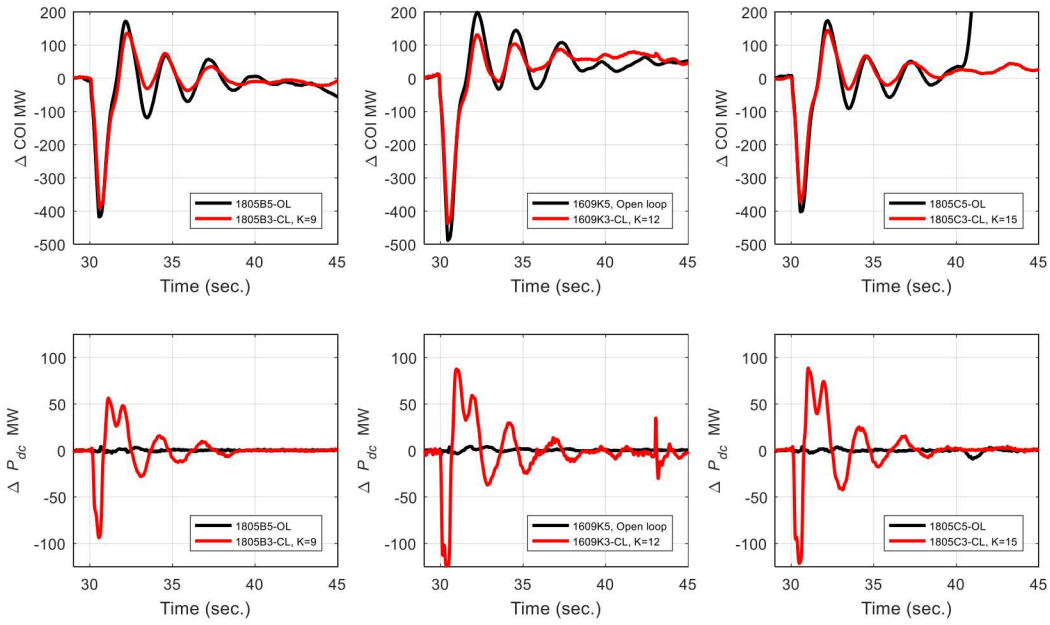

Figure 7-1. Total COI MW flow for three open-loop versus closed-loop Chief Jo brake tests (The open-loop and closed-loop tests are conducted back-to-back in time. The top row of plots shows the COI MW flow, the bottom row shows the ΔP_{dc} injected into the system by the DCON (red case). Each column of plots is a given test case with increasing gain going from left to right.)

7.1. NSB Mode

The signature signal for the NSB mode is the relative frequency between John Day and Malin. This is the primary feedback signal for the DCON and is well known to be dominated by the NSB mode; in fact, this is the reason it is used as the primary feedback [3].

Figures 7-2 and 7-3 show the signature signal for all six back-to-back Chief-Jo experiments. The top row of each figure shows the transient response in time while the bottom row shows the spectrum of the transient calculated via a windowed FFT. The peak in the spectrum near 0.4 Hz is the isolated NSB mode. Each column of plots corresponds to a test. Qualitatively, the added damping is best seen in the spectrum. Note that the peak of the spectrum significantly decreases in each case.

Table 7-1 shows the estimated frequency and damping of the NSB mode using Prony analysis for each test cases. The added damping from open-loop to closed-loop ranges from 1.3% to 6% depending on the gain and test date. Note that adding on-the-order of 3% or more to a mode represents a significant change in the mode. Because of the noise in the data and the high damping inherent in the system during the tests, the variance in the mode estimates from Prony analysis are fairly high. But, it is clear that in all cases, significant damping is added to the mode. Theory says that as the gain increases, the mode damping should increase. One might conclude this from Table 7-1; but, more experiments would be required to overcome the variance in the modal estimates.

The square-wave pulsing test utilizing the probing signal in Figure 4-2 also provides a qualitative view of the impact of the DCON on the NSB mode. Figure 7-4 shows the results for K_0 = 15 MW/mHz. This test is a good low-amplitude qualitative evaluation for the controller's impact on the NSB mode. As seen in the plot, the controller is clearly adding damping to the oscillation. Many more similar low-level tests were conducted with all indicating similar performance; these are shown in Appendix B.

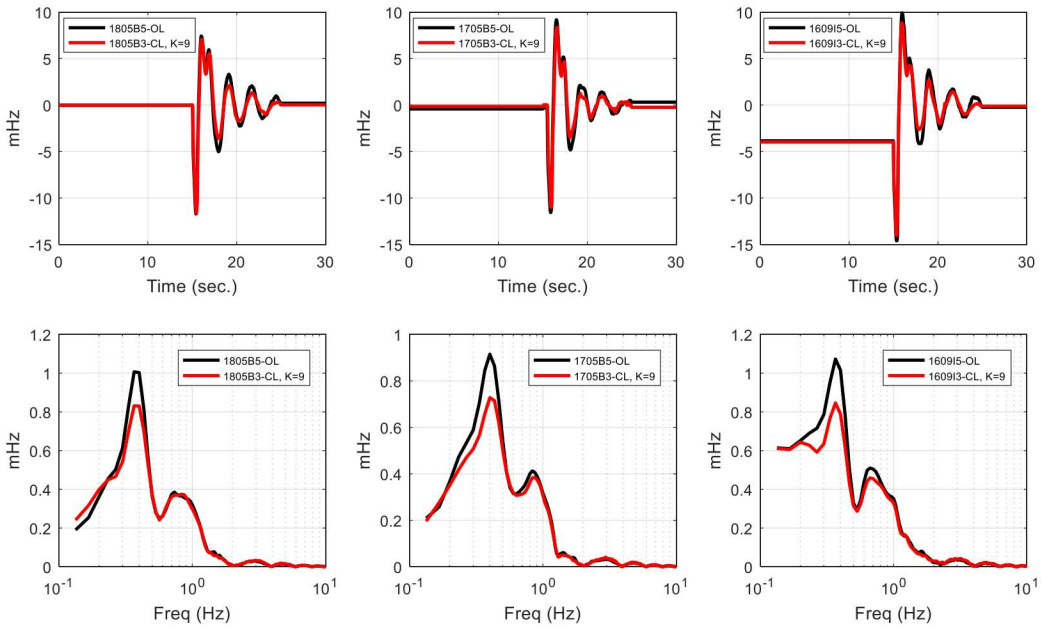

Figure 7-2. NSB signature signal (John Day - Malin freq error) response to Chief Jo brake pulse (Top row shows the time-domain response with the brake pulse at the 15 sec. point. Bottom row shows the spectrum of the time-domain response immediately above it. NSB mode is near 0.4 Hz. Open-loop vs. closed-loop comparisons for K_0 = 9.)

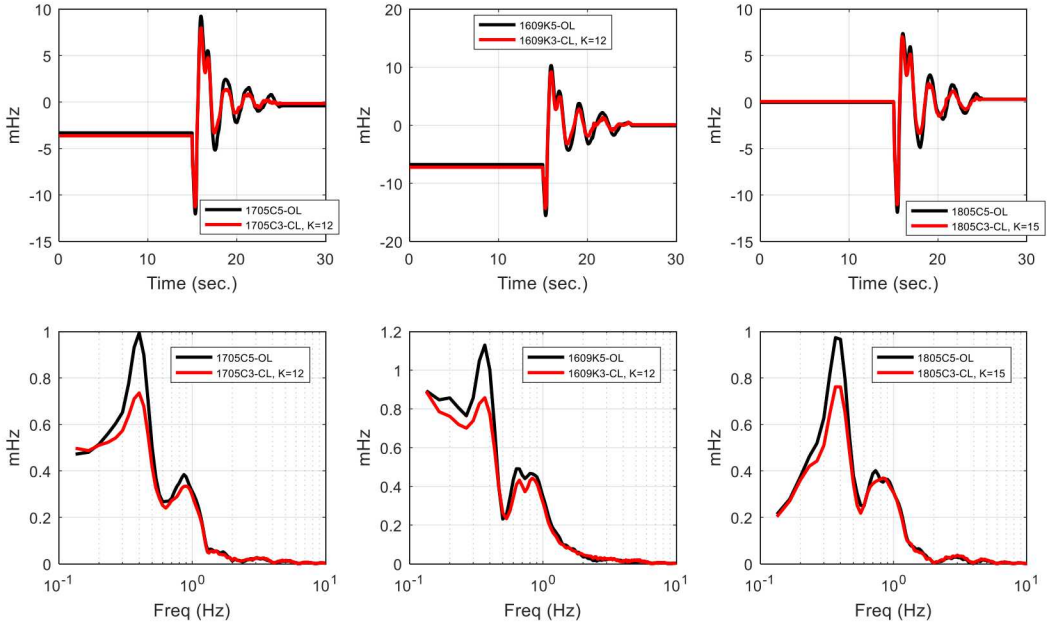

Figure 7-3. NSB signature signal (John Day - Malin freq error) response to Chief Jo brake pulse (Top row shows the time-domain response with the brake pulse at the 15 sec. point. Bottom row shows the spectrum of the time-domain response immediately above it. NSB mode is near 0.4 Hz. Open-loop vs. closed-loop comparisons for K_0 = 12 and 15.)

Table 7-1. NSB mode estimates for back-to-back Chief Jo tests (Modes estimated via Prony analysis.)

Test		Gain	Open Loop		Closed Loop		Change	
Open Loop	Closed Loop		F (Hz)	D (%)	F (Hz)	D (%)	F (Hz)	D (%)
1609I5	1609I3	9	0.383	11.7	0.364	16.1	-0.019	4.4
1705B5	1705B3	9	0.417	13.1	0.420	14.4	0.003	1.3
1805B5	1805B3	9	0.394	9.8	0.380	15.8	-0.014	6.0
1609K5	1609K3	12	0.390	12.7	0.385	17.8	-0.005	5.1
1705C5	1705C3	12	0.409	13.3	0.420	16.1	0.011	2.8
1805C5	1805C3	15	0.388	10.2	0.380	16.1	-0.008	5.9

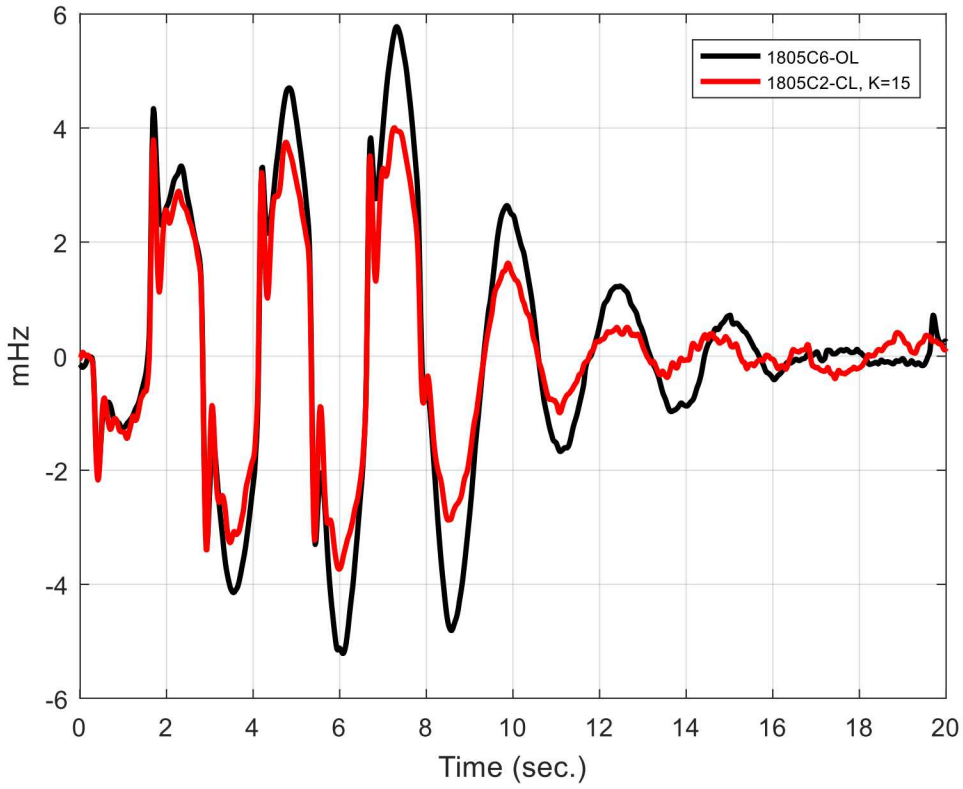

Figure 7-4. NSB signature signal (John Day - Malin freq error) response to square-wave pulse ((Figure 4-2) at ΔP_{to}. Open-loop versus closed-loop responses for K_0 = 15.)

7.2 NSA Mode

The NSA mode is very close in frequency to the NSB mode (typically 0.27 Hz vs. 0.4 Hz). In order to analyze the NSA mode, the goal is to construct a signature signal that has very little NSB mode content. The signature signal for the NSA mode is the addition of the frequency error at Sundance and Grand Coulee. Sundance has significant observability at both the NSA and NSB modes. Grand Coulee has significant content at the NSB mode and is 180° out of phase to Sundance at this mode. The content of the NSA mode at Coulee is relatively small. By adding the two signals, the NSB mode is cancelled leaving the NSA modal content.

The Chief Jo brake moderately excites the NSA mode. Figures 7-5 and 7-6 show the NSA signature signal for all six back-to-back Chief-Jo experiments. The top row of each figure shows the transient response in time while the bottom row shows the spectrum of the transient calculated via a windowed FFT. The peak in the spectrum near 0.25 to 0.3 Hz is the isolated NSA mode. Each column of plots corresponds to a test. Qualitatively, the added damping is best seen in the spectrum as a reduction in the peak while degraded damping is seen as an increase in the peak. Two tests (1805B and 1609I) show slight degrading of damping, one tests shows increased damping (1609K), and two tests show no change (1705C and 1805C). Because of the inconsistency of the results and the very high damping inherent in the system, these results indicate the DCON is having little, if any, impact on the NSA mode. The changes from one test to the next are more likely impacted by other system components and effects.

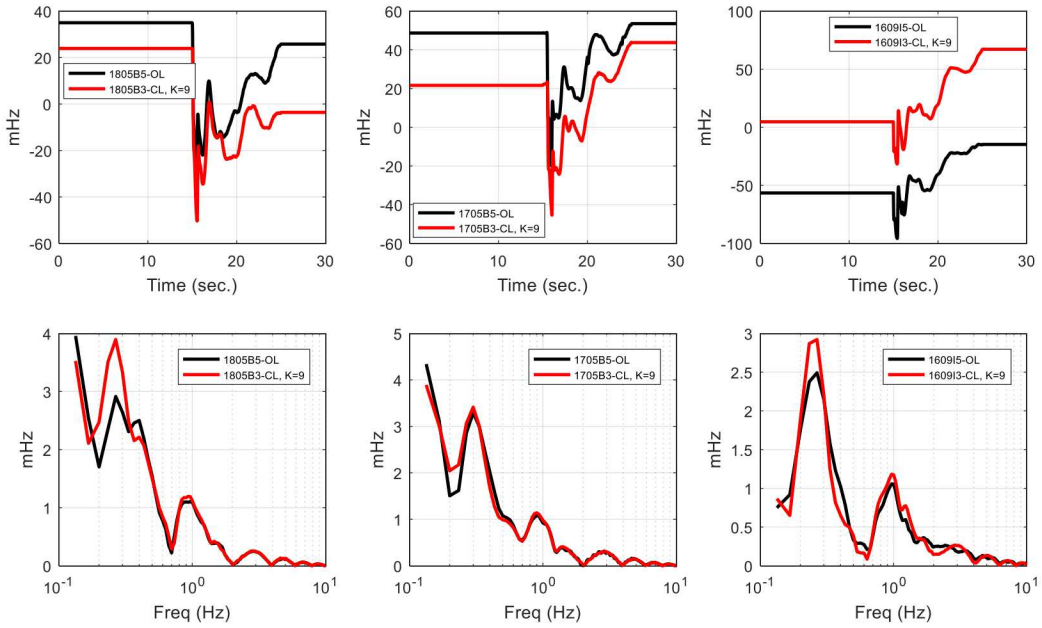

Figure 7-5. NSA signature signal (Sundance - Grand Coulee freq error) resp. to Chief Jo brake (Top row shows the time-domain response with the brake pulse at the 15 sec. point. Bottom row shows the spectrum of the time-domain response immediately above it. Open-loop vs. closed-loop comparisons for K_0 = 9.)

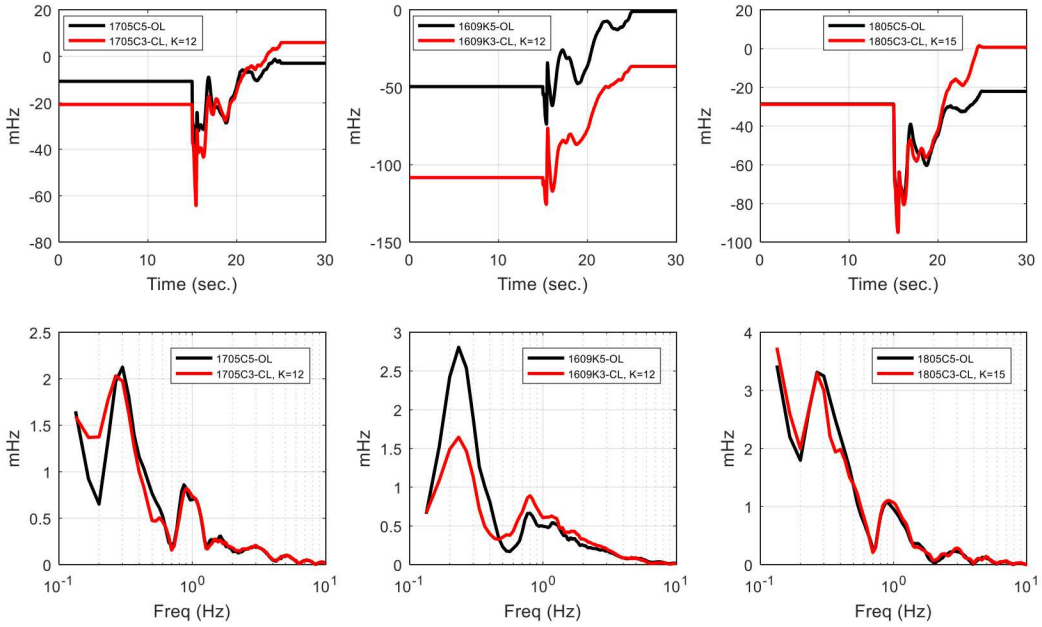

Figure 7-6. NSA signature signal (Sundance - Grand Coulee freq error) resp. to Chief Jo brake (Top row shows the time-domain response with the brake pulse at the 15 sec. point. Bottom row shows the spectrum of the time-domain response immediately above it. NSA mode is near 0.25 Hz. Open-loop vs. closed-loop comparisons for K_0 = 12 and 15.)

7.3 MT Mode

The MT mode has generators in Montana swinging against the system. The primary lead power plant is Colstrip. The signature signal for the MT mode is the relative frequency between Colstrip and Grand Coulee.

The Chief Jo brake excites the MT mode. Figure 7-7 shows the MT signature signal for the three back-to-back Chief-Jo experiments where Colstrip data was available. The top row of each figure shows the transient response in time while the bottom row shows the spectrum of the transient calculated via a windowed FFT. The peak in the spectrum near 0.8 Hz is the isolated MT mode. Each column of plots corresponds to a test. For all three cases, the response with the DCON in open-loop is nearly identical to the response with the DCON in closed loop. It is clear that the DCON has no impact on the MT mode.

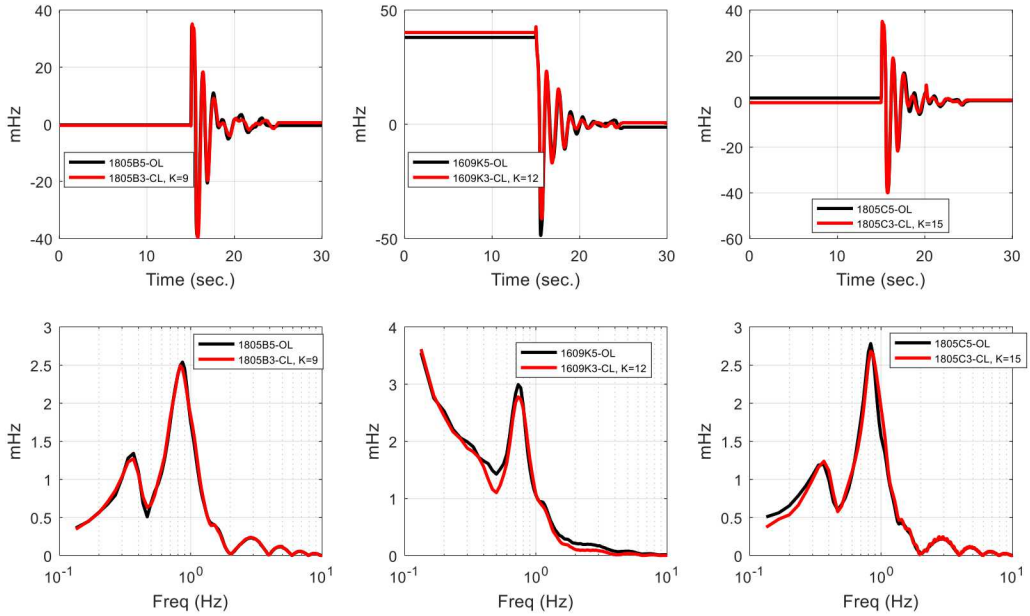

Figure 7-7. MT signature signal (Colstrip – Grand Coulee freq error) resp. to Chief Jo brake (Top row shows the time-domain response with the brake pulse at the 15 sec. point. Bottom row shows the spectrum of the time-domain response immediately above it. MT mode is the peak near 0.85 Hz. Open-loop vs. closed-loop comparisons for K_0 = 9, 12, and 15)

7.4 BC Mode

Model studies indicate that the BC mode has the Kemano power plant swinging against the system. The exact nature of this mode is not fully understood at this time. Under some conditions this mode melds with the MT mode and has the BC area oscillating against generation in MT. Unfortunately, PMU data from the BC area of the system is not available for this project. The best signature signal available is the relative frequency between Custer and John Day.

The Chief Jo brake excites the BC mode. Figures 7-8 and 7-9 show the BC signature signal for all six back-to-back Chief-Jo experiments. The top row of each figure shows the transient response in time while the bottom row shows the spectrum of the transient calculated via a windowed FFT. The peak in the spectrum near 0.85 Hz is the isolated BC mode. Because the frequency is so close to the frequency of the isolated mode in the MT signal (above section), it is possible that the BC

mode shown in Figures 7-8 and 7-9 is actually the MT mode. At any rate, the results show that DCON slightly decreases the amplitude of the mode near the 0.8 Hz.

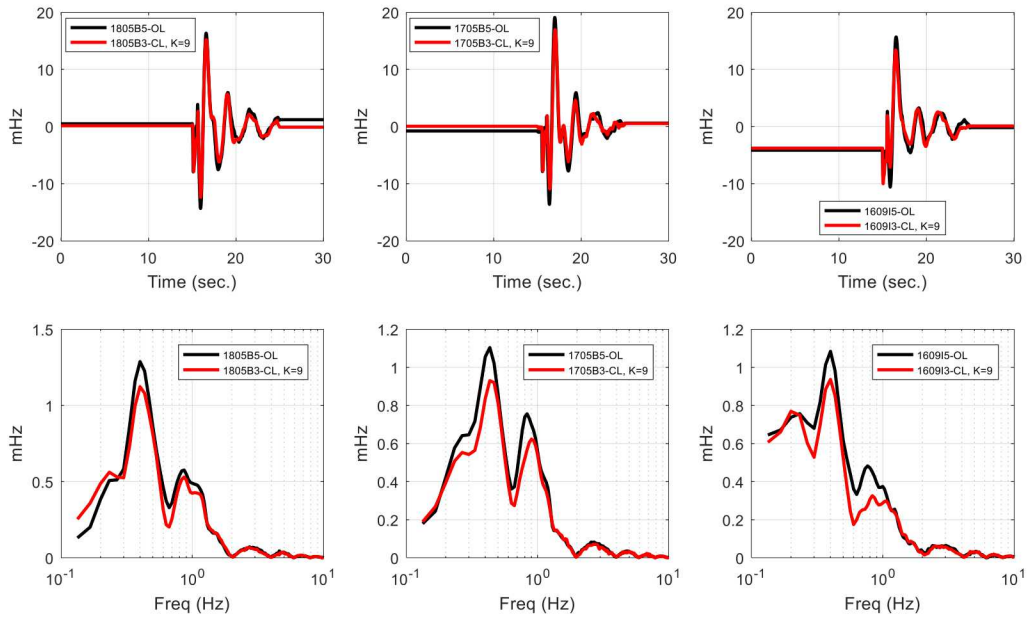

Figure 7-8. BC signature signal (Custer - John Day freq error) resp. to Chief Jo brake (Top row shows the time-domain response with the brake pulse at the 15 sec. point. Bottom row shows the spectrum of the time-domain response immediately above it. BC mode is the peak near 0.8 Hz. Open-loop vs. closed-loop comparisons for K_0 = 9.)

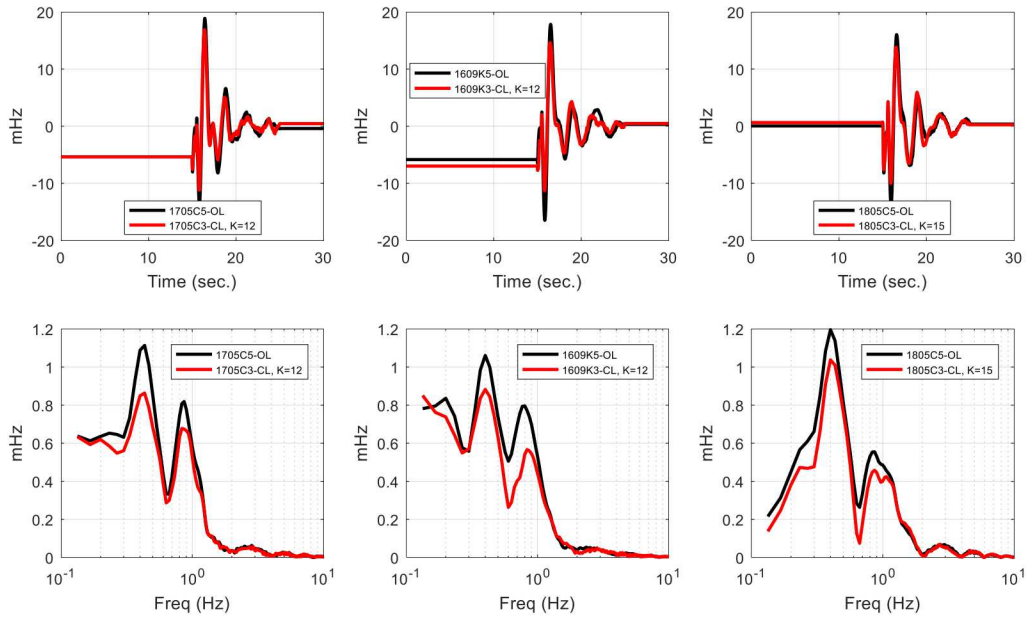

Figure 7-9. BC signature signal (Custer - John Day freq error) resp. to Chief Jo brake (Top row shows the time-domain response with the brake pulse at the 15 sec. point. Bottom row shows the spectrum of the time-domain response immediately above it. BC mode is the peak near 0.8 Hz. Open-loop vs. closed-loop comparisons for K_0 = 12 and 15)

This page left blank

8. FORCED OSCILLATIONS

Forced oscillations are common within the system. A natural question is: how does the DCON impact a forced oscillation. One perspective of the DCON controller is that it is an "eigenvalue shifting" controller. That is, it does not change the eigenvectors of the overall system; it simply does not have enough gain to modify the mode shape. Therefore, its impact on forced oscillations is minimal. Because it increases the damping within the system for all modes below one Hz, the gain from any input to any output is slightly reduced in this bandwidth. Above 1 Hz, the impact will be minimal since the gain into the system unless the forced oscillation emits from the PDCI itself.

Figure 8-1 shows the measured closed-loop transfer function $\Delta P_{dc}/P_{pi}$ for three different gain conditions. From this plot, one can calculate the impact of a forced oscillation emitting from the PDCI controls into the system. An open-loop comparison is shown in Figure 5-1. Because the closed-loop natural frequency of the PDCI system is near 4 Hz and is underdamped, the gain in the 3 to 5 Hz range is largest. Therefore, the PDCI would have the largest degrading impact on forced oscillations in the 3 to 5 Hz range. For forced oscillation below 1 Hz, the DCON will actually reduce the impact as the gain is below 0 dB. This is especially true for the interarea mode gain near 0.4 Hz as considerable damping is added to this mode.

Another useful perspective is the transfer function from the PDCI to the COI power flow shown in Figure 8-2. It is clear that below 1 Hz, forced oscillations from the PDCI will not emit into the system with much effect. The gain is well below 0 dB.

Several forced oscillation closed-loop versus open-loop tests were conducted at 0.4 Hz, 1 Hz, 3 Hz, and 5 Hz in 2017 and 2018 (test series 1705F and 1805F). Figures 8-3, 8-4, and 8-5 show the responses to the 0.4-Hz tests. It is clear that the DCON reduces the amplitude of the forced oscillation when in closed loop. The 1-Hz results are shown in Figures 8-6, 8-7, and 8-8. In this case, the FO amplitude within the system (Figure 8-7) is considerably smaller than the 0.4 Hz. The DCON slightly decreases the amplitude of the FO as it emits into the system.

Results for 3 Hz and 5 Hz forced oscillations are shown in Figures 8-9 through 8-14. In this case, the closed-loop DCON slightly amplifies the FO. This is expected as the PDCI has its natural frequency in this range. But, the amplitude of the FO at his frequency is quite small for both the open-loop and closed-loop cases as forced oscillations at these higher frequencies don't transmit throughout the system.

Appendix C shows the response of the modal signature signals to the forced oscillations. These plots further verify the observations described above.

In summary, one can conclude that the DCON will actually reduce the impact of forced oscillations for all cases except when the forced oscillation is in the 3 to 5 Hz range. In this case, the DCON could slightly amplify the oscillation. But, this is likely of little concern because the overall system has very low gain in this higher frequency range. That is, forced oscillations above 1 Hz do not emit very far from their source as the overall system gain is much lower.

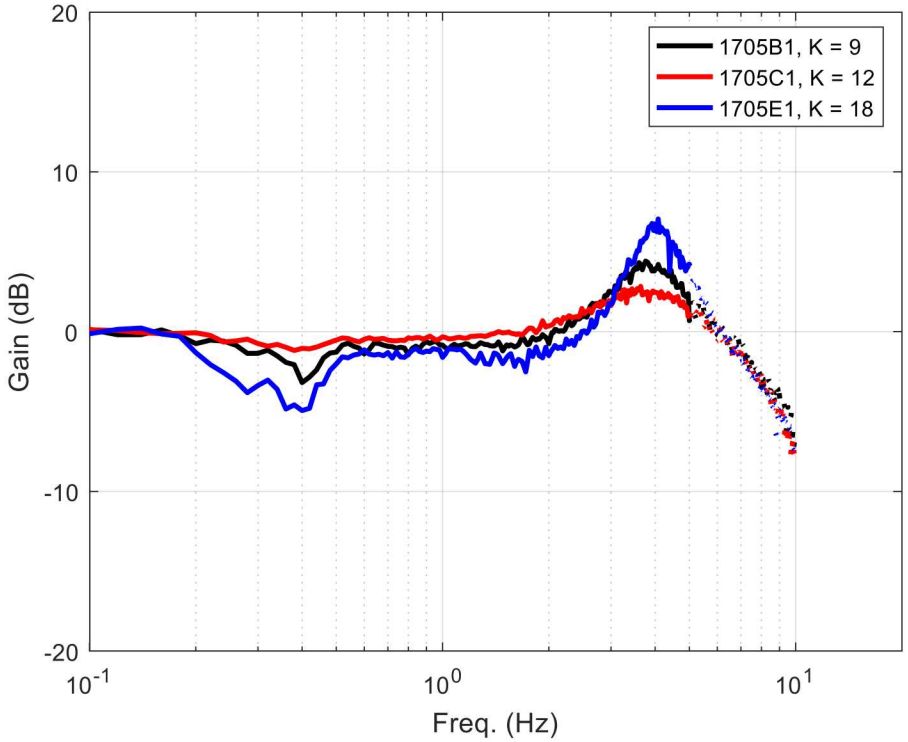

Figure 8-1. Measured closed-loop transfer-functions $\Delta P_{dc}/P_{pi}$ for several gains

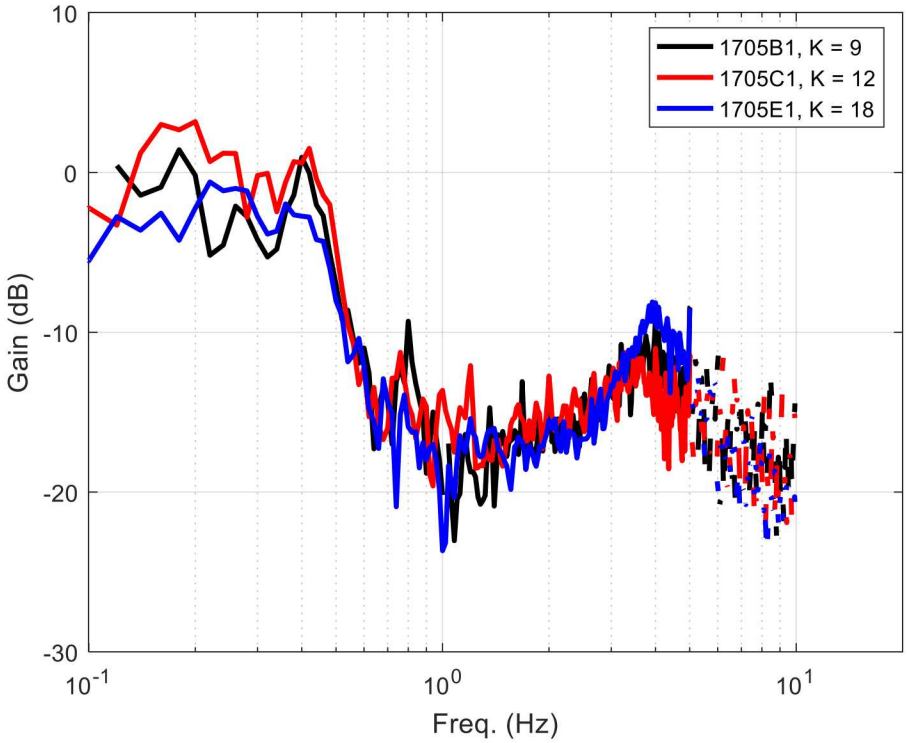

Figure 8-2. Measured closed-loop transfer-functions $\Delta P_{COl}/P_{pi}$ for several gains

8.1. 0.4 Hz

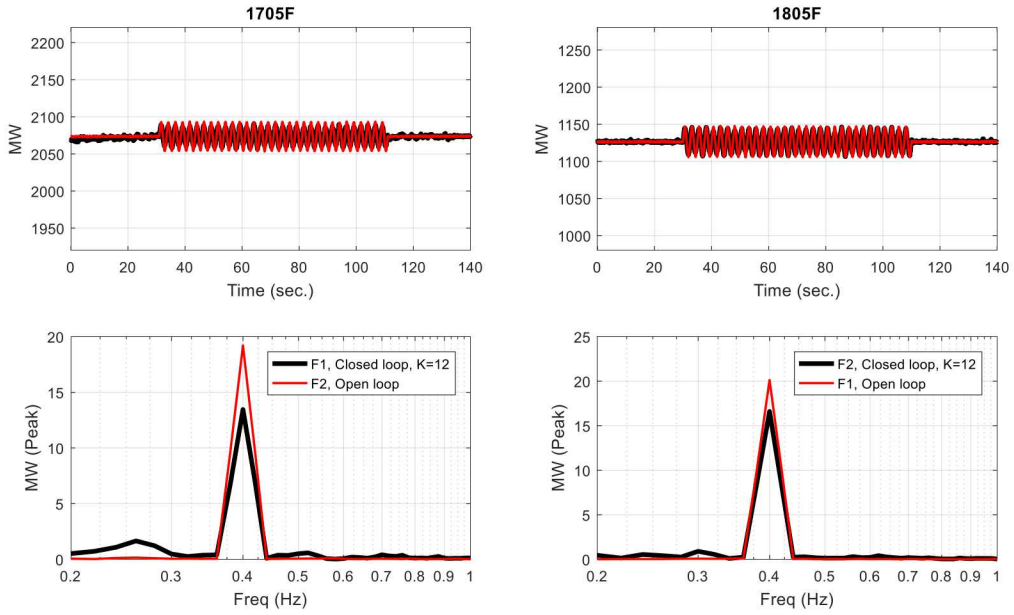

Figure 8-3. P_{dc} response to a 0.4-Hz ±20-MW forced oscillation at P_{po} in Figure 3-1 (Top row shows the time-domain response with the FO starting at the 30 sec. point and ending at the 110 sec. point. Bottom row shows the spectrum of time-domain response over a 60 sec. span of the FO. Open-loop response is shown in red, closed-loop response is shown in black. Left column of plots is from test series 1705F1 and 1705F2. Right column is from test series 1805F1 and 1805F2.)

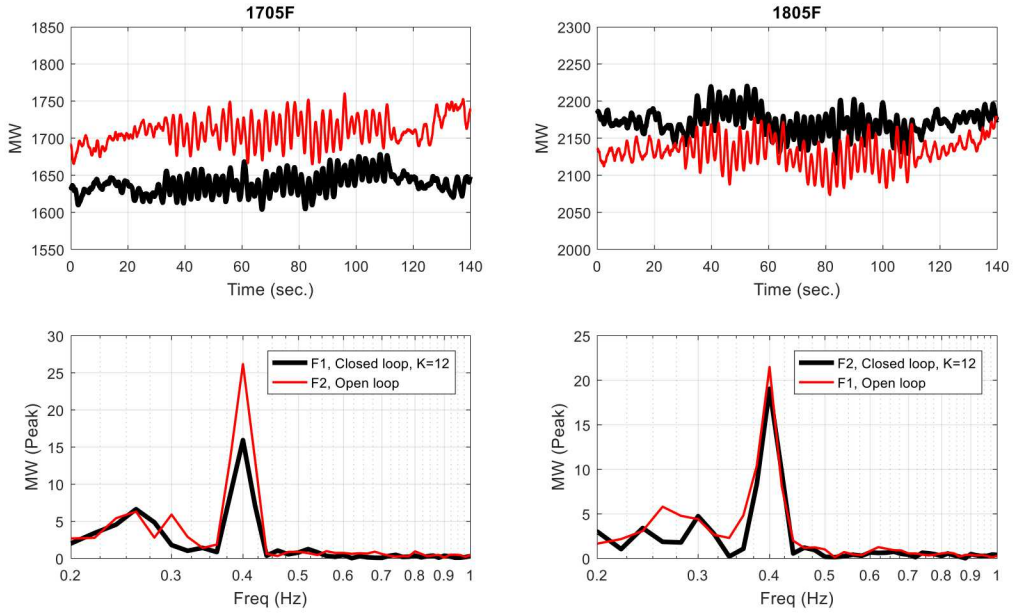

Figure 8-4. COI MW response to a 0.4-Hz ±20-MW forced oscillation at P_{po} in Figure 3-1 (Top row shows the time-domain response with the FO starting at the 30 sec. point and ending at the 110 sec. point. Bottom row shows the spectrum of time-domain response over a 60 sec. span of the FO. Open-loop response is shown in red, closed-loop response is shown in black. Left column of plots is from test series 1705F1 and 1705F2. Right column is from test series 1805F1 and 1805F2.)

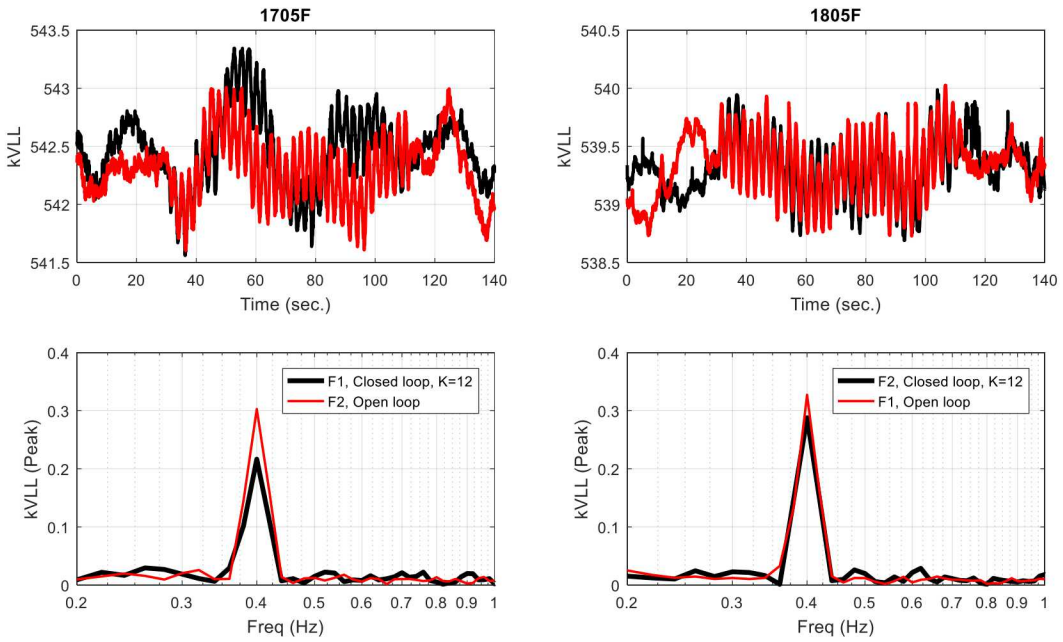

Figure 8-5. Big Eddy voltage response to 0.4-Hz ±20-MW forced oscillation at P_{po} in Figure 3-1 (Top row shows the time-domain response with the FO starting at the 30 sec. point and ending at the 110 sec. point. Bottom row shows the spectrum of time-domain response over a 60 sec. span of the FO. Open-loop response is shown in red, closed-loop response is shown in black. Left column is from test series 1705F1 & 1705F2. Right column is from test series 1805F1 & 1805F2.)

8.2. 1 Hz

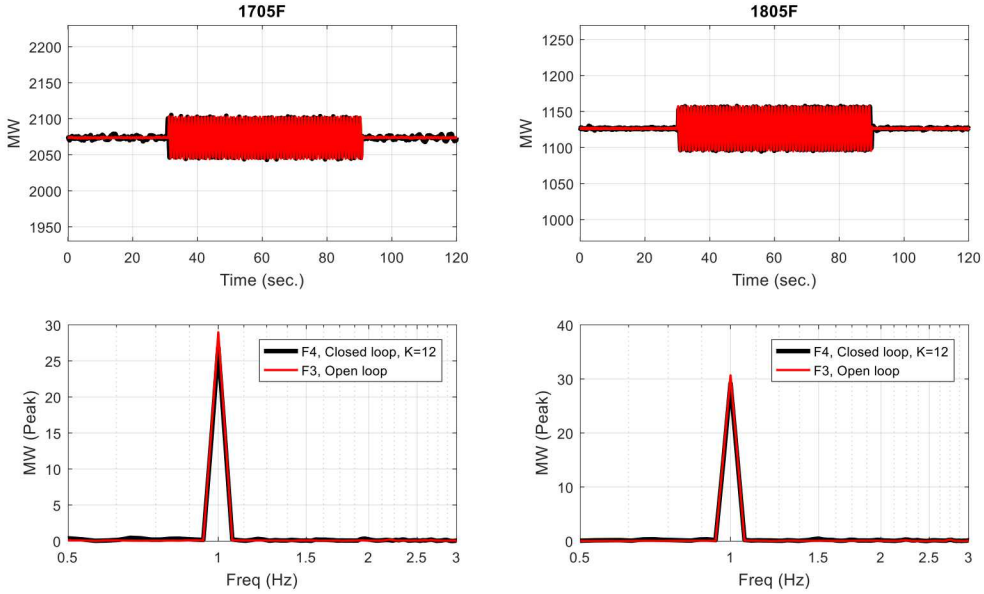

Figure 8-6. P_{dc} response to 1-Hz ±30-MW forced oscillation at P_{po} in Figure 3-1 (Top row shows the time-domain response with the FO starting at the 30 sec. point and ending at the 90 sec. point. Bottom row shows the spectrum of time-domain response over a 30 sec. span of the FO. Open-loop response is shown in red, closed-loop response is shown in black. Left column of plots is from test series 1705F1 and 1705F2. Right column of plots is from test series 1805F1 and 1805F2.)

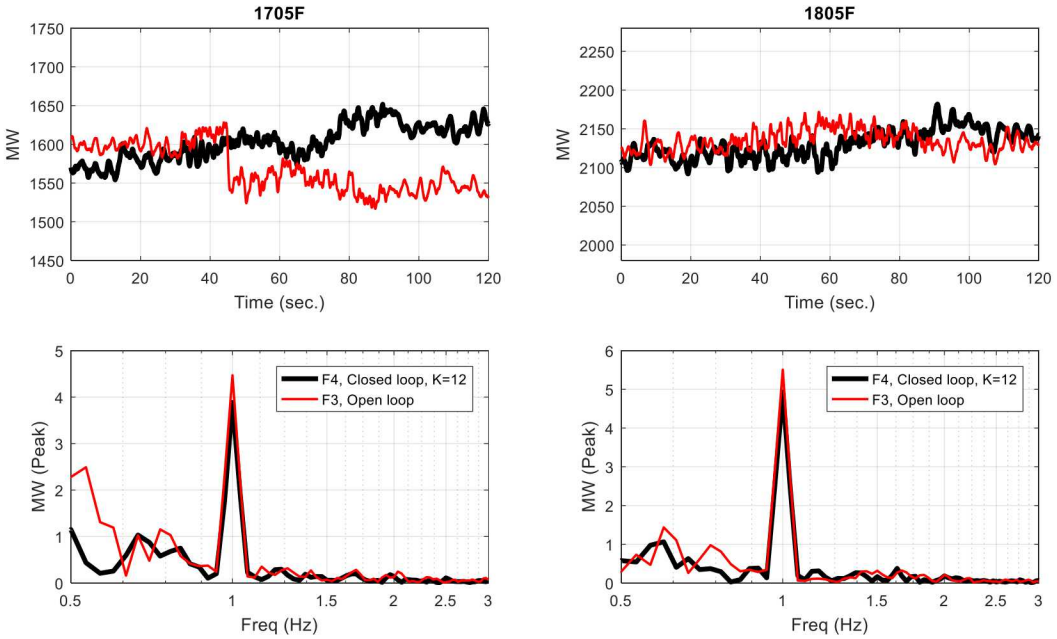

Figure 8-7. COI MW response to 1-Hz ±30-MW forced oscillation at P_{po} in Figure 3-1 (Top row shows the time-domain response with the FO starting at the 30 sec. point and ending at the 90 sec. point. Bottom row shows the spectrum of time-domain response over a 30 sec. span of the FO. Open-loop response is shown in red, closed-loop response is shown in black. Left column of plots is from test series 1705F1 and 1705F2. Right column is from test series 1805F1 and 1805F2.)

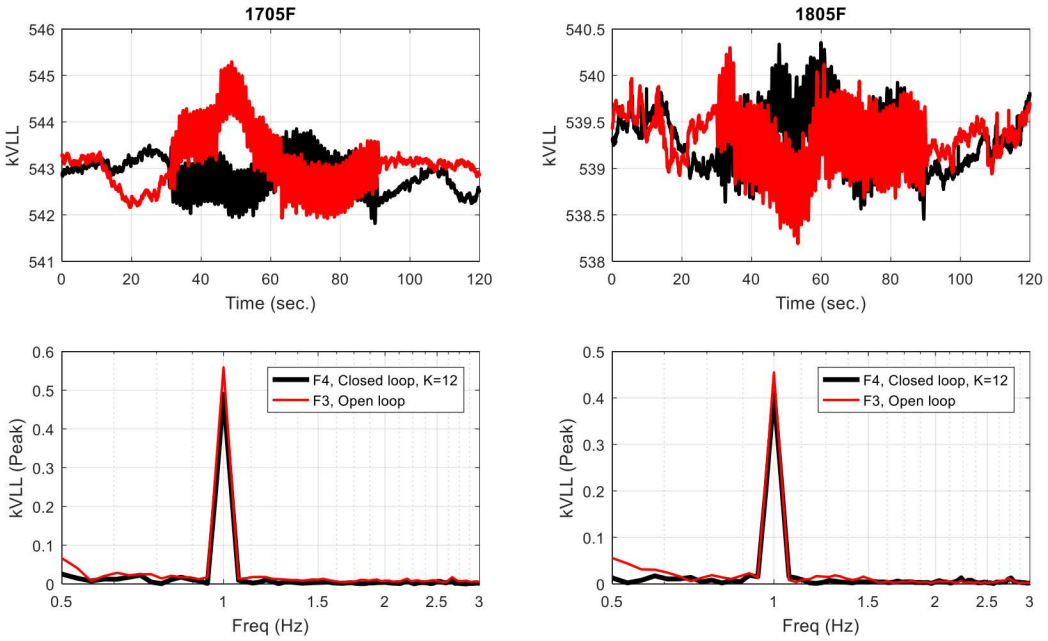

Figure 8-8. Big Eddy voltage response to 1-Hz ±30-MW forced oscillation at P_{po} in Figure 3-1 (Top row shows the time-domain response with the FO starting at the 30 sec. point and ending at the 90 sec. point. Bottom row shows the spectrum of time-domain response over a 30 sec. span of the FO. Open-loop response is shown in red, closed-loop response is shown in black. Left column of plots is from test series 1705F1 and 1705F2. Right column is from test series 1805F1 and 1805F2.)

8.3. 3 Hz

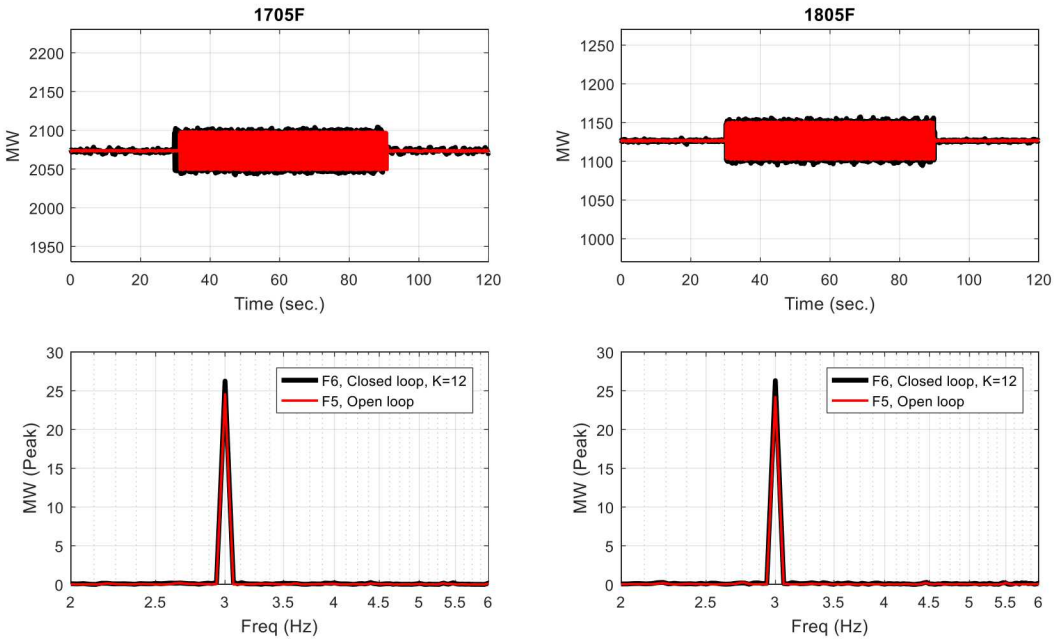

Figure 8-9. P_{dc} response to 3-Hz ±20-MW forced oscillation at P_{po} in Figure 3-1 (Top row shows the time-domain response with the FO starting at the 30 sec. point and ending at the 90 sec. point. Bottom row shows the spectrum of time-domain response over a 30 sec. span of the FO. Open-loop response is shown in red, closed-loop response is shown in black. Left column of plots is from test series 1705F1 and 1705F2. Right column of plots is from test series 1805F1 and 1805F2.)

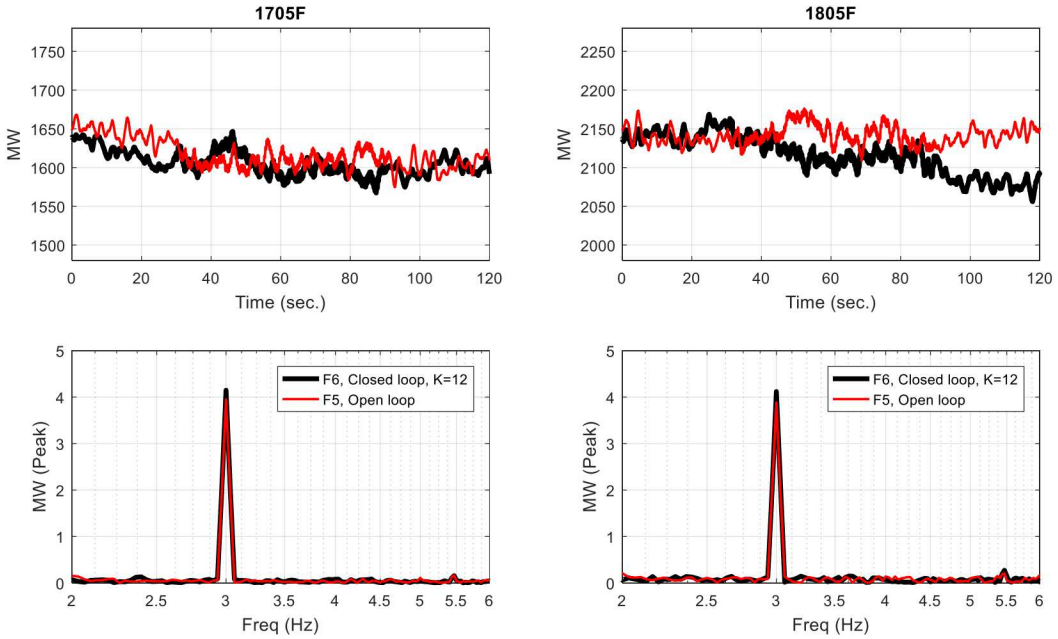

Figure 8-10. COI MW response to 3-Hz ±20-MW forced oscillation at P_{po} in Figure 3-1 (Top row shows the time-domain response with the FO starting at the 30 sec. point and ending at the 90 sec. point. Bottom row shows the spectrum of time-domain response over a 30 sec. span of the FO. Open-loop response is shown in red, closed-loop response is shown in black. Left column of plots is from test series 1705F1 and 1705F2. Right column is from test series 1805F1 and 1805F2.)

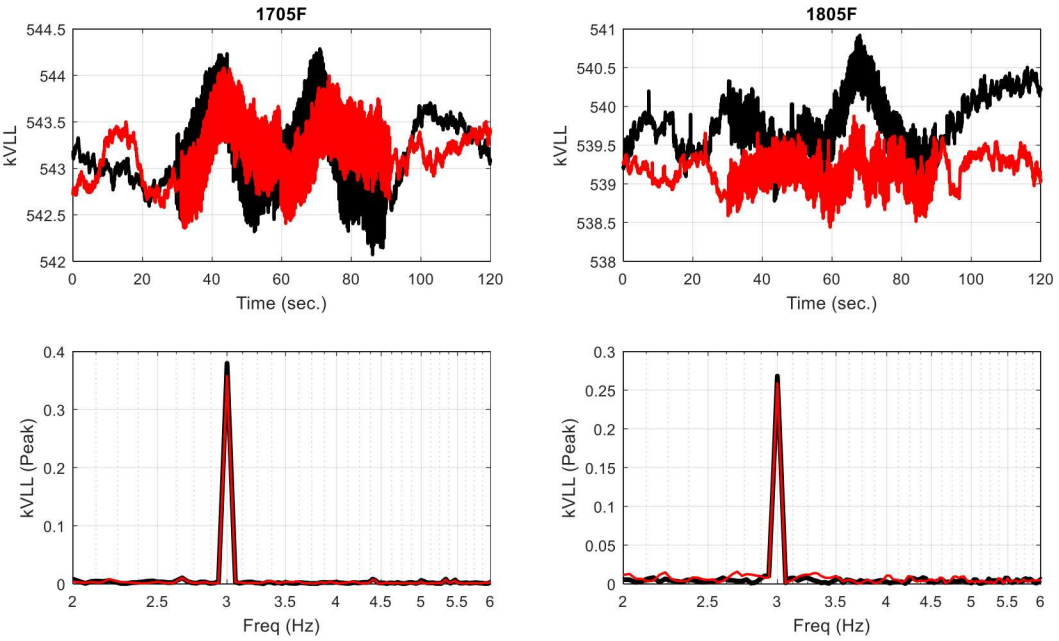

Figure 8-11. Big Eddy voltage response to 3-Hz ±20-MW forced oscillation at P_{po} in Figure 3-1 (Top row shows the time-domain response with the FO starting at the 30 sec. point and ending at the 90 sec. point. Bottom row shows the spectrum of time-domain response over a 30 sec. span of the FO. Open-loop response is shown in red, closed-loop response is shown in black. Left column of plots is from test series 1705F1 and 1705F2. Right column is from test series 1805F1 and 1805F2.)

8.4. 5 Hz

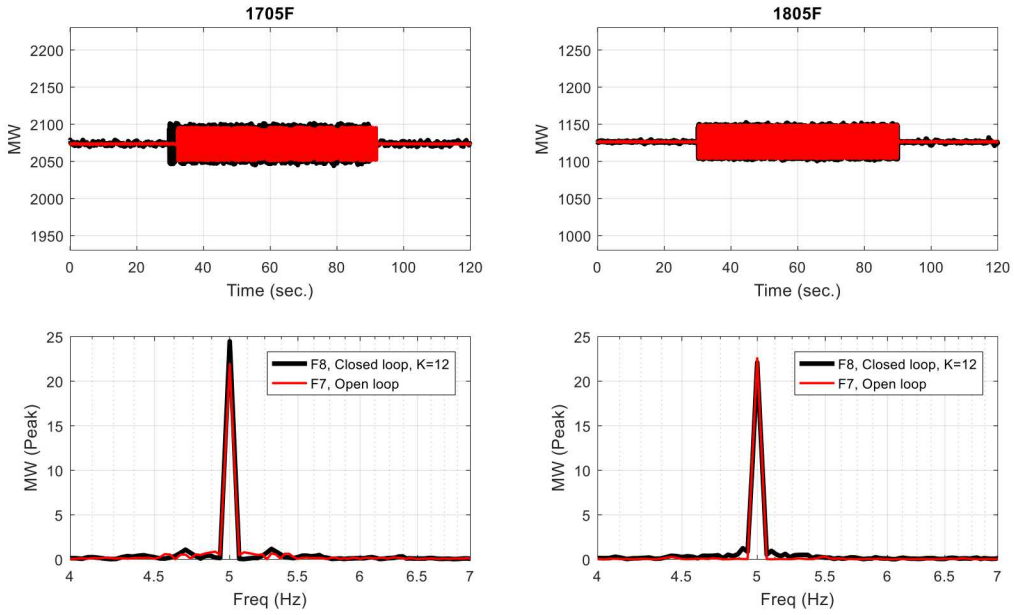

Figure 8-12. P_{dc} response to 5-Hz ±20-MW forced oscillation at P_{po} in Figure 3-1 (Top row shows the time-domain response with the FO starting at the 30 sec. point and ending at the 90 sec. point. Bottom row shows the spectrum of time-domain response over a 30 sec. span of the FO. Open-loop response is shown in red, closed-loop response is shown in black. Left column of plots is from test series 1705F1 and 1705F2. Right column of plots is from test series 1805F1 and 1805F2.)

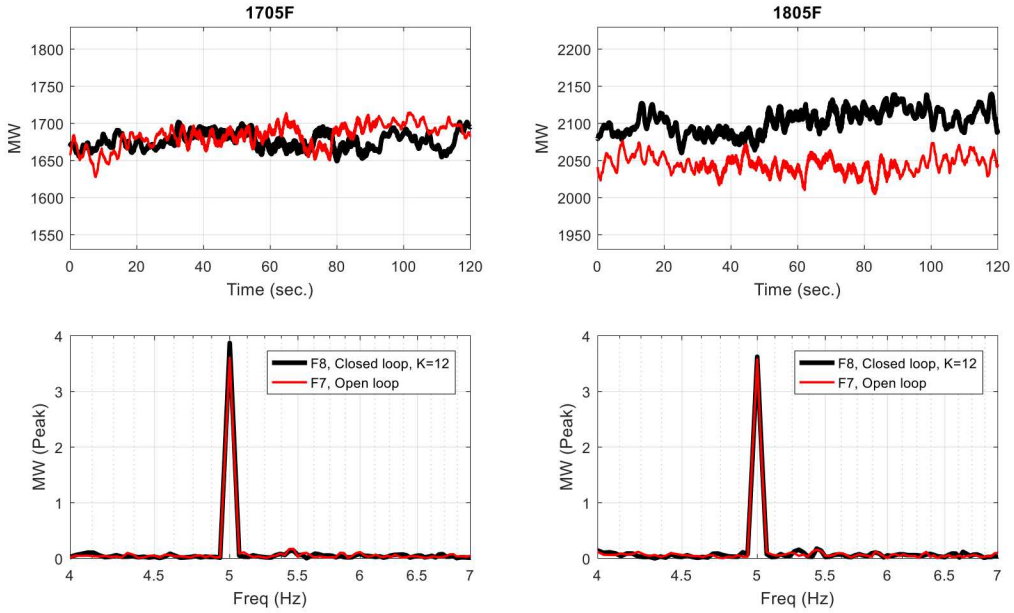

Figure 8-13. COI MW response to 5-Hz ±20-MW forced oscillation at P_{po} in Figure 3-1 (Top row shows the time-domain response with the FO starting at the 30 sec. point and ending at the 90 sec. point. Bottom row shows the spectrum of time-domain response over a 30 sec. span of the FO. Open-loop response is shown in red, closed-loop response is shown in black. Left column of plots is from test series 1705F1 and 1705F2. Right column is from test series 1805F1 and 1805F2.)

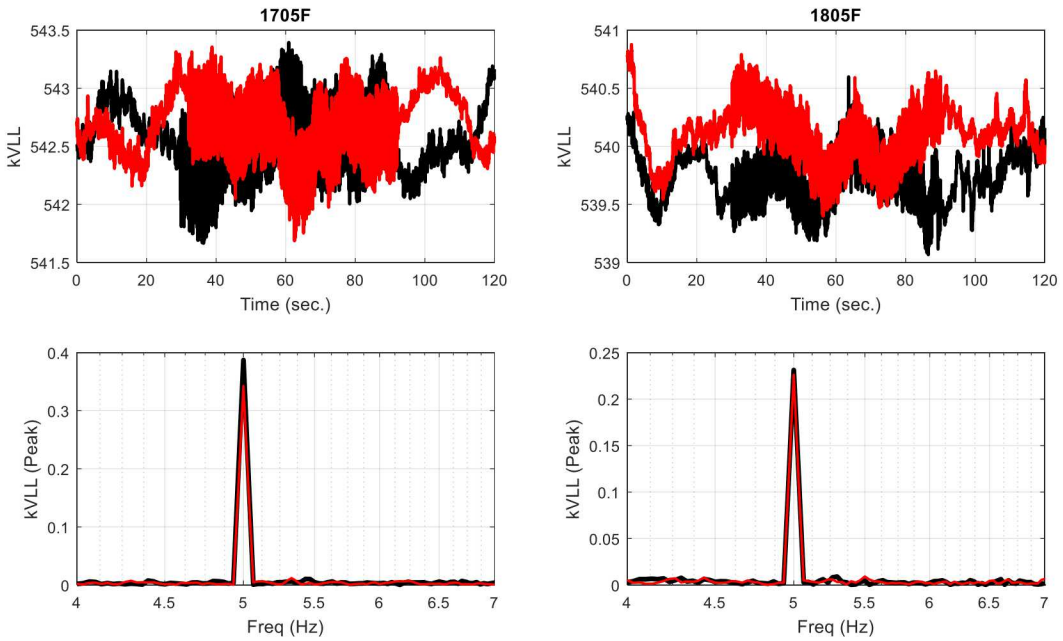

Figure 8-14. Big Eddy voltage response to 5-Hz ±20-MW forced oscillation at P_{po} in Figure 3-1 (Top row shows the time-domain response with the FO starting at the 30 sec. point and ending at the 90 sec. point. Bottom row shows the spectrum of time-domain response over a 30 sec. span of the FO. Open-loop response is shown in red, closed-loop response is shown in black. Left column of plots is from test series 1705F1 and 1705F2. Right column is from test series 1805F1 and 1805F2.)

This page left blank

9. WALK AWAY TESTS

Following the specific tests conducted on the PDCI on May 24, 2018, the DCON was configured to operate in an unattended mode (24/7 operation for 4 weeks until June 21, 2018) in which there were no DCON project team members present at the Celilo converter station. For this test, the DCON was limited to a control authority of +/- 25 MW instead of the +/- 125 MW limits for the single day attended tests. Though these lower limits reduced the ability of the DCON to significantly improve damping, it was clear upon subsequent analysis of test results that the DCON performed exactly as it was designed to with no harmful side effects. The following subsections provide plots and analysis of some of the more interesting events that occurred during this 4 week period.

9.1. DCON Performance During Unattended Operation

The plots in Figures 9-1 thru 9-6, document the performance of the DCON for three specific events that occurred during the 4 weeks of unattended operation. For each of these events, there are two plots per event: local & remote frequencies and the PDCI power flow. The events are:

- PDCI event on June 1, 2018 at 20:29 UTC (Figures 9-1 and 9-2).
- PDCI event on June 11, 2018 at 7:42 UTC (Figures 9-3 and 9-4).
- Frequency excursion event on June 21, 2018 at 3:20 UTC (Figures 9-5 and 9-6).

Both PDCI events depict significant power flow drops quickly followed by successful restarts. These events were caused by pole 3 trips on the PDCI. The frequency excursion event is most likely caused by a drop in generation on the AC side. In all events, the DCON quickly responds with the correct damping action. Due to the lower control limits, the results are not as noticeable as would likely be the case with the full +/- 125 MW limits.

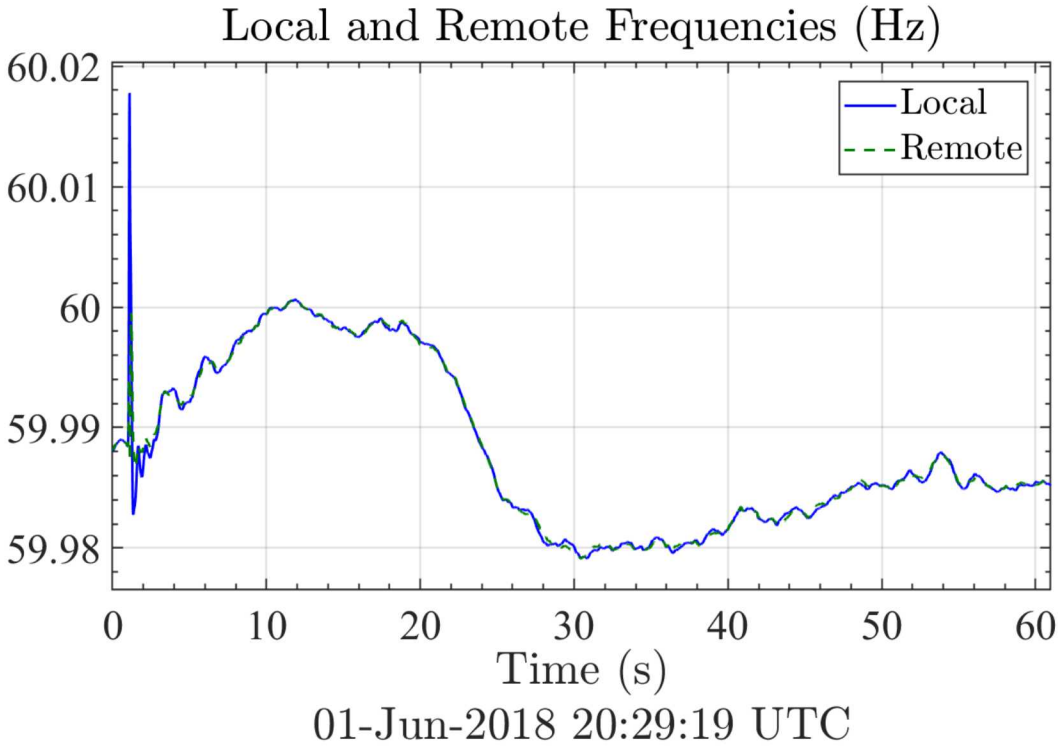

Figure 9-1. Local and remote frequencies during June 1, 2018 event

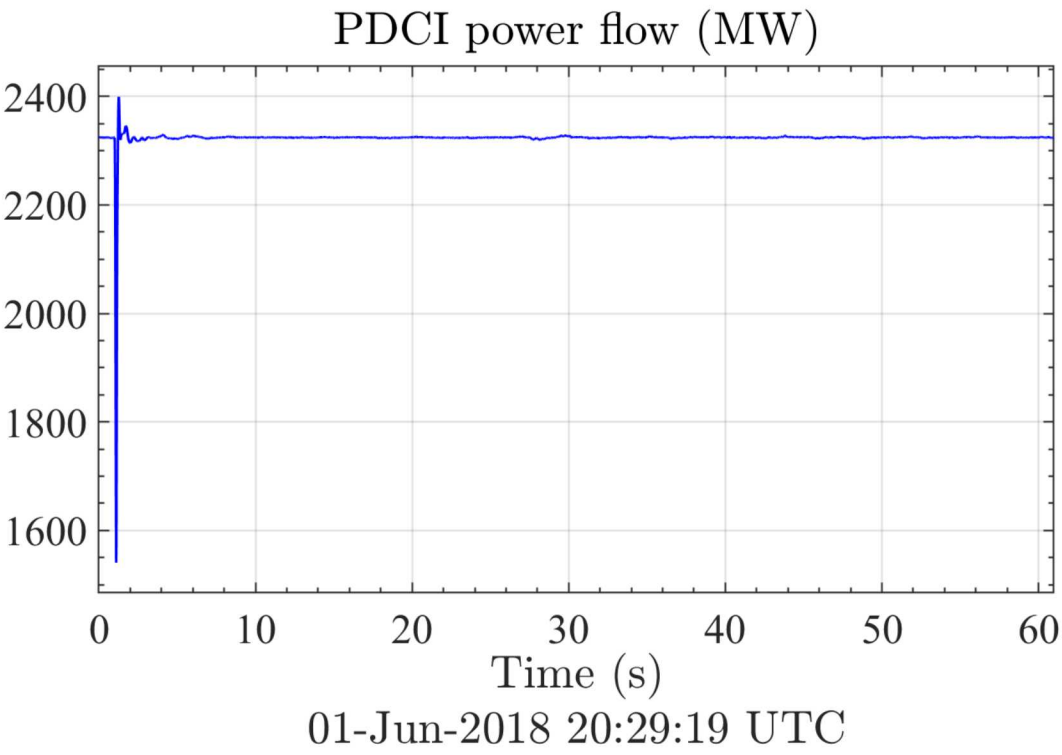

Figure 9-2. PDCI power flow during June 1, 2018 event

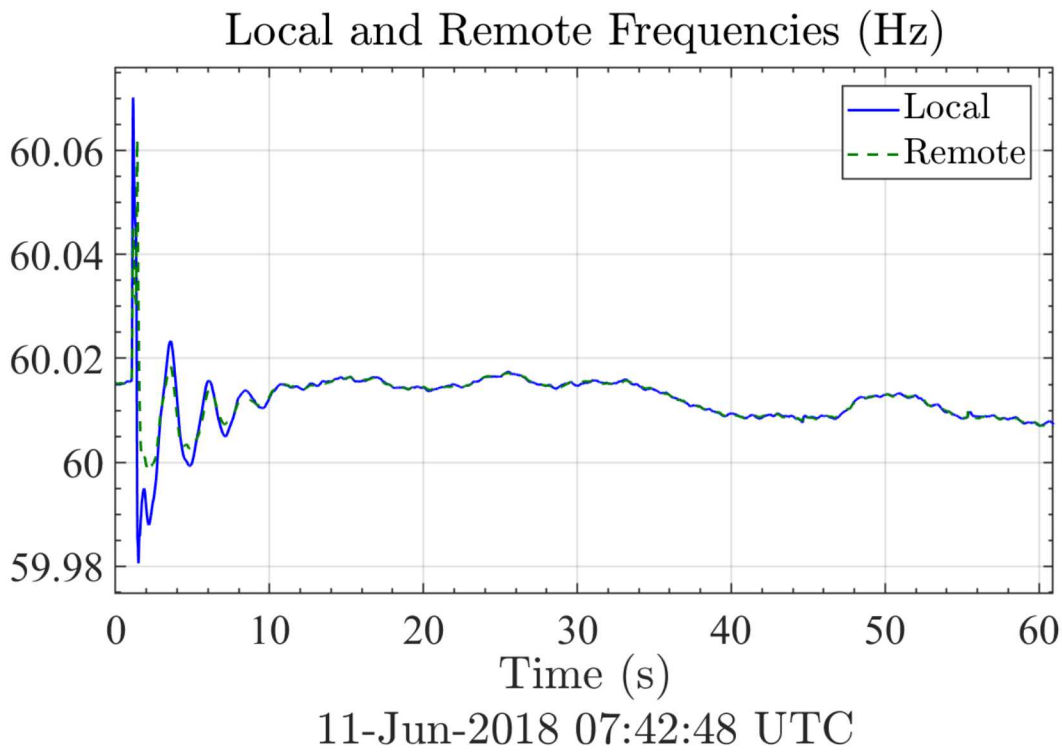

Figure 9-3. Local and remote frequencies during June 11, 2018 event

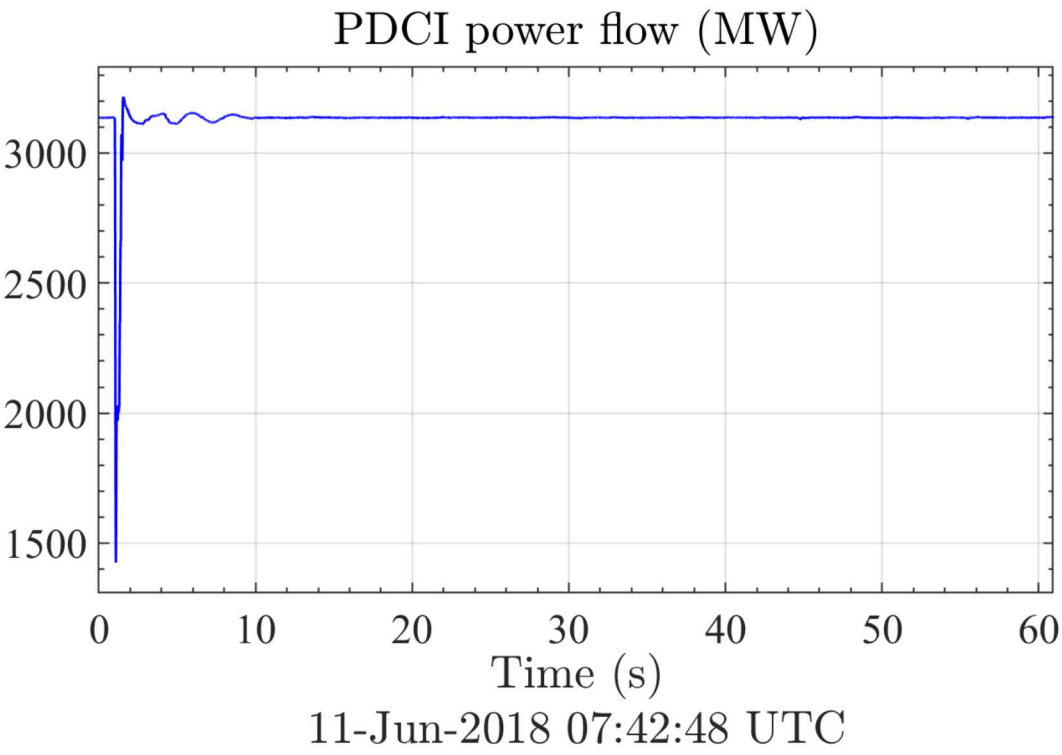

Figure 9-4. PDCI power flow during June 11, 2018 event

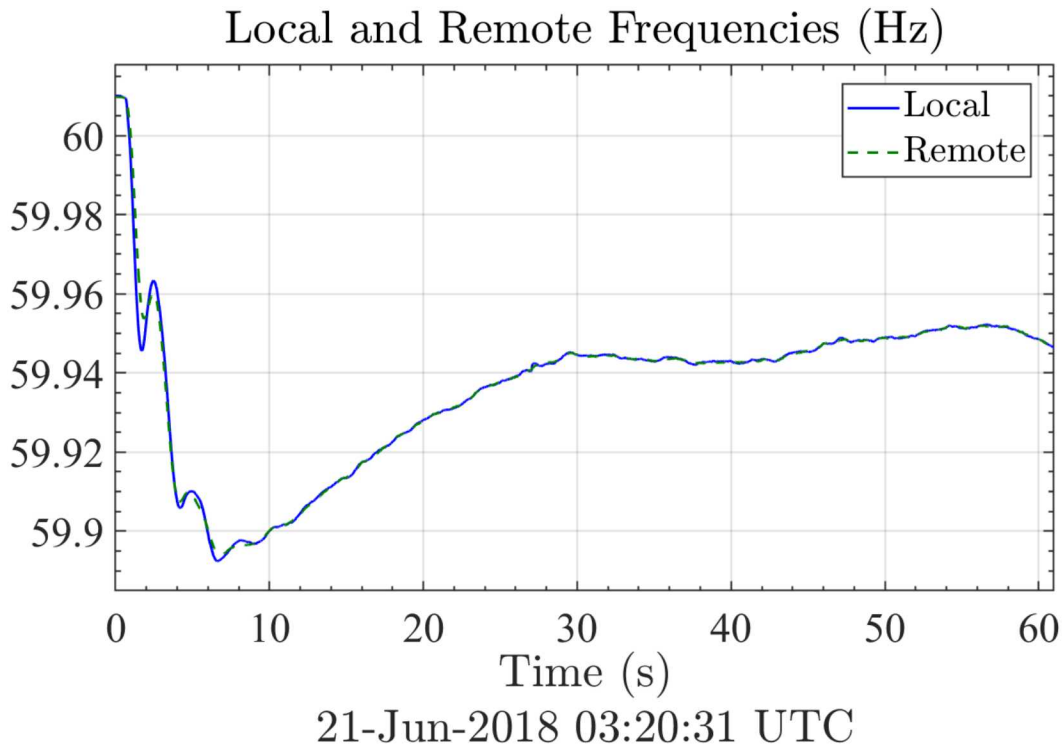

Figure 9-5. Local and remote frequencies during June 21, 2018 event

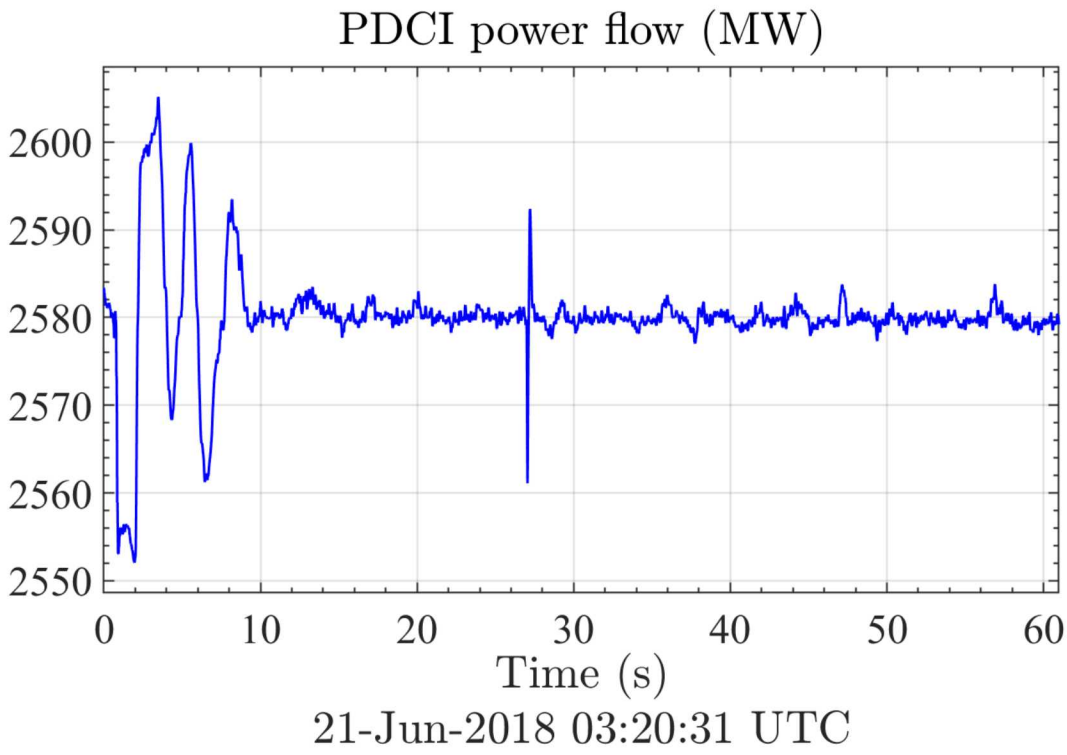

Figure 9-6. PDCI power flow during June 21, 2018 event

9.2. Comparison of DCON Performance to Disconnected State

In this subsection, the DCON performance for the PDCI event on June 11, 2018 is compared to a similar event on May 6, 2018 in which the DCON was not connected to the PDCI. Both of these events involved Pole 3 of the PDCI. This analysis provides some insight as to the improvement the DCON is capable of providing for events that occur on the DC side. Figures 9-7 and 9-8 depict the PDCI power flow for both dates (minus the steady state scheduled power flow in order to avoid graph scaling issues) over a 12-second period during the events. Figure 9-8 zooms in on the y-axis to provide better resolution of the power flow. Figure 9-9 shows the DCON power command during the event. The power command signal for the May 6 event was zero since the DCON was not connected to the PDCI at that time. Figure 9-10 depicts the frequency error between the John Day and Malin PMU sites. Figure 9-9 shows the DCON response to the power flow drop in the PDCI and the subsequent recovery. The DCON power command is exactly as it should be considering the frequency error in Figure 9-10. The damping improvement is not especially dramatic, however, the control authority of the DCON was limited to +/- 25 MW during the unattended test compared to +/- 125 MW control authority for single day tests. The important takeaway is that the DCON responded appropriately during this event.

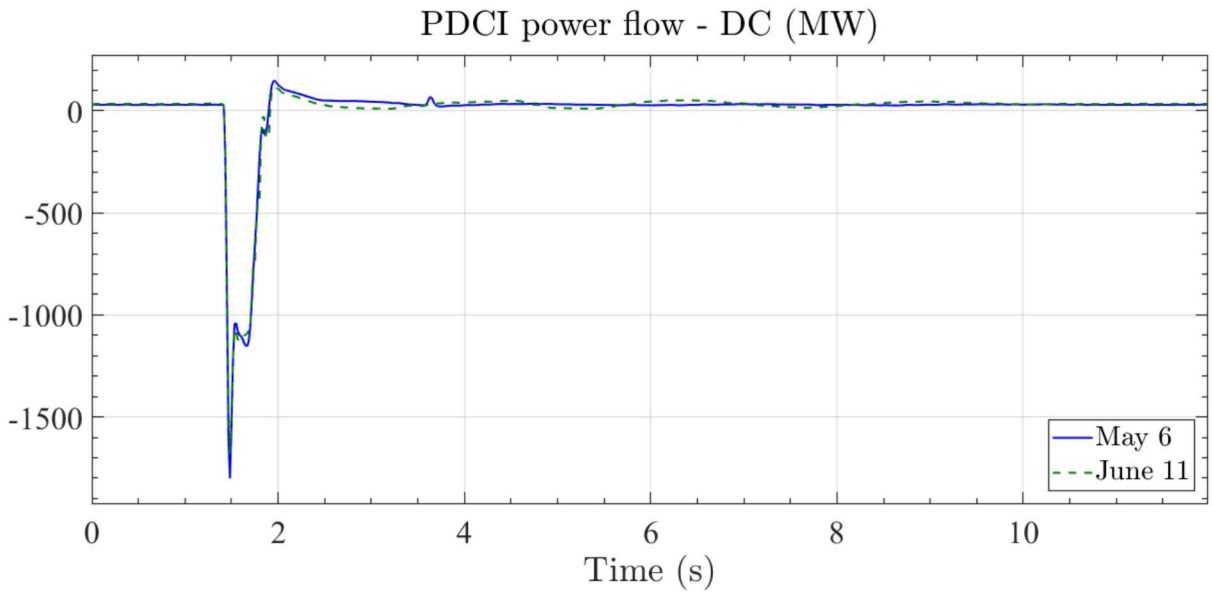

Figure 9-7. PDCI power flow minus the scheduled steady state power flow

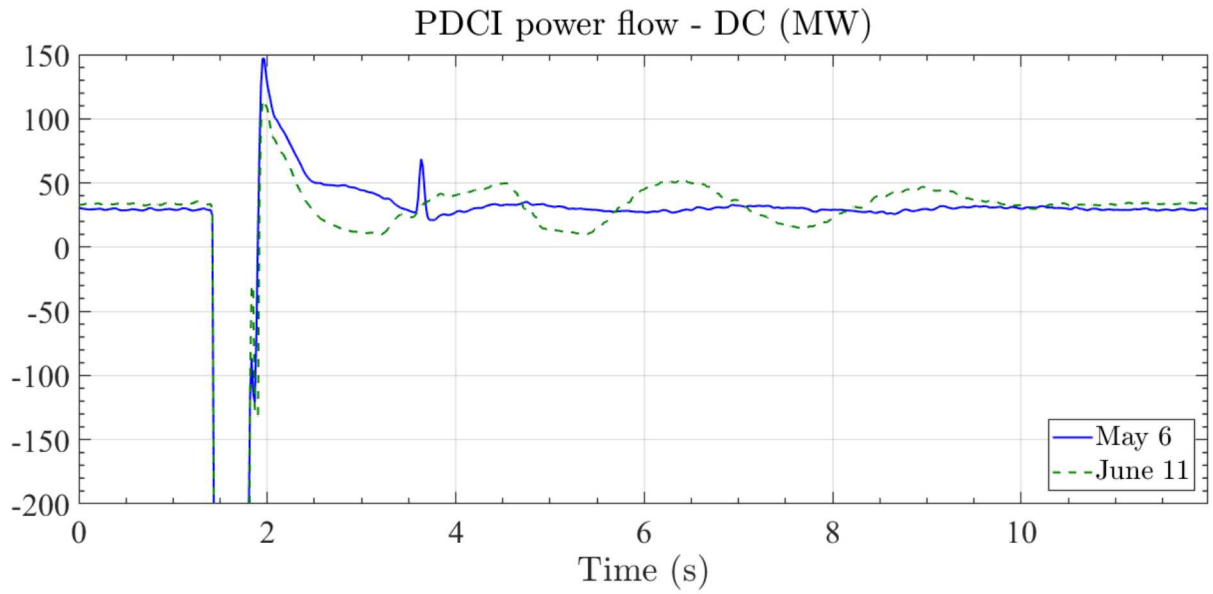

Figure 9-8. PDCI power flow with zoomed-in y-axis

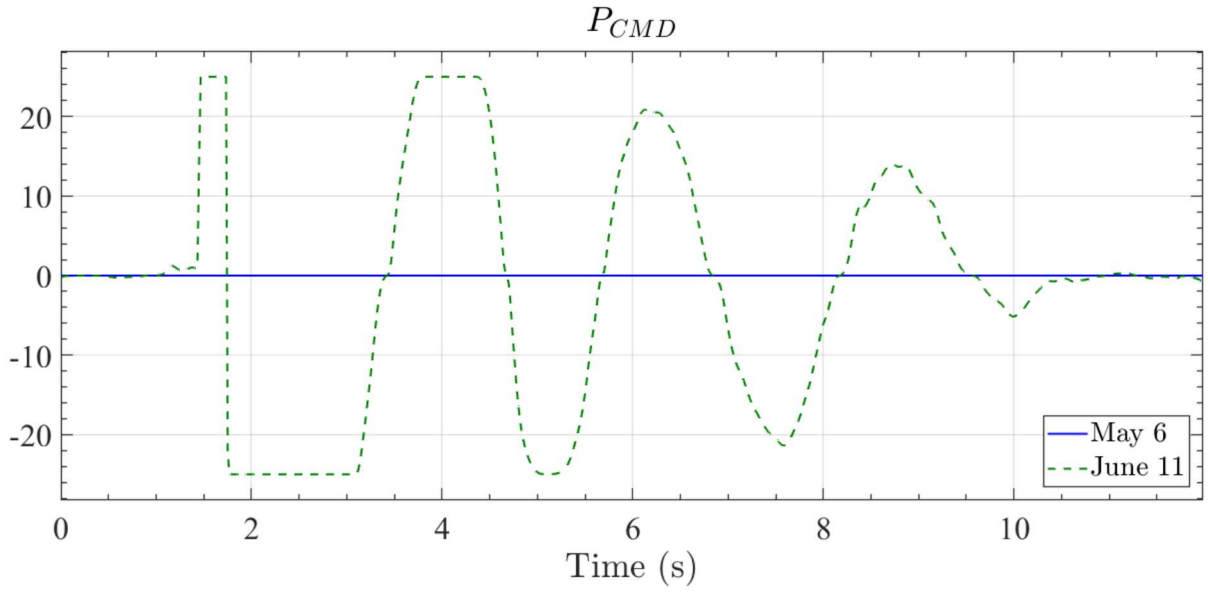

Figure 9-9. DCON power command signal

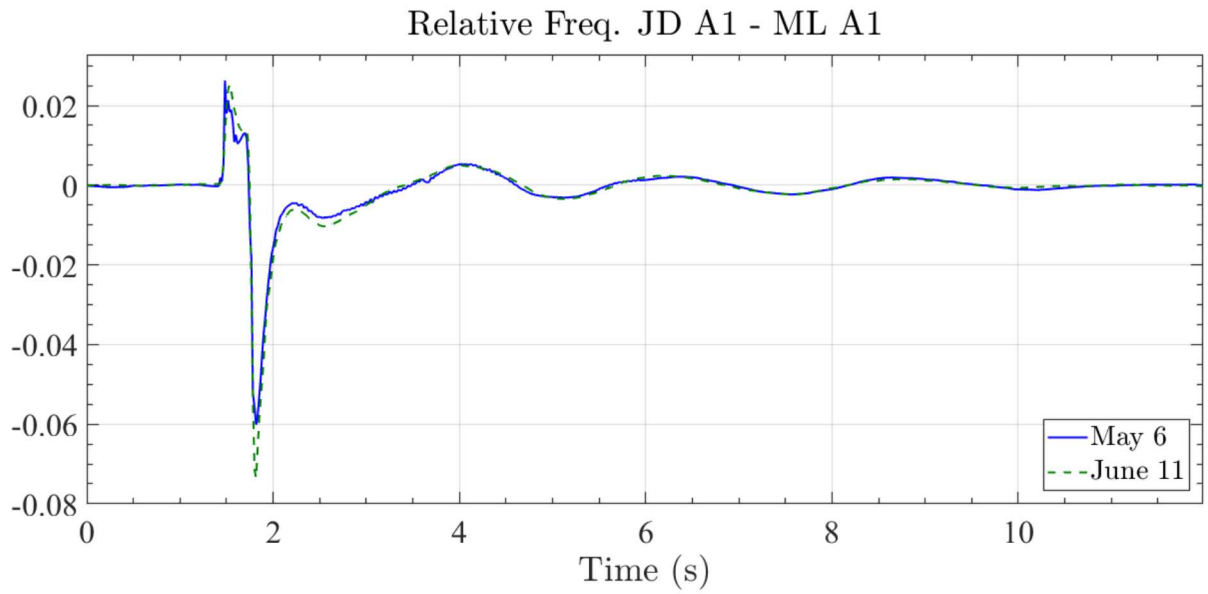

Figure 9-10. Relative frequency error for John Day and Malin PMU sites

9.3. Additional DCON Performance Details for a Specific Event

The plots in Figures 9-11 thru 9-15 provide more detail on DCON performance for a PDCI event that occurred on June 21, 2018. These plots depict the PDCI power flow (Figure 9-11), the local and remote frequencies (Figure 9-12), the local and remote voltage magnitudes (Figures 9-13 and 9-14), and the DCON power command (Figure 9-15) for a 6 second period during the event. The DCON power command signal in Figure 9-15, though limited to +/- 25 MW, does respond appropriately to the event. The control action improves damping as can be seen in Figure 9-12, in which the frequency excursion is significantly reduced in a couple seconds.

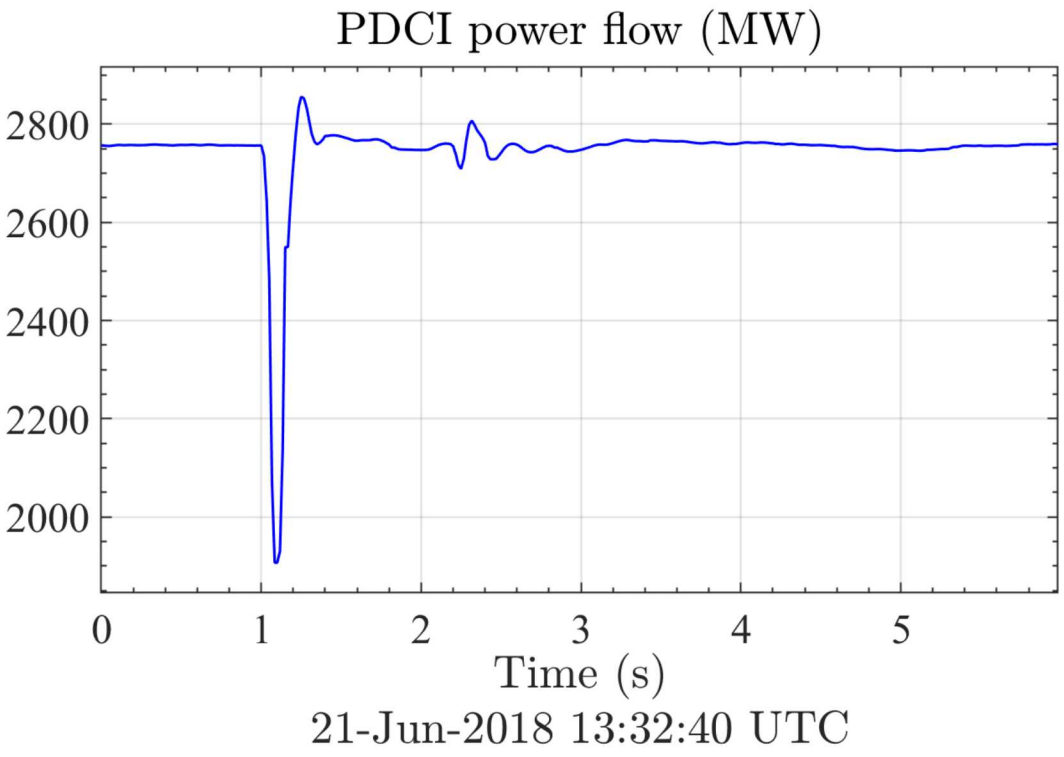

Figure 9-11. PDCI power flow during June 21, 2018 event

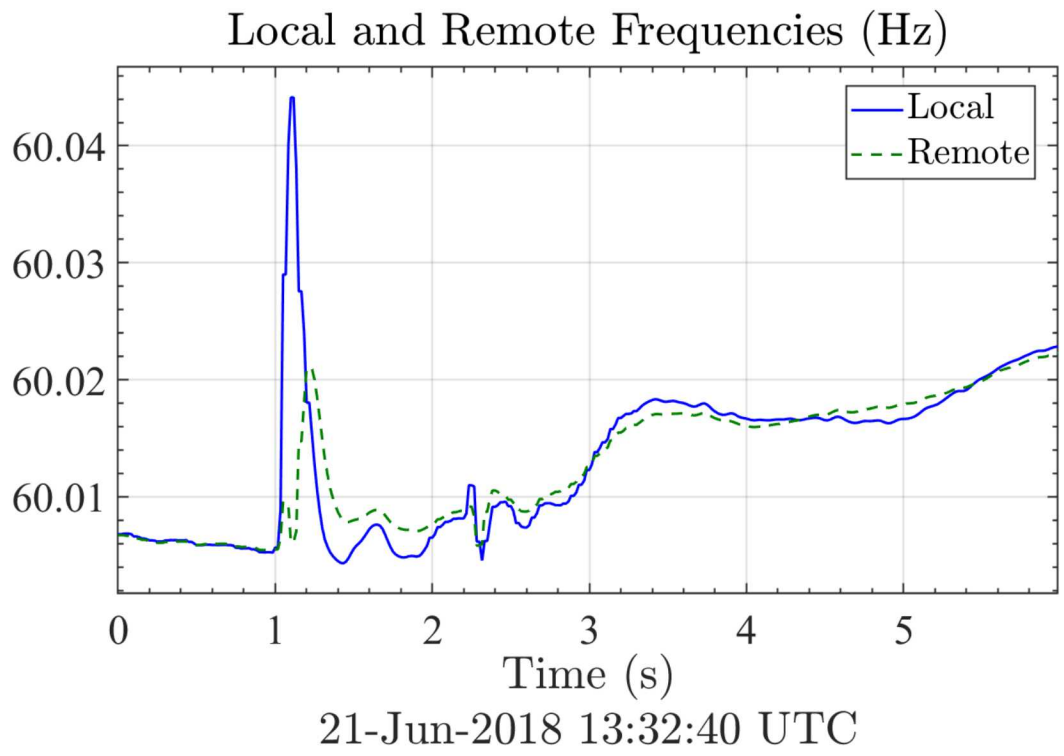

Figure 9-12. Local and remote frequencies during June 21, 2018 event

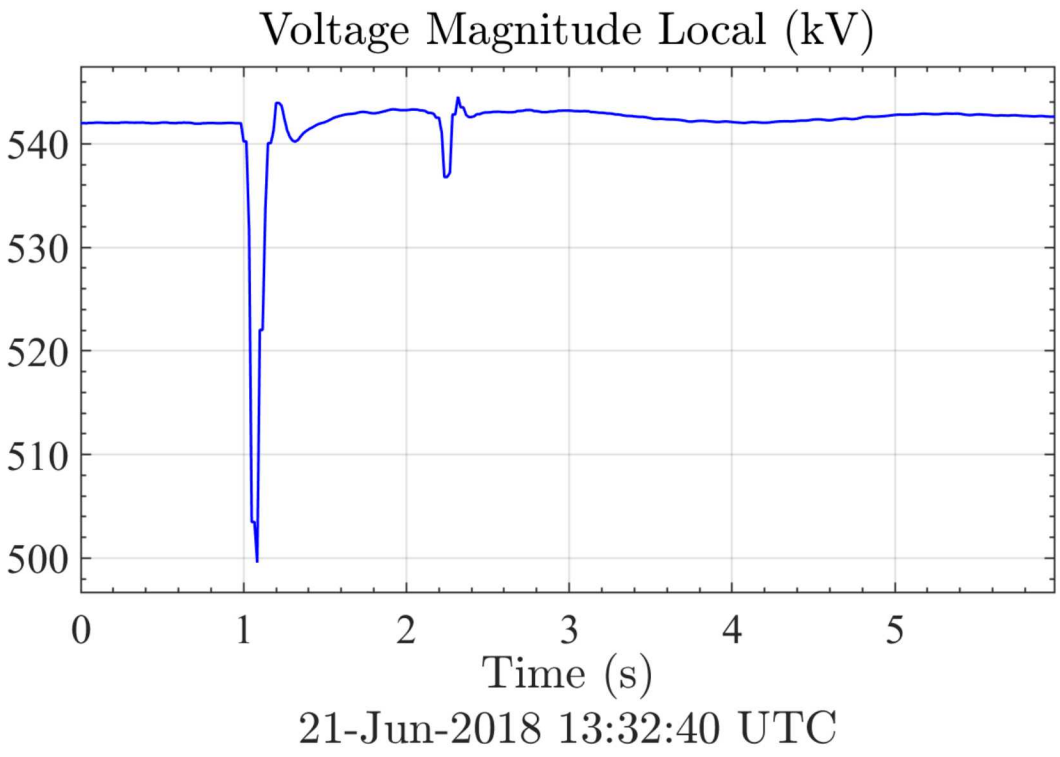

Figure 9-13. Local voltage magnitude during June 21, 2018 event

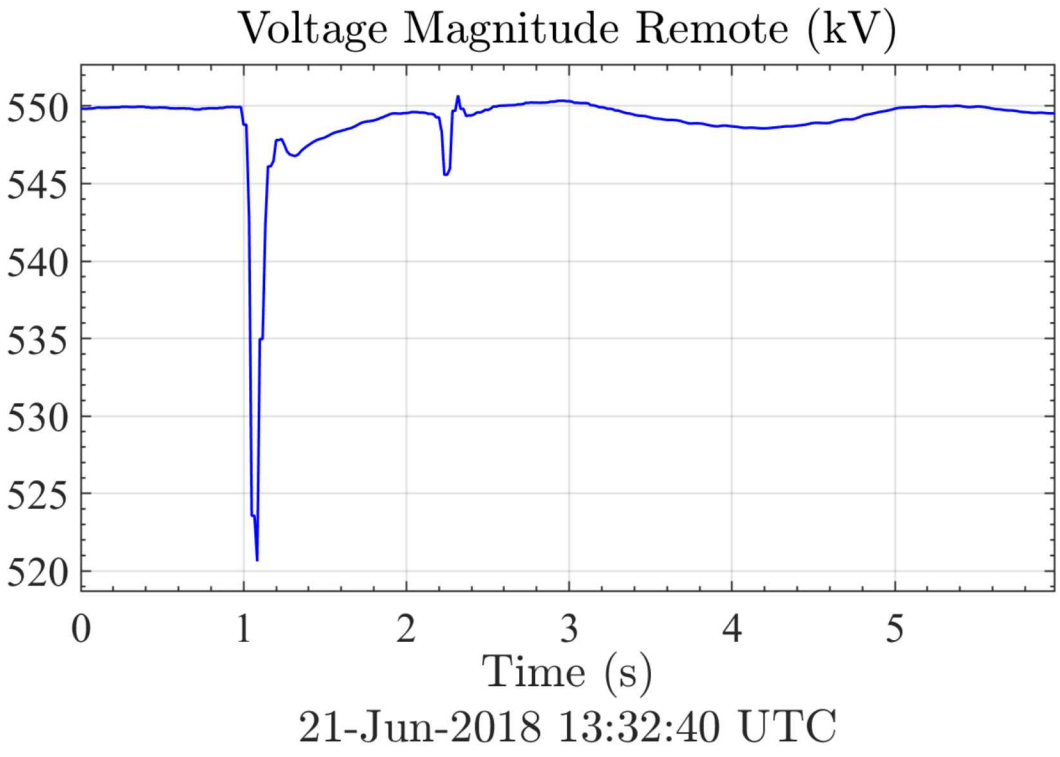

Figure 9-14. Remote voltage magnitude during June 21, 2018 event

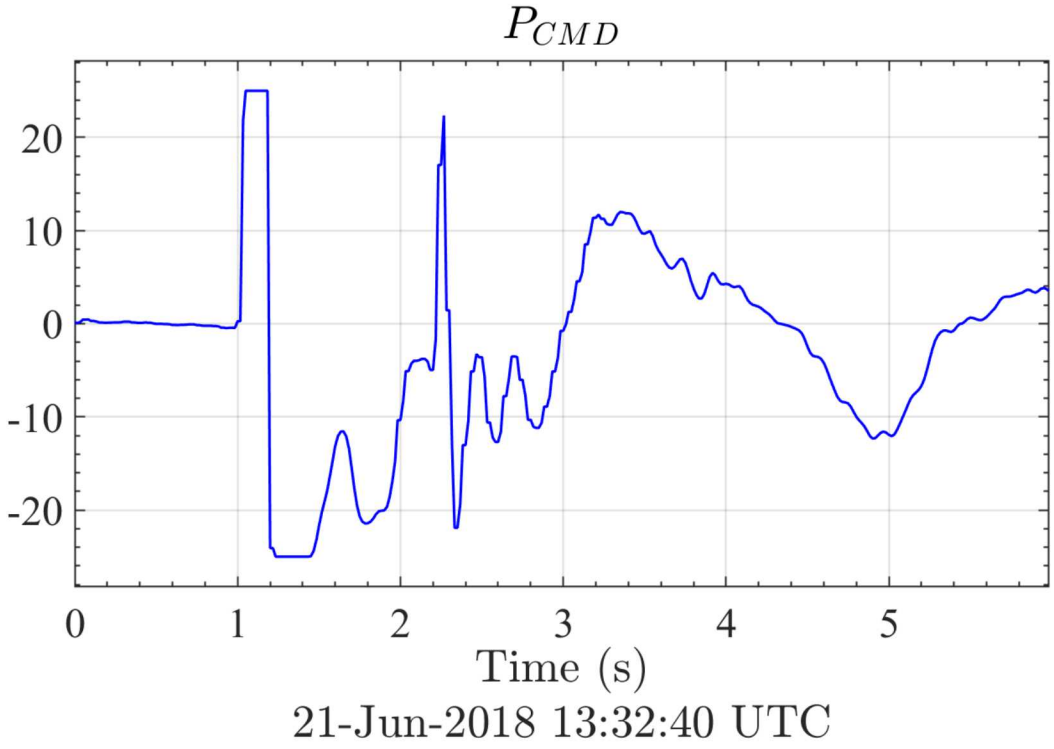

Figure 9-15. DCON power command signal during June 21, 2018 event

This page left blank

10. CONCLUSIONS

In addition to providing a project summary and bibliography, this report describes results from a series of three tests conducted in 2016, 2017, and 2018. This includes extensive closed-loop tests. These tests included inducing transients into the WI and observing the performance of the damping controller over many days of operation. Key conclusions include:

- The PDCI system is an excellent actuator for damping the wide-spread and most critical NSB mode. The PDCI response time is more than fast enough for damping any mode below one Hz. The system also has excellent noise rejection properties. The system showed excellent consistency, repeatability, and linearity for the many tests conducted over the three years of testing.
- The DCON control strategy has excellent robustness properties. For the nearly 100 open-loop measurements conducted over the past several years, all demonstrated that the controller would add damping to any mode in the 0.1 to 1 Hz range. The controllability is especially strong for the NSB mode while the impact on other known modes is minimal. This robustness maintains in the critical condition of when Alberta disconnects from the system which tends to decrease the damping on the NSB mode.
- The maximum prudent gain for the controller is K_0 = 14 MW/mHz (the gain for John Day PMU as the local signal). If the gain exceeds 14 MW/mHz, the gain margin could degrade below 6 dB and results in the DC system response being overly underdamped with a natural frequency near 4 Hz. Reliable performance is achieved with a gain in the 9 to 12 MW/mHz and represents the recommended range. The DCON automatically halves the gain for the Big Eddy PMU local signals to be half that of the John Day signals to preserve this gain margin. The result is less added damping performance. Therefore, John Day is the preferred local PMU.
- The DCON reduces the impact of forced oscillations for all cases except when the forced oscillation is in the 3 to 5 Hz range. In this case, the DCON could slightly amplify the oscillation over the open-loop condition. But, this is likely of little concern because the overall system has very low gain in this higher frequency range. That is, forced oscillations above 1 Hz do not emit very far from their source as the overall system gain is much lower.
- A key step in the testing process of the DCON was to configure the DCON to operate in an unattended mode (24/7 operation). This was done in order to capture DCON performance during a wider range of typical events on the WI than would otherwise be possible in a single day of testing. Further, successful unattended operation over a longer stretch of time (e.g., 4 weeks) would provide additional confidence that the DCON is safe and reliable for potential permanent operational status in the future. The unattended test was conducted for 4 weeks from May 24, 2018 until June 21, 2018 in which there were no DCON project team members present at the Celilo converter station. For this test, the DCON was limited to a control authority of +/- 25 MW instead of the +/- 125 MW limits for the single day attended tests. Though these lower limits reduced the ability of the DCON to significantly improve damping, it was clear upon subsequent analysis of test results that the DCON performed exactly as it was designed to with no harmful side effects. Additional analysis proved insightful to the potential improvement the DCON is capable of providing for events that occur on the DC side, which was observed during the unattended test.

REFERENCES

[1] Kosterev, D.N., Taylor, C.W., and Mittelstadt, W.A., "Model validation for the August 10, 1996 WSCC system outage," *IEEE Trans. Power Syst.*, vol. 14, pp. 967–979, 1999.

[2] Cresap, R.L., Mittelstadt, W.A., Scott, D.N., and Taylor, C.W., "Operating experience with modulation of the Pacific HVDC Intertie," *IEEE Trans. Power Apparatus and Syst.*, vol. 97, no. 4, pp. 1053-1059, 1978.

[3] Trudnowski, D.J., Kosterev, D.N., and Undrill, J., "PDCI damping control analysis for the western North American Power System," *2013 IEEE Power and Energy Soc. General Meeting.* IEEE, Vancouver, BC, Canada, July 2013.

[4] D. Trudnowski, D. Kosterev, and J. Wold, "Open-loop PDCI probing tests for the wester north American power system," IEEE PES General Meeting, July 2014.

[5] D. Trudnowski, "2014 Probing Test Analysis," TIP 289 project report to BPA, Jan. 2014.

[6] D. J. Trudnowski, B. J. Pierre, F. Wilches-Bernal, D. A. Schoenwald, R. T. Elliott, J. C. Neely, R. H. Byrne, and D. N. Kosterev, "Initial Closed-Loop Testing Results for the Pacific DC Intertie Wide Area Damping Controller," IEEE Power & Energy Society General Meeting, Chicago, IL, July 16-20, 2017.

[7] JSIS Modal paper.

[8] K. Wingert, "BPA puts modernized Celilo Converter Station into service," BPA News Release, PR 03-16, Jan. 2016.

[9] J. Bendat and A. Piersol, Engineering Applications of Correlation and Spectral Analysis, 2nd Ed., John Wiley & Sons, Inc., 1993.

[10] B. J. Pierre, R. T. Elliott, D. A. Schoenwald, J. C. Neely, R. H. Byrne, D. J. Trudnowski, and J. Colwell, "Supervisory System for a Wide Area Damping Controller Using PDCI Modulation and Real-Time PMU Feedback," IEEE Power & Energy Society General Meeting, Boston, MA, July 17-21, 2016.

[11] D. A. Copp, F. Wilches-Bernal, D. A. Schoenwald, and I. Gyuk, "Power System Damping Control via Power Injections from Distributed Energy Storage," SPEEDAM 2018, Amalfi Coast, Italy, June 20-22, 2018.

[12] B. J. Pierre, F. Wilches-Bernal, D. A. Schoenwald, R. T. Elliott, R. H. Byrne, J. C. Neely, and D. J. Trudnowski, "The Pacific DC Intertie Wide Area Damping Controller Utilizing Real-Time PMU Feedback," North American Synchrophasor Initiative (NASPI) Spring Meeting, Albuquerque, NM, April 24-26, 2018.

[13] F. Wilches-Bernal, D. Schoenwald, R. Fan, M. Elizondo, and H. Kirkham, "Analysis of the Effect of Communication Latencies on HVDC-Based Damping Control," 2018 IEEE PES T&D Conference & Exposition, Denver, CO, April 16-19, 2018.

[14] D. A. Copp, F. Wilches-Bernal, I. Gravagne, and D. A. Schoenwald, "Time Domain Analysis of Power System Stability with Damping Control and Asymmetric Feedback Delays," 2017 North American Power Symposium, Morgantown, WV, September 2017.

[15] D. A. Schoenwald, "Active Damping of Inter-Area Oscillations in the Western Interconnection: Recent Developments," *IEEE Smart Grid Newsletter*, http://smartgrid.ieee.org/newsletters/july-2017, July 2017.

[16] F. Wilches-Bernal, R. Concepcion, J. C. Neely, D. A. Schoenwald, R. H. Byrne, B. J. Pierre, and R. T. Elliott, "Effect of Time Delay Asymmetries in Power System Damping Control," IEEE Power & Energy Soc. General Meeting, Chicago, IL, July 16-20, 2017.

[17] F. Wilches-Bernal, B. J. Pierre, R. T. Elliott, D. A. Schoenwald, R. H. Byrne, J. C. Neely, and D. J. Trudnowski, "Time Delay Definitions and Characterizations in the Pacific DC Intertie Wide Area Damping Controller," IEEE Power & Energy Society General Meeting, Chicago, IL, July 16-20, 2017.

[18] B. J. Pierre, F. Wilches-Bernal, R. T. Elliott, D. A. Schoenwald, J. C. Neely, R. H. Byrne, and D. J. Trudnowski, "Simulation Results for the Pacific DC Intertie Wide Area Damping Controller," IEEE Power & Energy Society General Meeting, Chicago, IL, July 16-20, 2017.

[19] D. A. Schoenwald, B. J. Pierre, F. Wilches-Bernal, and D. J. Trudnowski, "Design and Implementation of a Wide-Area Damping Controller Using High Voltage DC Modulation and Synchrophasor Feedback," IFAC World Congress, Toulouse, France, July 9-14, 2017.

[20] B. Pierre, F. Wilches-Bernal, D. Schoenwald, R. Elliott, J. Neely, R. Byrne, "Open-Loop Testing Results for the Pacific DC Intertie Wide Area Damping Controller," 12th IEEE Power & Energy Society PowerTech Conference, Manchester, UK, June 18 – 22, 2017.

[21] R. Byrne, D. Trudnowski, J. Neely, D. Schoenwald, D. Wilson, and L. Rashkin, "Small Signal Stability Analysis and Distributed Control with Communications Uncertainty," SPEEDAM2016, Capri, Italy, June 2016.

[22] J. C. Neely, R. H. Byrne, D. A. Schoenwald, R. T. Elliott, D. J. Trudnowski, and M. K. Donnelly, "Optimal Control of Distributed Networked Energy Storage for Improved Small-Signal Stability," Proceedings of the 2015 Biennial International Conference on Electrical Energy Storage Applications and Technologies (EESAT 2015), San Diego, CA, Sept 2015.

[23] J. C. Neely, J. Johnson, R. H. Byrne, and R. T. Elliott, "Structured Optimization for Parameter Selection of Frequency-Watt Grid Support Functions for Wide-Area Damping," *International J. Distributed Energy Resources and Smart Grids*, pp. 69-94, Vol. 11, No. 1, Jan. 2015.

[24] R. H. Byrne, D. J. Trudnowski, J. C. Neely, R. T. Elliott, D. A. Schoenwald, and M. K. Donnelly, "Optimal Locations for Energy Storage Damping Systems in the Western North American Interconnect,", IEEE Power & Energy Society General Meeting, National Harbor, MD, July 27-31, 2014.

[25] J. C. Neely, R. T. Elliott, R. H. Byrne, D. A. Schoenwald, and D. J. Trudnowski, "The Benefits of Energy Storage Combined with HVDC Transmission Power Modulation for Mitigating Inter-Area Oscillations," Proceedings of the 2013 Biennial International Conference on Electrical Energy Storage Applications and Technologies (EESAT 2013), San Diego, CA, Oct 20-23, 2013.

[26] J. C. Neely, R. H. Byrne, C. A. Silva Monroy, R. T. Elliott, D. A. Schoenwald, D. Trudnowski, and M. Donnelly, "Damping of Inter-Area Oscillations using Energy Storage," IEEE Power & Energy Soc. General Meeting, Vancouver, Canada, July 2013.

[27] Shelton, M.L., Mittelstadt, W.A., Winkelman, P.F., and Bellerby, W.J., "Bonneville Power Administration 1400 MW Braking Resistor," *IEEE Trans. on Power Apparatus and Systems*, vol. 94, no. 2, pp. 602-611, 1975.

[28] Trudnowski, D.J. and Undrill, J., "Modal and Controllability Analysis of the MiniWECC System Model: Year 2 report of BPA contract 37508," Bonneville Power Administration, Portland, OR, USA, 2009.

[29] Pierre, B. J., F. Wilches-Bernal, D. A. Schoenwald, R. T. Elliott, D. J. Trudnowski, R. H. Byrne, and J. C. Neely, "Design of the Pacific DC Intertie Wide Area Damping Controller," *IEEE Trans. on Power Systems*, DOI 10.1109/TPWRS.2019.2903782, 2019.

[30] F. Wilches-Bernal, B. Pierre, R. Elliott, D. Schoenwald, R. Byrne, J. Neely, D. Trudnowski, and M. Donnelly, "PDCI Wide-Area Damping Control: PSLF Simulations of the 2017 Test Plan - Dual Export Case," Sandia National Laboratories Technical Report, SAND2017-6196, Albuquerque, NM, June 2017.

[31] F. Wilches-Bernal, B. Pierre, R. Elliott, D. Schoenwald, R. Byrne, J. Neely, D. Trudnowski, and M. Donnelly, "PDCI Wide-Area Damping Control: PSLF Simulations of the 2017 Test Plan - Heavy Summer Case," Sandia National Laboratories Technical Report, SAND2017-6195, Albuquerque, NM, June 2017.

[32] F. Wilches-Bernal, B. Pierre, R. Elliott, D. Schoenwald, R. Byrne, J. Neely, D. Trudnowski, and M. Donnelly, "PDCI Wide-Area Damping Control: PSLF Simulations of the 2017 Test Plan - Light Summer Case," Sandia National Laboratories Technical Report, SAND2017-6194, Albuquerque, NM, June 2017.

[33] F. Wilches-Bernal, B. Pierre, R. Elliott, D. Schoenwald, R. Byrne, J. Neely, D. Trudnowski, and M. Donnelly, "PDCI Wide-Area Damping Control: PSLF Simulations of the 2016 Open and Closed Loop Test Plan," Sandia National Laboratories Technical Report, SAND2017-2755, Albuquerque, NM, March 2017.

APPENDIX A. OPEN LOOP TRANSFER FUNCTION PLOTS

The following plots are the Open-loop transfer function -ΔPc/ΔPcmd for the 12 feedback pairs in Table 3-1 and K^0 = 9 MW/mHz. It is the same as Figure 6-1 but for all pairs.

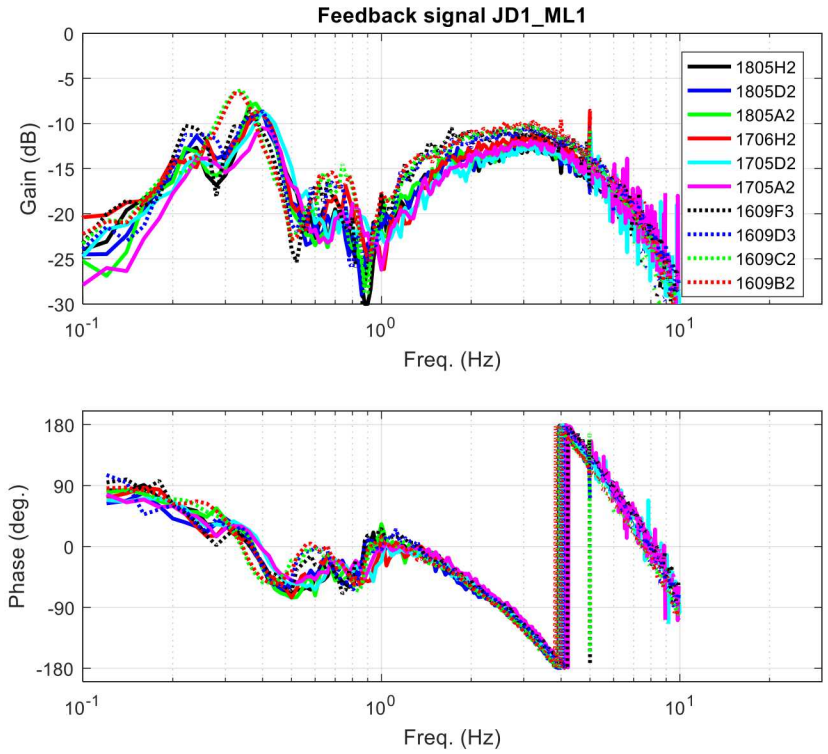

Figure A-1. Open loop transfer function gain and phase plots for feedback signal JD1_ML1.

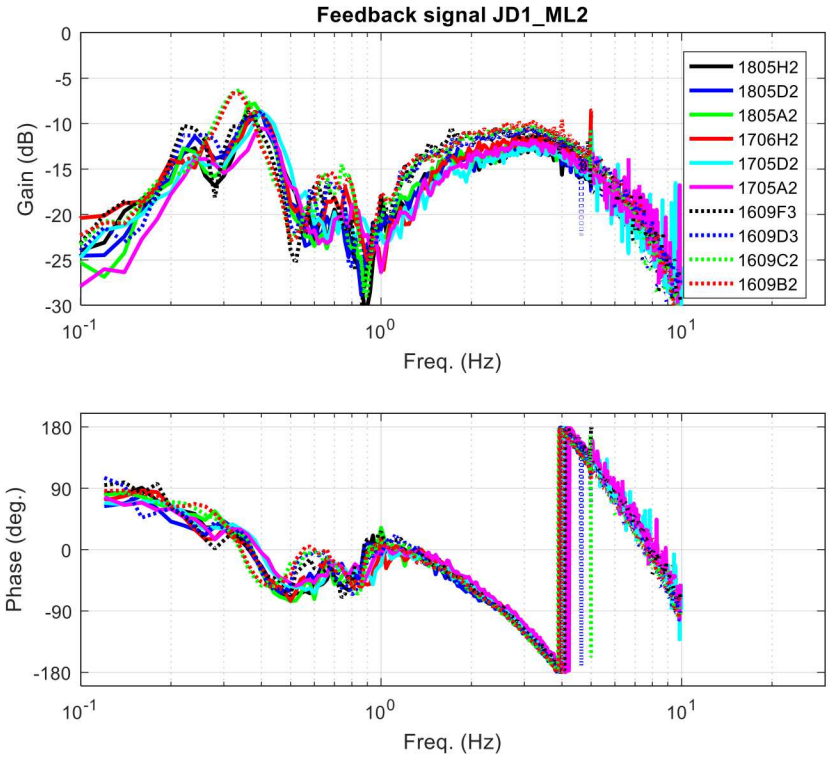

Figure A-2. Open loop transfer function gain and phase plots for feedback signal JD1_ML2.

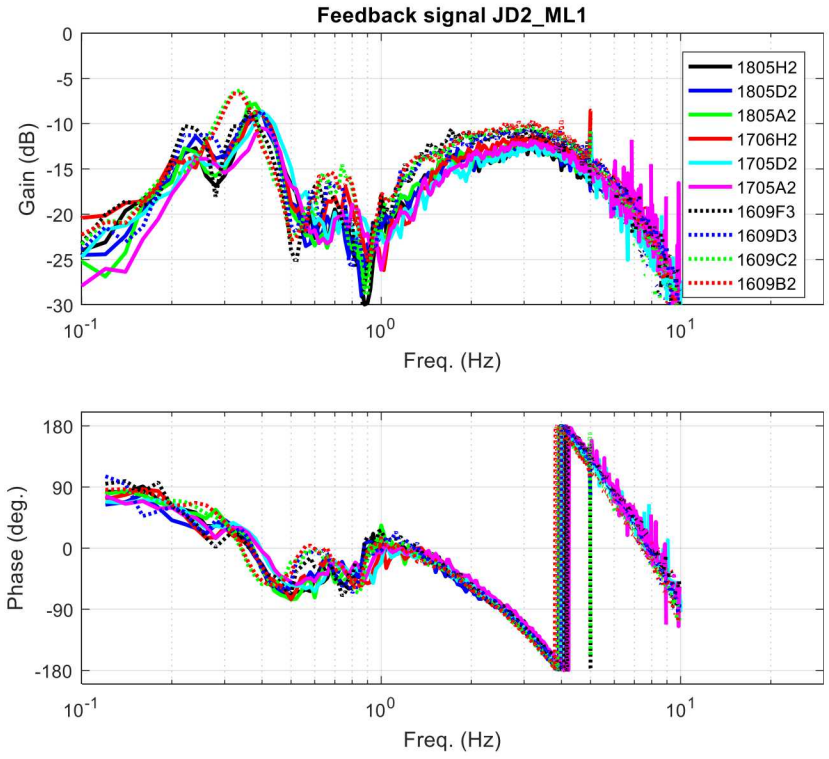

Figure A-3. Open loop transfer function gain and phase plots for feedback signal JD2_ML1.

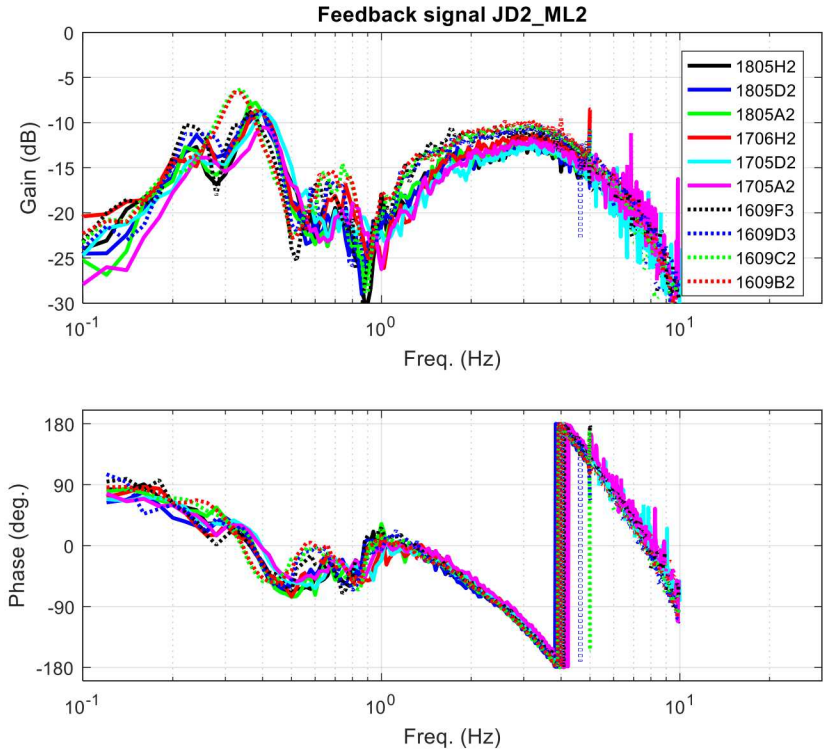

Figure A-4. Open loop transfer function gain and phase plots for feedback signal JD2_ML2.

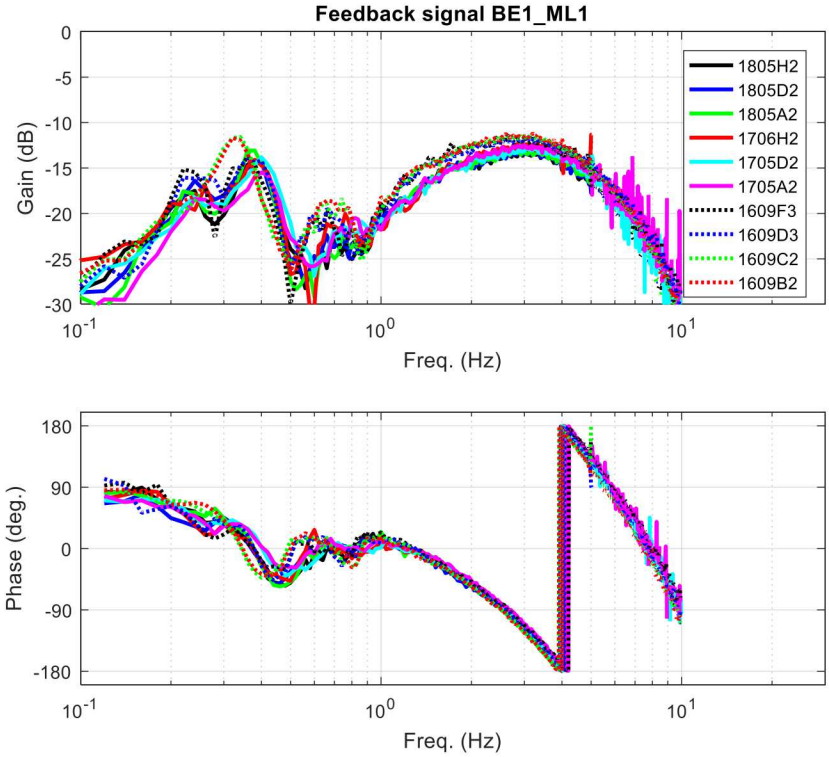

Figure A-5. Open loop transfer function gain and phase plots for feedback signal BE1_ML1.

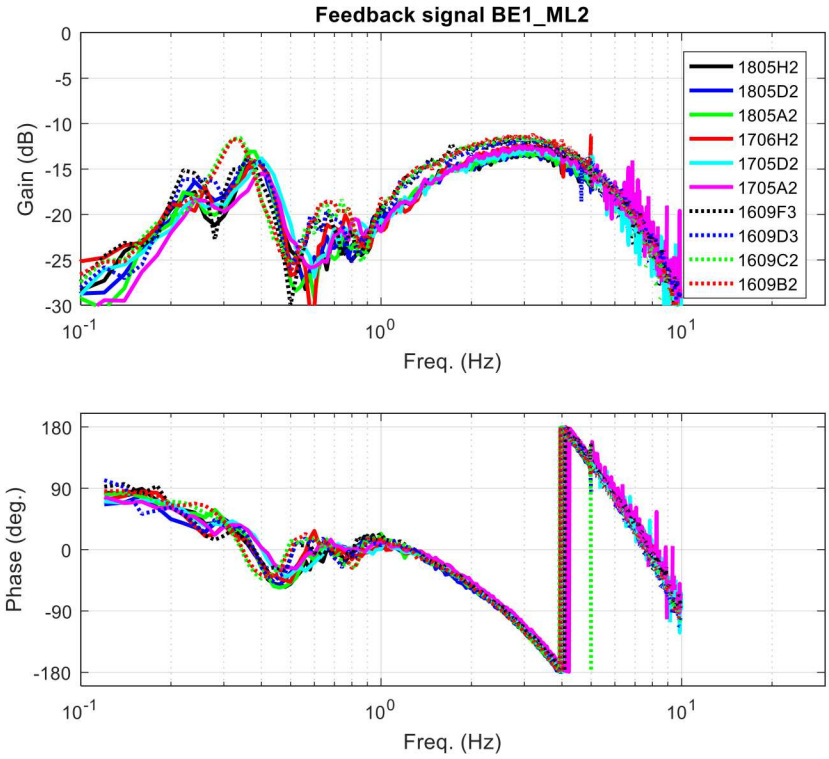

Figure A-6. Open loop transfer function gain and phase plots for feedback signal BE1_ML2.

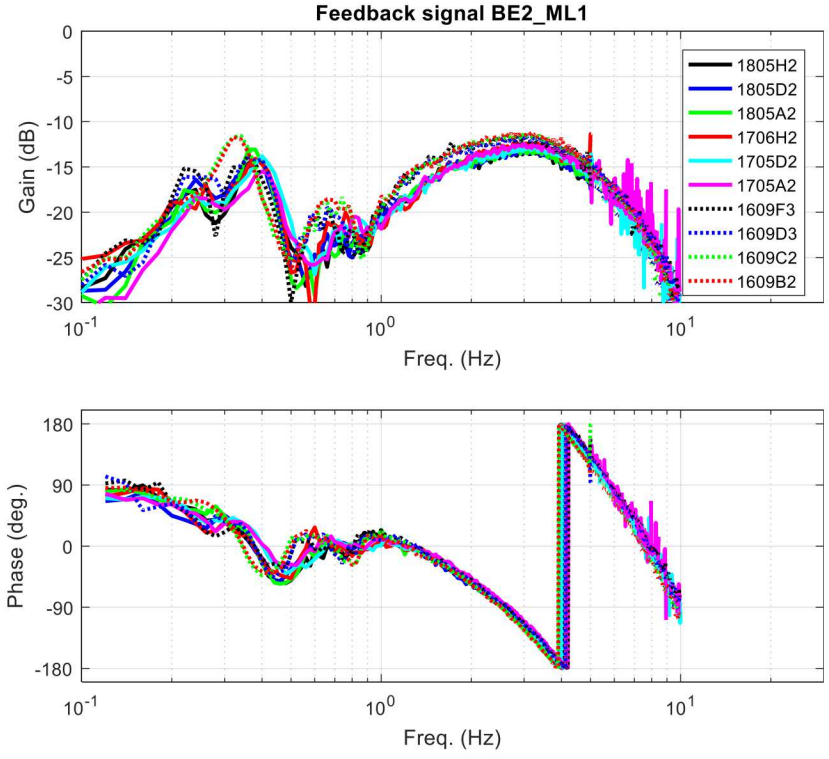

Figure A-7. Open loop transfer function gain and phase plots for feedback signal BE2_ML1.

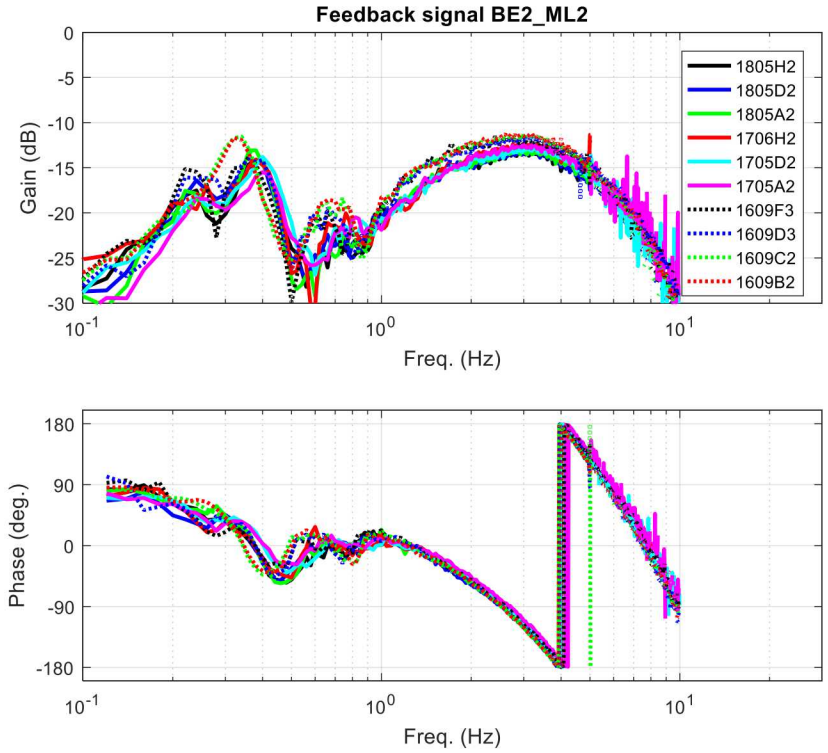

Figure A-8. Open loop transfer function gain and phase plots for feedback signal BE2_ML2.

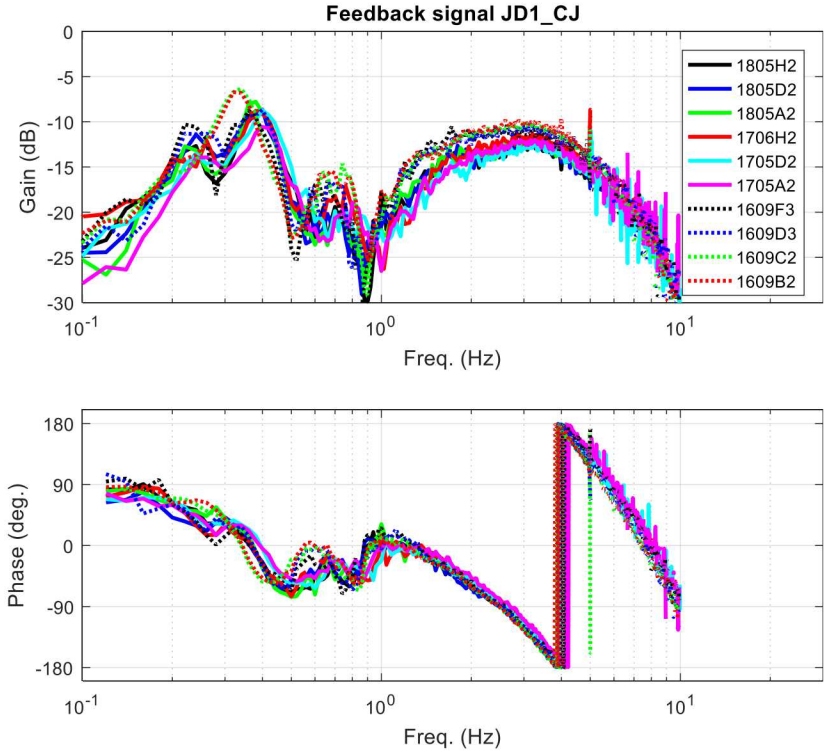

Figure A-9. Open loop transfer function gain and phase plots for feedback signal JD1_CJ.

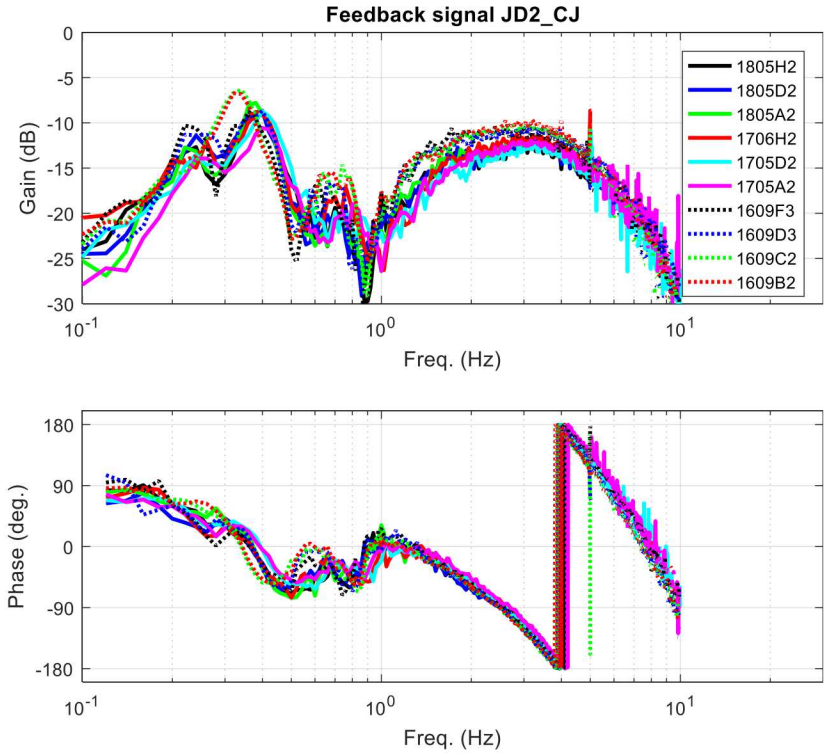

Figure A-10. Open loop transfer function gain and phase plots for feedback signal JD2_CJ.

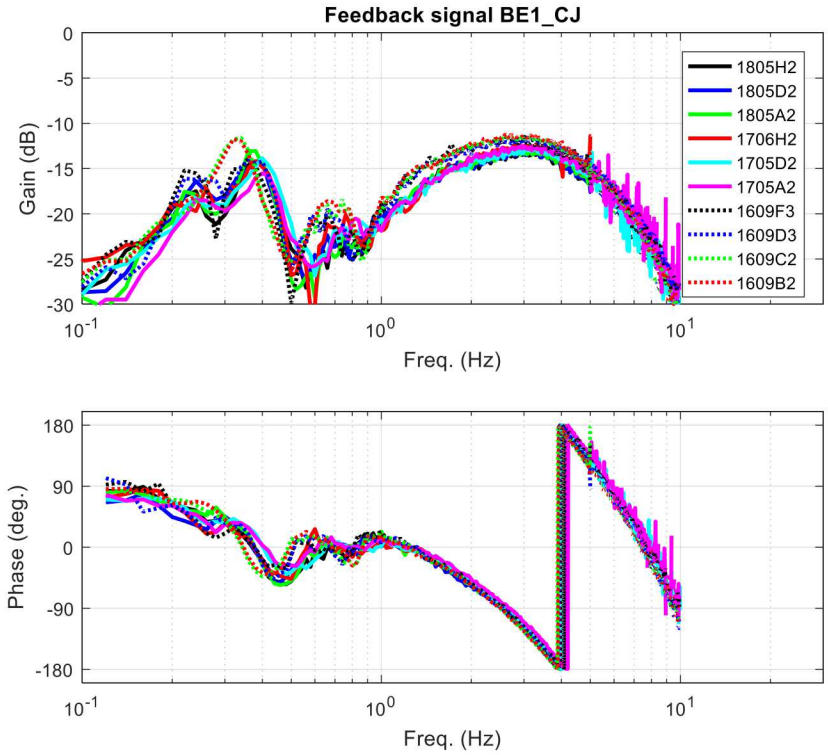

Figure A-11. Open loop transfer function gain and phase plots for feedback signal BE1_CJ.

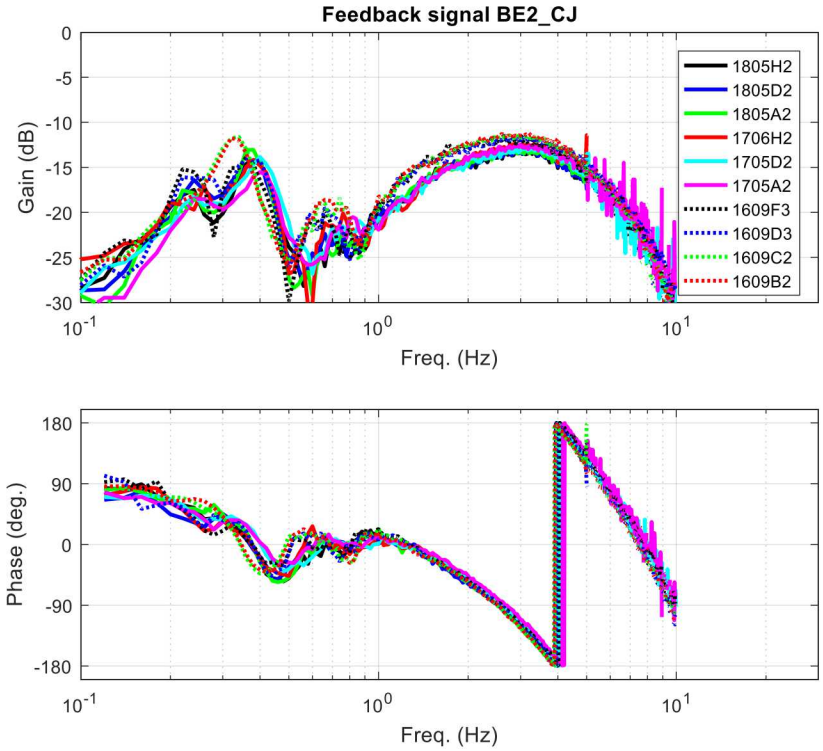

Figure A-12. Open loop transfer function gain and phase plots for feedback signal BE2_CJ.

This page left blank

APPENDIX B. SQUARE-WAVE PULSING RESPONSES

The following plots are the NSB signature signal (John Day - Malin freq error) response to the square-wave pulse (Figure 4-2) at ΔP_{to}; open-loop versus closed-loop responses for several gain values. These plots are the same as Figure 7-4 but for several other gain values.

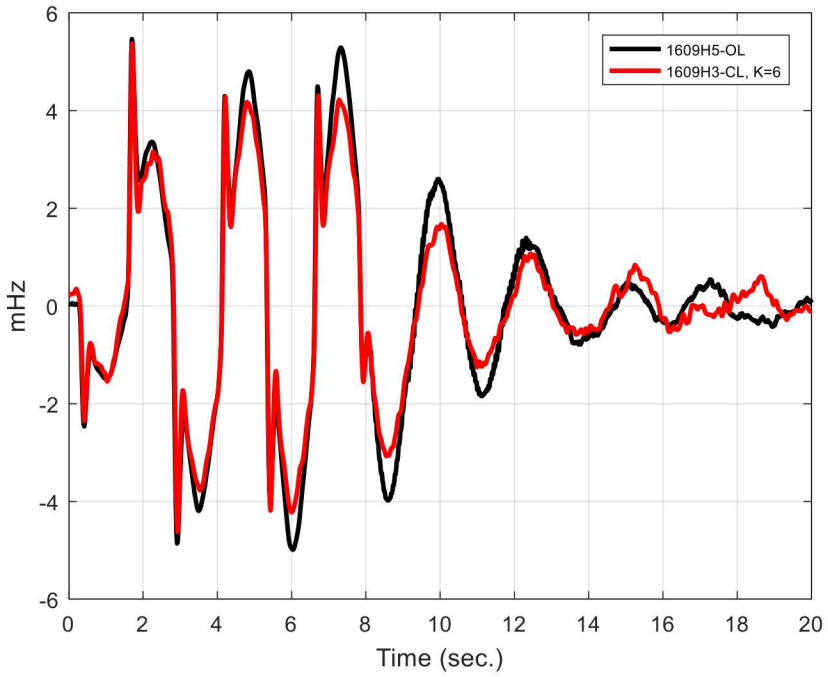

Figure B-1. NSB signature signal response (JD1_ML1 signal) to square-wave pulse for $K_0 = 6$.

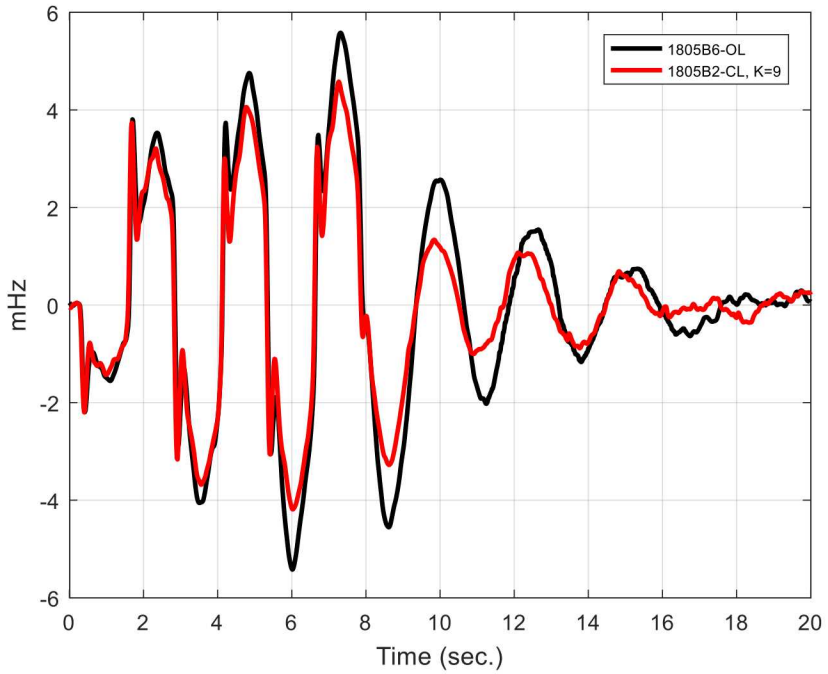

Figure B-2. NSB signature signal response (JD1_ML1 signal) to square-wave pulse for $K_0 = 9$.

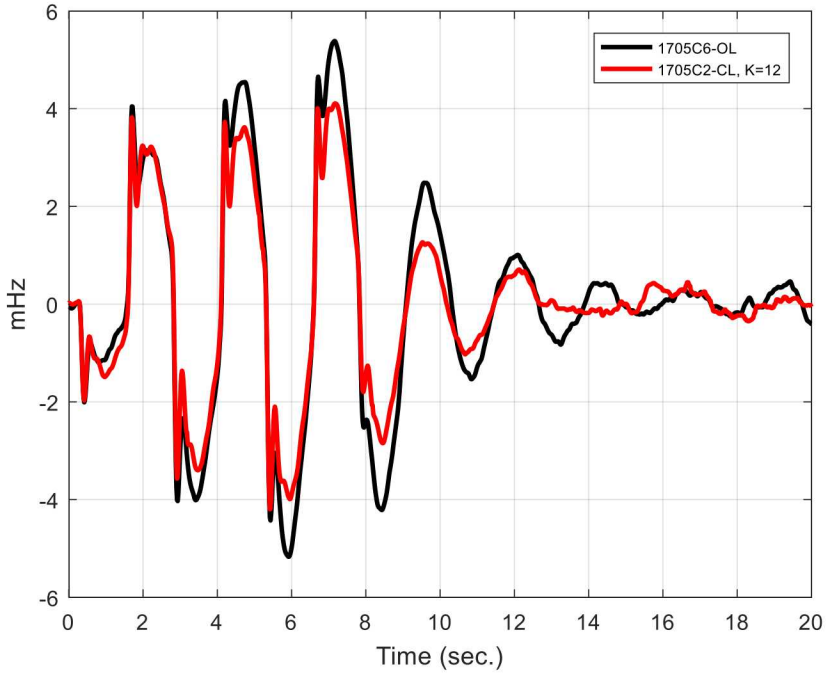

Figure B-3. NSB signature signal response (JD1_ML1 signal) to square-wave pulse for K_0 = 12.

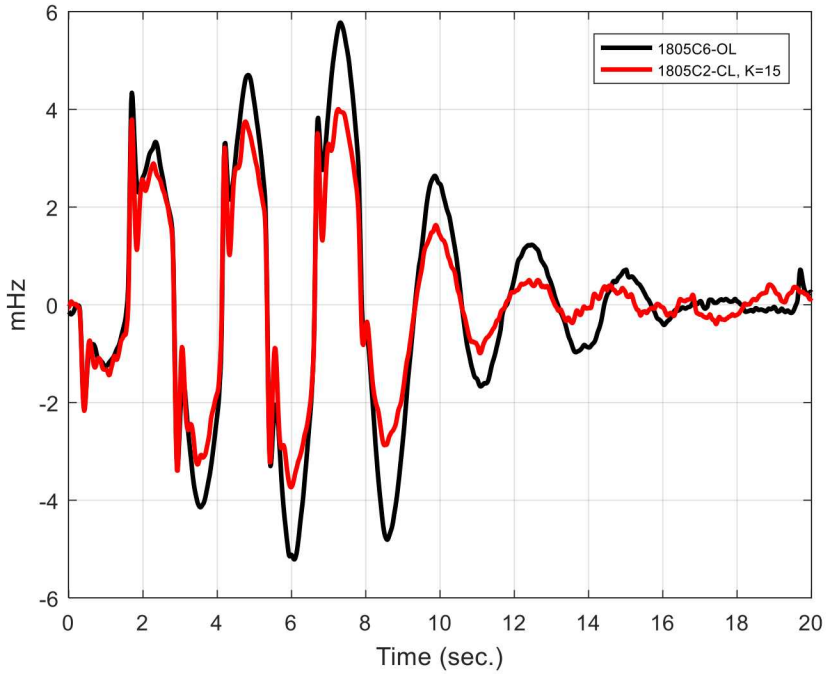

Figure B-4. NSB signature signal response (JD1_ML1 signal) to square-wave pulse for K_0 = 15.

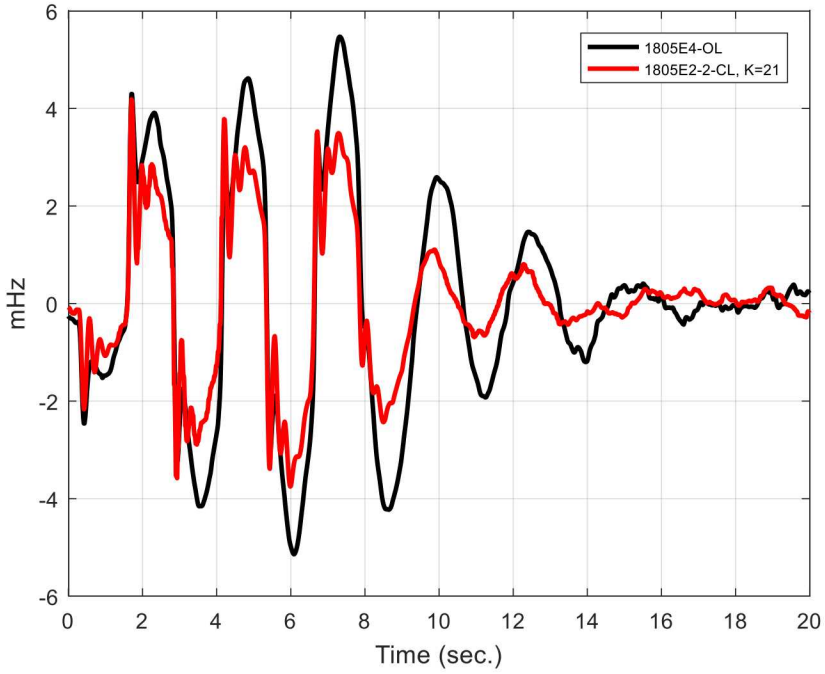

Figure B-4. NSB signature signal response (JD1_ML1 signal) to square-wave pulse for K_0 = 15.

This page left blank

APPENDIX C. FORCED OSCILLATION PLOTS

C.1. 0.4 Hz

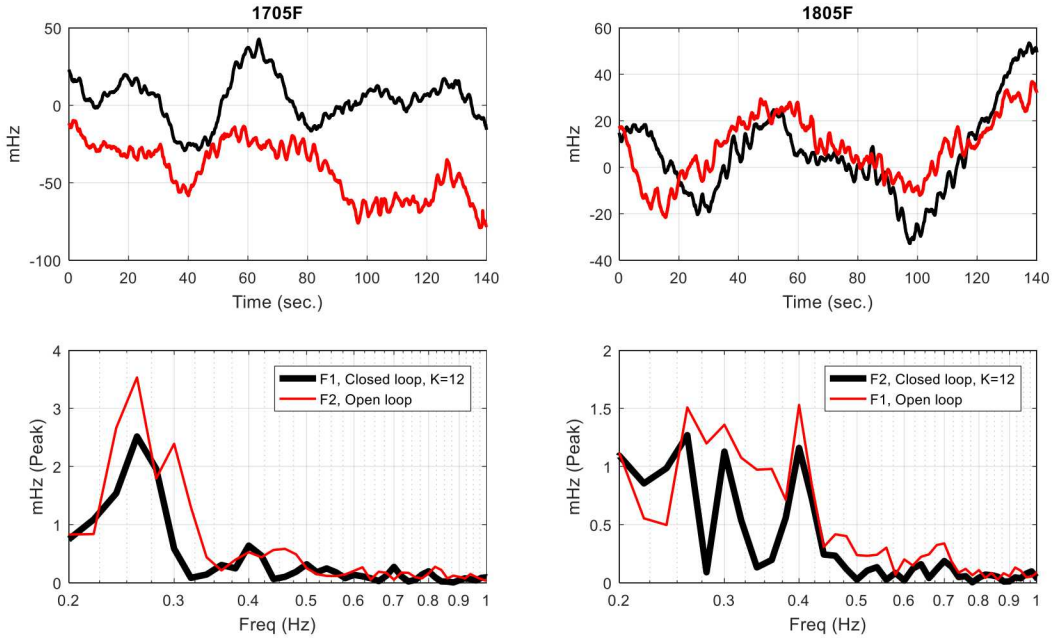

Figure C-1. NSA signature (Sundance - Grand Coulee freq error) to 0.4-Hz FO at P_{po} in Fig. 3-1 (Top row shows the time-domain response with the FO starting at the 30 sec. point and ending at the 110 sec. point. Bottom row shows the spectrum of time-domain response over a 60 sec. span of the FO. Open-loop response is shown in red, closed-loop response is shown in black. Left column is from test series 1705F1 & 1705F2. Right column is from test series 1805F1 & 1805F2.)

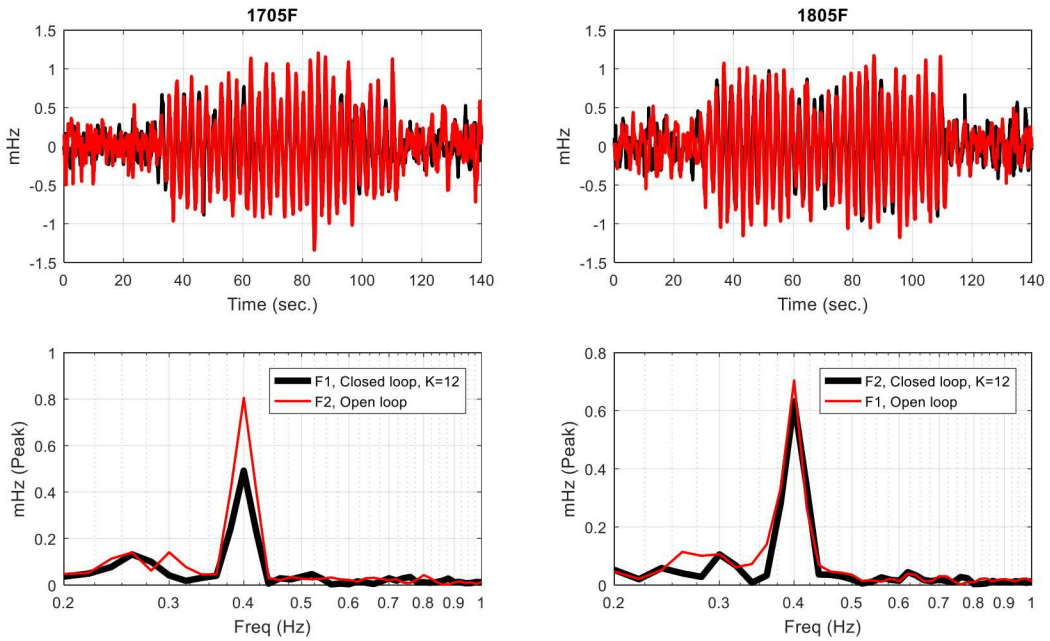

Figure C-2. NSB signature (John Day - Malin freq error) to 0.4-Hz FO at P_{po} in Fig. 3-1 (Top row shows the time-domain response with the FO starting at the 30 sec. point and ending at the 110 sec. point. Bottom row shows the spectrum of time-domain response over a 60 sec. span of the FO. Open-loop response is shown in red, closed-loop response is shown in black. Left column of plots is from test series 1705F1 and 1705F2. Right column is from test series 1805F1 and 1805F2.)

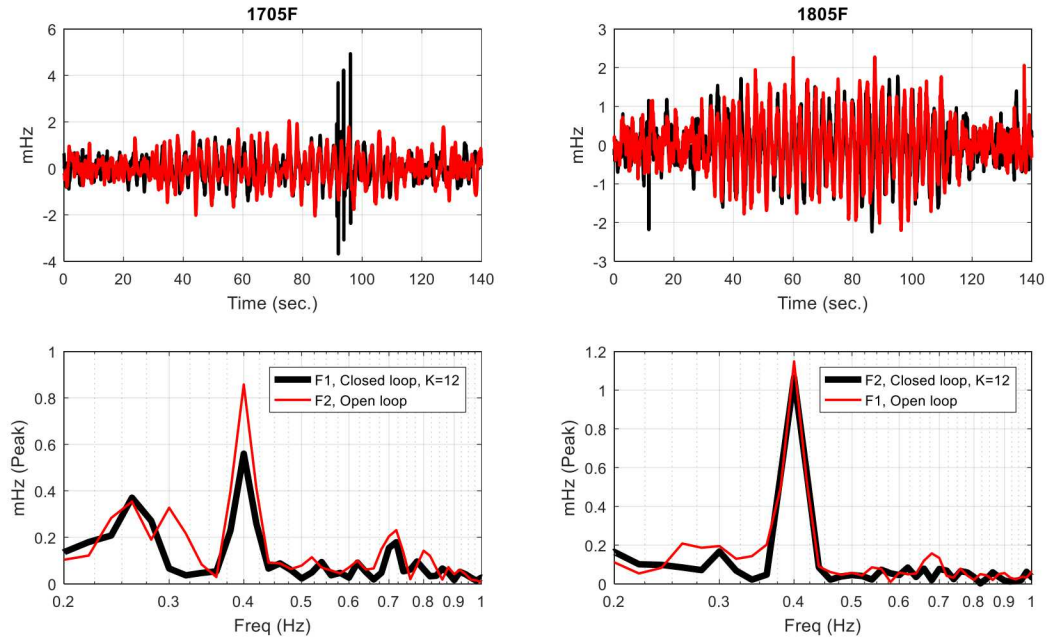

Figure C-3. BC signature (Custer – John Day freq error) to 0.4-Hz FO at P_{po} in Fig. 3-1 (Top row shows the time-domain response with the FO starting at the 30 sec. point and ending at the 110 sec. point. Bottom row shows the spectrum of time-domain response over a 60 sec. span of the FO. Open-loop response is shown in red, closed-loop response is shown in black. Left column of plots is from test series 1705F1 and 1705F2. Right column is from test series 1805F1 and 1805F2.)

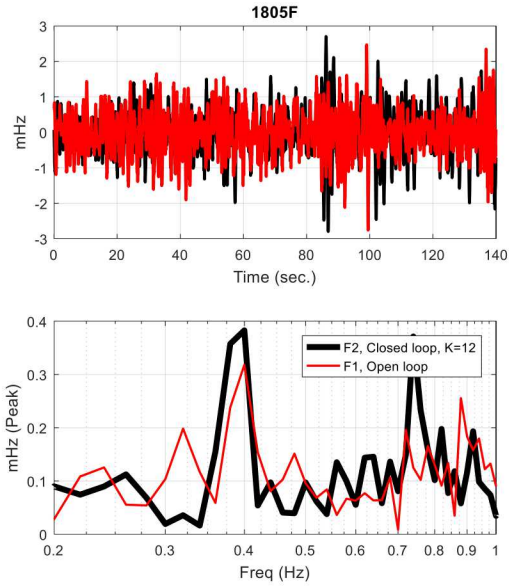

Figure C-4. MT signature (Colstrip – Grand Coulee freq error) to 0.4-Hz FO at P_{po} in Fig. 3-1 (Top row shows the time-domain response with the FO starting at the 30 sec. point and ending at the 110 sec. point. Bottom row shows the spectrum of time-domain response over a 60 sec. span of the FO. Open-loop response is shown in red, closed-loop response is shown in black. Left column is from test series 1705F1 & 1705F2. Right column is from test series 1805F1 & 1805F2.)

C.2. 1 Hz

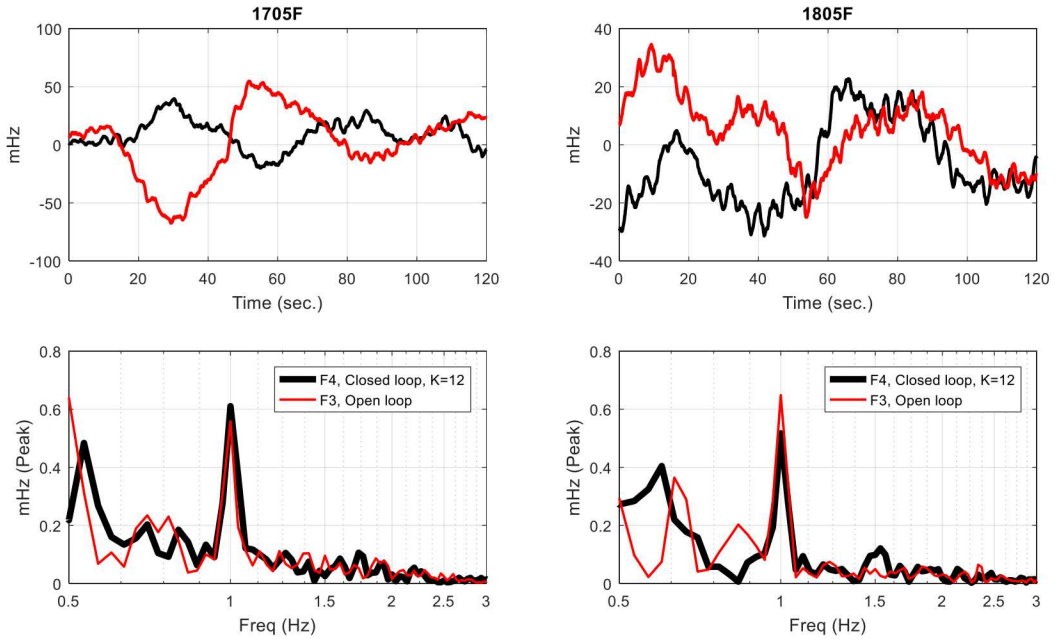

Figure C-5. NSA signature (Sundance - Grand Coulee freq error) to 1-Hz FO at P_{po} in Fig. 3-1 (Top row shows the time-domain response with the FO starting at the 30 sec. point and ending at the 90 sec. point. Bottom row shows the spectrum of time-domain response over a 30 sec. span of the FO. Open-loop response is shown in red, closed-loop response is shown in black. Left column of plots is from test series 1705F1 and 1705F2. Right column is from test series 1805F1 and 1805F2.)

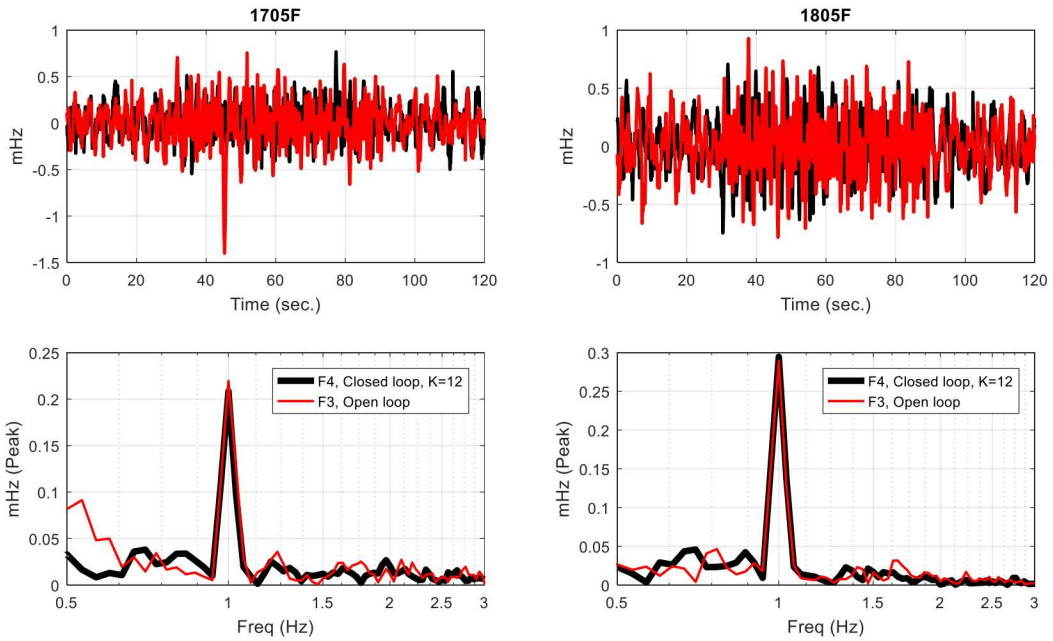

Figure C-6. NSB signature (John Day - Malin freq error) to 1-Hz FO at P_{po} in Fig. 3-1 (Top row shows the time-domain response with the FO starting at the 30 sec. point and ending at the 90 sec. point. Bottom row shows the spectrum of time-domain response over a 30 sec. span of the FO. Open-loop response is shown in red, closed-loop response is shown in black. Left column of plots is from test series 1705F1 and 1705F2. Right column is from test series 1805F1 and 1805F2.)

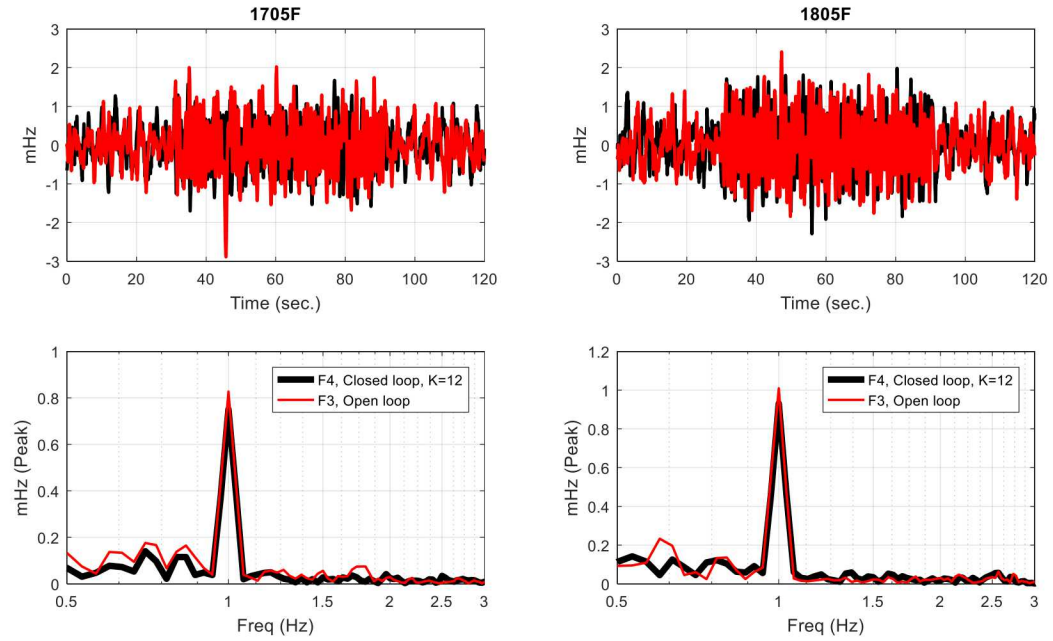

Figure C-7. BC signature (Custer – John Day freq error) to 1-Hz FO at P_{po} in Fig. 3-1 (Top row shows the time-domain response with the FO starting at the 30 sec. point and ending at the 90 sec. point. Bottom row shows the spectrum of time-domain response over a 30 sec. span of the FO. Open-loop response is shown in red, closed-loop response is shown in black. Left column of plots is from test series 1705F1 and 1705F2. Right column is from test series 1805F1 and 1805F2.)

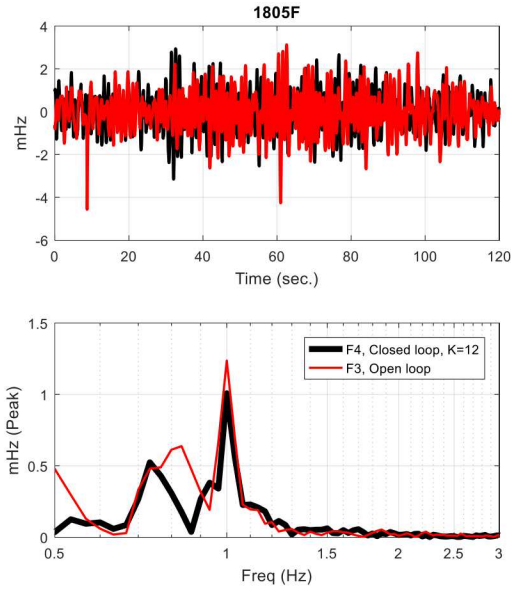

Figure C-8. MT signature (Colstrip – Grand Coulee freq error) to 1-Hz FO at P_{po} in Fig. 3-1 (Top row shows the time-domain response with the FO starting at the 30 sec. point and ending at the 90 sec. point. Bottom row shows the spectrum of time-domain response over a 30 sec. span of the FO. Open-loop response is shown in red, closed-loop response is shown in black. Taken from test series 1805F1 and 1805F2.)

C.3. 3 Hz

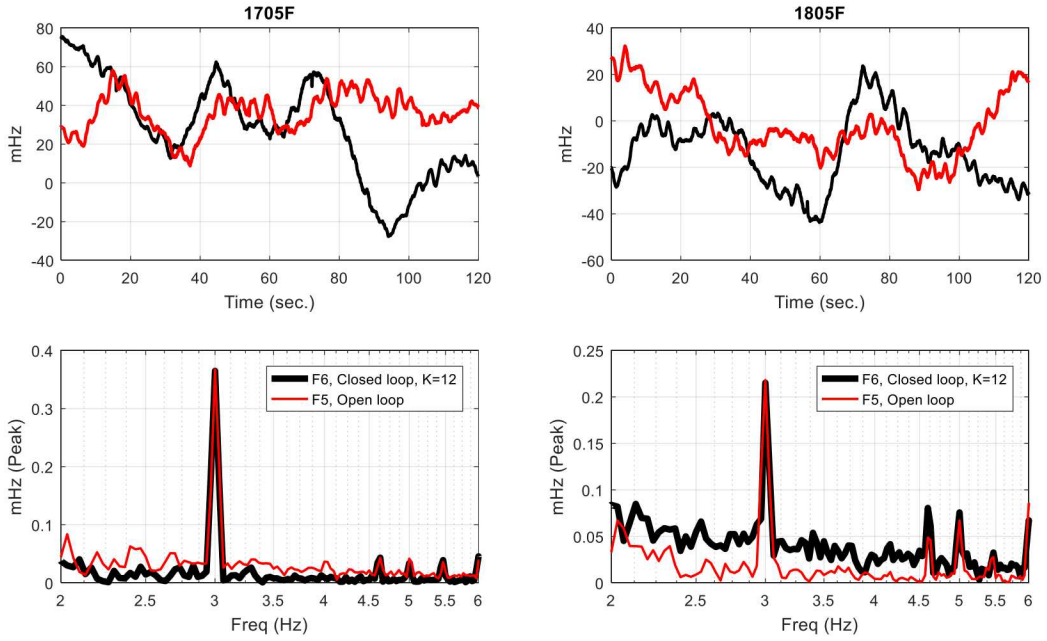

Figure C-9. NSA signature (Sundance - Grand Coulee freq error) to 3-Hz FO at P_{po} in Fig. 3-1 (Top row shows the time-domain response with the FO starting at the 30 sec. point and ending at the 90 sec. point. Bottom row shows the spectrum of time-domain response over a 30 sec. span of the FO. Open-loop response is shown in red, closed-loop response is shown in black. Left column of plots is from test series 1705F1 and 1705F2. Right column is from test series 1805F1 and 1805F2.)

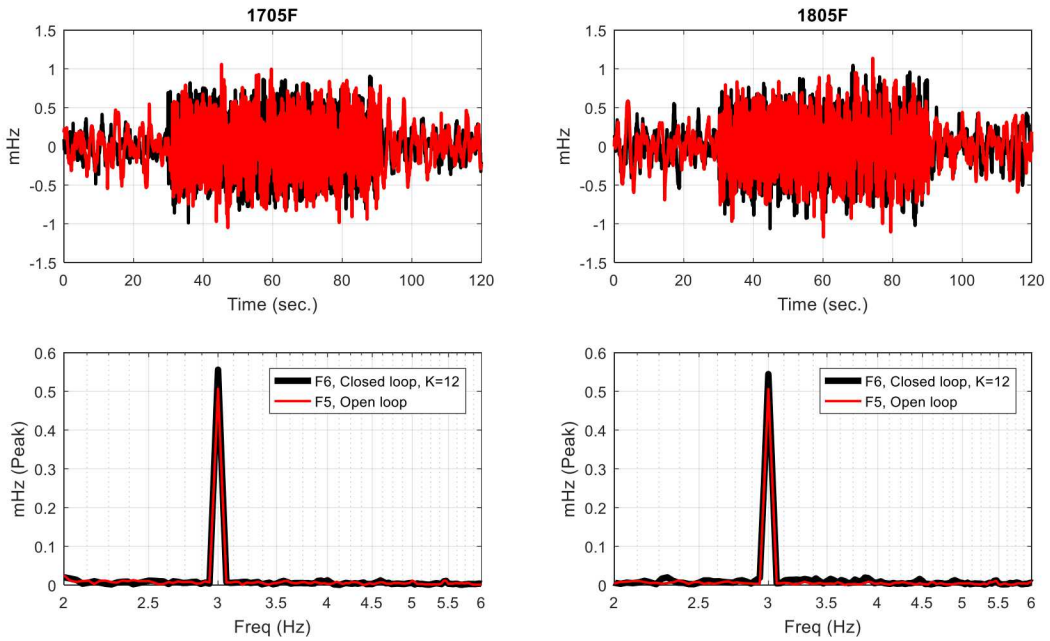

Figure C-10. NSB signature (John Day - Malin freq error) to 3-Hz FO at P_{po} in Fig. 3-1 (Top row shows the time-domain response with the FO starting at the 30 sec. point and ending at the 90 sec. point. Bottom row shows the spectrum of time-domain response over a 30 sec. span of the FO. Open-loop response is shown in red, closed-loop response is shown in black. Left column of plots is from test series 1705F1 and 1705F2. Right column is from test series 1805F1 and 1805F2.)

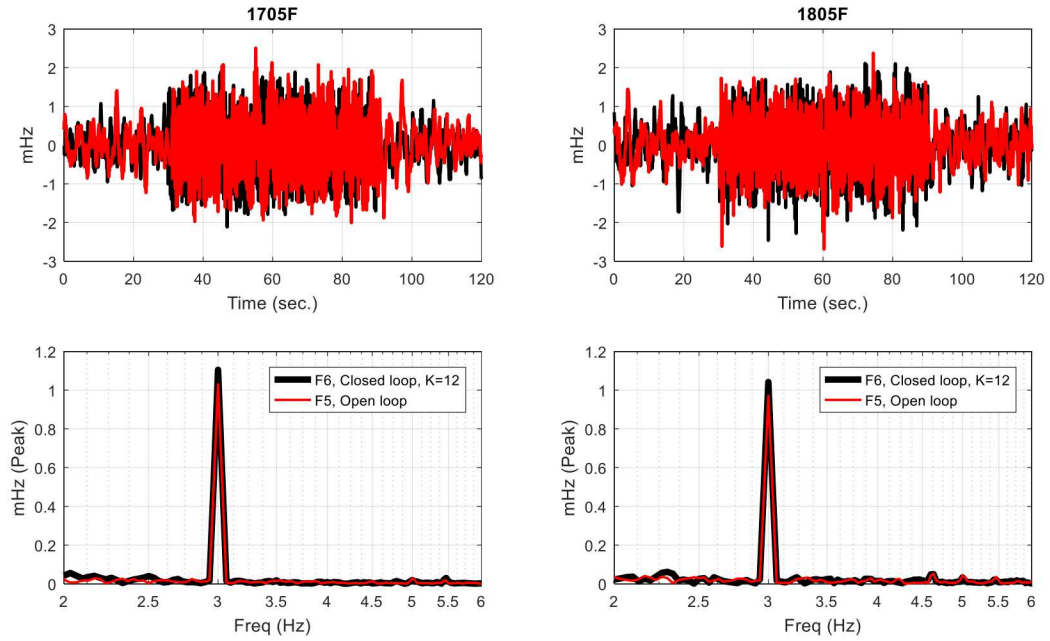

Figure C-11. BC signature (Custer – John Day freq error) to 3-Hz FO at P_{po} in Fig. 3-1 (Top row shows the time-domain response with the FO starting at the 30 sec. point and ending at the 90 sec. point. Bottom row shows the spectrum of time-domain response over a 30 sec. span of the FO. Open-loop response is shown in red, closed-loop response is shown in black. Left column of plots is from test series 1705F1 and 1705F2. Right column is from test series 1805F1 and 1805F2.)

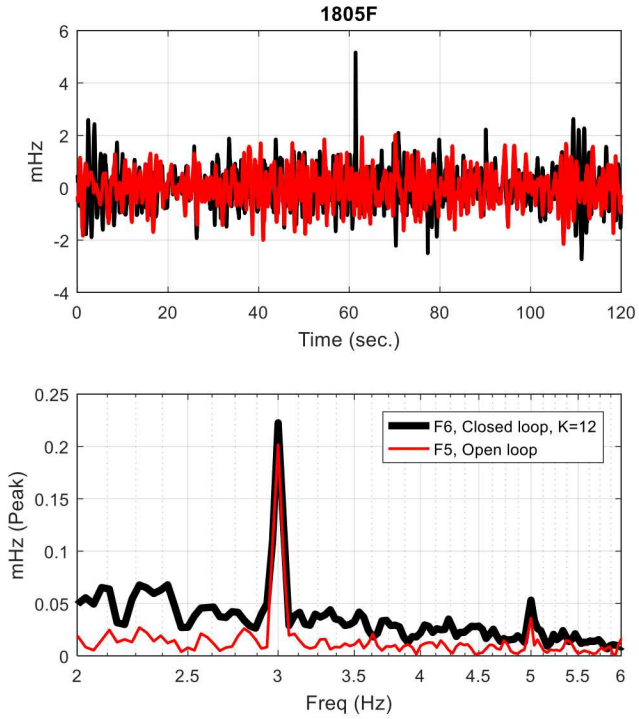

Figure C-12. MT signature (Colstrip – Grand Coulee freq error) to 3-Hz FO at P_{po} in Fig. 3-1 (Top row shows the time-domain response with the FO starting at the 30 sec. point and ending at the 90 sec. point. Bottom row shows the spectrum of time-domain response over a 30 sec. span of the FO. Open-loop response is shown in red, closed-loop response is shown in black. Taken from test series 1805F1 and 1805F2.)

This page left blank

APPENDIX D. SUMMARY OF PROJECT ACHIEVEMENTS

The following sub-sections provide a project overview, list of project innovations, list of relevant awards attained by project staff during the tenure of the project, project patent application filed, list of journal papers, list of conference papers, list of project reports, and a list of project presentations, respectively.

D.1. Project Overview

Supplementing the PDCI with a real-time damping controller dates back to the 1970s when BPA engineers experimented with the concept. Review of this work via reports and oral interviews with engineers in charge of the project revealed two primary conclusions: 1) the HVDC modulation considerably improved inter-area mode damping; and 2) the feedback signal, which was derived from a localized AC power flow, actually caused the PDCI controller to make oscillations at a higher frequency worse. This issue, along with lack of a WAMS, was a primary reason that the control was not considered for production.

Based upon several low-damping events, BPA initiated the TIP-50 project in 2007. The goal was to investigate several potential solutions to improve system oscillatory stability. One component of TIP-50 was to re-visit PDCI damping control. Initial research focused on understanding why the 1970s experiments failed and if a safe PDCI damping control strategy could actually be constructed. The primary results were presented in conference paper [25] below which was an IEEE prize paper. This paper explained why the 1970s approach failed and why wide-area feedback was needed to safely implement a PDCI damping controller. The paper demonstrated an effective and safe control strategy via simulation.

After the successful conclusions from TIP-50, the TIP-289 project was initiated to fully investigate and demonstrate a PDCI damping controller. The primary deliverable of TIP 289 was the design, simulation, testing, and demonstration of a wide-area damping control system that modulates the power flow on the PDCI based on real-time wide-area feedback information acquired from PMUs located throughout the BPA region. Major breakthroughs include:

- An effective and safe feedback control strategy based upon further refinement of the concept developed under TIP-50. This included thousands of simulation tests to verify the approach.
- An automated supervisory system to monitor and operate the controller to maintain system safety and integrity. This system utilizes state-of-the-art algorithms to assure the safe operation of the damping controller under all conditions.
- The first wide-area large-scale damping controller ever constructed and operated in the world. This system utilizes real-time PMU feedback from hundreds of miles to stabilize the entire interconnect. To our knowledge, no other system has ever been built and operated on an actual system.

D.2. Project Innovations

The following list describes the primary innovations to come out of the DCON project.

1. First successful demonstration of wide-area control using real-time PMU feedback in North America ➔ much knowledge gained for networked control systems on the grid.
2. Control design is actuator agnostic ➔ easily adaptable to other sources of power injection (e.g., wind turbines, energy storage).

3. Supervisory system architecture and design is modular and readily reusable for future real-time control systems to ensure "Do No Harm" to the grid.
4. Algorithms, models, and simulations created to support future implementation of control strategies using distributed grid assets.
5. Extensive eigensystem analysis, visualization, and mapping tools developed to support simulation studies and analysis of test results.
6. Model development and validation supports multiple levels of fidelity in analysis, design, and simulation studies.

D.3. Awards

The following list enumerates the awards attained by project staff during the tenure of the project. All of these awards have a significant component directly related to the work of this project.

1. David A. Schoenwald, Brian J. Pierre, Felipe Wilches-Bernal, Ryan T. Elliott, Raymond H. Byrne, Jason C. Neely, Daniel J. Trudnowski, and Dmitry N. Kosterev, "Control System for Active Damping of Inter-Area Oscillations," R&D 100 Award, 2017.
2. David A. Schoenwald, Brian J. Pierre, Felipe Wilches-Bernal, Ryan T. Elliott, Raymond H. Byrne, and Jason C. Neely, "Power Grid Oscillation Damping Control Design Team," Sandia Employee Recognition Award, 2017.
3. David A. Schoenwald, Outstanding Engineer, Albuquerque IEEE Section, 2017, "For contributions to the development and realization of next generation Smart Grid technologies."
4. Daniel J. Trudnowski, "Lifetime Distinguished Researcher" Award, Montana Technological University, 2017
5. Felipe Wilches-Bernal, Outstanding Young Engineer Award, Albuquerque IEEE Section, 2019 "For outstanding development of control algorithms for distributed energy resources and wide area damping control."
6. Daniel J. Trudnowski, Dmitry N. Kosterev, and John Undrill, "PDCI Damping Control Analysis for the western North American Power System," Best of the Best Paper Award, IEEE Power & Energy Soc. General Meeting, Vancouver, Canada, July 21-25, 2013.
7. Brian J. Pierre, Ryan T. Elliott, David A. Schoenwald, Jason C. Neely, Raymond H. Byrne, Daniel J. Trudnowski, and James Colwell, "Supervisory System for a Wide Area Damping Controller Using PDCI Modulation and Real-Time PMU Feedback," Best Conference Paper Session Award, IEEE Power & Energy Society General Meeting, Boston, MA, July 17-21, 2016.
8. Felipe Wilches-Bernal, Brian J. Pierre, Ryan T. Elliott, David A. Schoenwald, Raymond H. Byrne, Jason C. Neely, and Daniel J. Trudnowski, "Time Delay Definitions and Characterizations in the Pacific DC Intertie Wide Area Damping Controller," Best Conference Paper Session Award, IEEE Power & Energy Society General Meeting, Chicago, IL, July 16-20, 2017.

D.4. Patent Application

The following patent application, based on work from this project, is pending as of May 2019.

1. David A. Schoenwald, Raymond H. Byrne, Ryan T. Elliott, Jason C. Neely, Brian J. Pierre, Felipe Wilches-Bernal, and Daniel J. Trudnowski, "Systems and Methods for Active Damping Control of Inter-Area Oscillations in Large-Scale Interconnected Power Systems," Non-Provisional Patent Application filed with the US Patent and Trademark Office, Application Number: 15/926,658, Filed: March 20, 2018.

D.5. Journal Papers

The following list provides the citations for published journal papers whose content was primarily derived from this project.

1. B. J. Pierre, F. Wilches-Bernal, D. A. Schoenwald, R. T. Elliott, D. J. Trudnowski, R. H. Byrne, and J. C. Neely, "Design of the Pacific DC Intertie Wide Area Damping Controller," DOI 10.1109/TPWRS.2019.2903782, *IEEE Transactions on Power Systems*, 2019.
2. C. Lackner, F. Wilches-Bernal, B.J. Pierre, D. A. Schoenwald, "A Tool to Characterize Delays and Packet Losses in Power Systems with Synchrophasor Data," *IEEE Power and Energy Technology Systems Journal*, Vol. 5, Issue 4, pp.117-128, December 2018.
3. M. Elizondo, R. Fan, H. Kirkham, M. Ghosal, F. Wilches-Bernal, D. Schoenwald, and J. Lian, "Interarea Oscillation Damping Control Using High Voltage DC Transmission: A Survey," *IEEE Trans. Power Syst.*, Vol. 33, Issue 6, pp. 6915 – 6923, November 2018.
4. D. A. Schoenwald, B. J. Pierre, F. Wilches-Bernal, and D. J. Trudnowski, "Design and Implementation of a Wide-Area Damping Controller Using High Voltage DC Modulation and Synchrophasor Feedback," *IFAC-PapersOnLine*, ISSN 2405-8963, Vol. 50, Issue 1, pp. 67-72, July 2017.
5. D. A. Schoenwald, "Active Damping of Inter-Area Oscillations in the Western Interconnection: Recent Developments," *IEEE Smart Grid Newsletter*, http://smartgrid.ieee.org/newsletters/july-2017, July 2017.
6. J. C. Neely, J. Johnson, R. H. Byrne, and R. T. Elliott, "Structured Optimization for Parameter Selection of Frequency-Watt Grid Support Functions for Wide-Area Damping," *International Journal of Distributed Energy Resources and Smart Grids*, pp. 69-94, Vol. 11, No. 1, January 2015.

D.6. Conference Papers

The following list provides the citations for published conference papers whose content was primarily derived from this project.

1. D. A. Schoenwald, F. Wilches-Bernal, B. J. Pierre, R. T. Elliott, and D. J. Trudnowski, "Data Considerations in Real-Time PMU Feedback Control Systems," North American SynchroPhasor Initiative (NASPI) Work Group Meeting, San Diego, CA, April 15-17, 2019.
2. F. Wilches-Bernal, D. A. Copp, G. Bacelli, and R. H. Byrne, "Structuring the Optimal Output Feedback Control Gain: A Soft Constraint Approach," 57th IEEE Conference on Decision and Control, Miami Beach, FL, December 17-19, 2018.
3. R. A. Biroon, P. Pisu, and D. A. Schoenwald, "Inter-Area Oscillation Damping in Large-Scale Power Systems using Decentralized Control," 2018 ASME Dynamic Systems and Control Conference, Atlanta, GA, September 30-October 3, 2018.

4. F. Wilches-Bernal, D. A. Copp, D. A. Schoenwald, and I. Gravagne, "Stability Criteria for Power Systems with Damping Control and Asymmetric Feedback Delays," 50th North American Power Symposium, Fargo, ND, September 9-11, 2018.
5. F. Wilches-Bernal, B. J. Pierre, D. A. Schoenwald, R. T. Elliott, and D. J. Trudnowski, "Time Synchronization in Wide Area Damping Control of Power Systems," 2018 Probabilistic Methods Applied to Power Systems (PMAPS) Conference, Boise, ID, June 24-28, 2018.
6. D. A. Copp, F. Wilches-Bernal, D. A. Schoenwald, and I. Gyuk, "Power System Damping Control via Power Injections from Distributed Energy Storage," SPEEDAM 2018, Amalfi Coast, Italy, June 20-22, 2018.
7. B. J. Pierre, F. Wilches-Bernal, D. A. Schoenwald, R. T. Elliott, R. H. Byrne, J. C. Neely, and D. J. Trudnowski, "The Pacific DC Intertie Wide Area Damping Controller Utilizing Real-Time PMU Feedback," North American Synchrophasor Initiative (NASPI) Spring Meeting, Albuquerque, NM, April 24-26, 2018.
8. F. Wilches-Bernal, D. Schoenwald, R. Fan, M. Elizondo, and H. Kirkham, "Analysis of the Effect of Communication Latencies on HVDC-Based Damping Control," 2018 IEEE PES T&D Conference & Exposition, Denver, CO, April 16-19, 2018.
9. R. Fan, M. Elizondo, H. Kirkham, F. Wilches-Bernal, and D. Schoenwald, "Oscillation Damping Control Using Multiple High Voltage DC Transmission Lines: Controllability Exploration," 2018 IEEE PES T&D Conference & Exposition, Denver, CO, April 16-19, 2018.
10. D. A. Copp, F. Wilches-Bernal, I. Gravagne, and D. A. Schoenwald, "Time Domain Analysis of Power System Stability with Damping Control and Asymmetric Feedback Delays," 49th North American Power Symposium, Morgantown, WV, September 17-19, 2017.
11. F. Wilches-Bernal, R. Concepcion, J. C. Neely, D. A. Schoenwald, R. H. Byrne, B. J. Pierre, and R. T. Elliott, "Effect of Time Delay Asymmetries in Power System Damping Control," IEEE Power & Energy Soc. General Meeting, Chicago, IL, July 16-20, 2017.
12. F. Wilches-Bernal, B. J. Pierre, R. T. Elliott, D. A. Schoenwald, R. H. Byrne, J. C. Neely, and D. J. Trudnowski, "Time Delay Definitions and Characterizations in the Pacific DC Intertie Wide Area Damping Controller," IEEE Power & Energy Society General Meeting, Chicago, IL, July 16-20, 2017.
13. D. J. Trudnowski, B. J. Pierre, F. Wilches-Bernal, D. A. Schoenwald, R. T. Elliott, J. C. Neely, R. H. Byrne, and D. N. Kosterev, "Initial Closed-Loop Testing Results for the Pacific DC Intertie Wide Area Damping Controller," IEEE Power & Energy Society General Meeting, Chicago, IL, July 16-20, 2017.
14. B. J. Pierre, F. Wilches-Bernal, R. T. Elliott, D. A. Schoenwald, J. C. Neely, R. H. Byrne, and D. J. Trudnowski, "Simulation Results for the Pacific DC Intertie Wide Area Damping Controller," IEEE Power & Energy Society General Meeting, Chicago, IL, July 16-20, 2017.
15. D. A. Schoenwald, B. J. Pierre, F. Wilches-Bernal, and D. J. Trudnowski, "Design and Implementation of a Wide-Area Damping Controller Using High Voltage DC Modulation and Synchrophasor Feedback," IFAC World Congress, Toulouse, France, July 9-14, 2017.
16. B. Pierre, F. Wilches-Bernal, D. Schoenwald, R. Elliott, J. Neely, R. Byrne, "Open-Loop Testing Results for the Pacific DC Intertie Wide Area Damping Controller," 12th IEEE Power & Energy Society PowerTech Conference, Manchester, UK, June 18 – 22, 2017.

17. B. J. Pierre, R. T. Elliott, D. A. Schoenwald, J. C. Neely, R. H. Byrne, D. J. Trudnowski, and J. Colwell, "Supervisory System for a Wide Area Damping Controller Using PDCI Modulation and Real-Time PMU Feedback," IEEE Power & Energy Society General Meeting, Boston, MA, July 17-21, 2016.
18. R. H. Byrne, D. J. Trudnowski, J. C. Neely, D. A. Schoenwald, D. G. Wilson, and L. J. Rashkin, "Small Signal Stability Analysis and Distributed Control with Communications Uncertainty," SPEEDAM 2016, Capri Island, Italy, June 22-24, 2016.
19. R. H. Byrne, R. J. Concepcion, J. C. Neely, F. Wilches-Bernal, R. T. Elliott, O. Lavrova, and J. E. Quiroz, "Small Signal Stability of the Western North American Power Grid with High Penetrations of Renewable Generation," 2016 IEEE 43rd Photovoltaic Specialists Conference (PVSC 2016), Portland, OR, June 5-10, 2016.
20. J. C. Neely, R. H. Byrne, D. A. Schoenwald, R. T. Elliott, D. J. Trudnowski, and M. K. Donnelly, "Optimal Control of Distributed Networked Energy Storage for Improved Small-Signal Stability," Proceedings of the 2015 Biennial International Conference on Electrical Energy Storage Applications and Technologies (EESAT 2015), San Diego, CA, September 21-24, 2015.
21. R. H. Byrne, D. J. Trudnowski, J. C. Neely, R. T. Elliott, D. A. Schoenwald, and M. K. Donnelly, "Optimal Locations for Energy Storage Damping Systems in the Western North American Interconnect,", IEEE Power & Energy Society General Meeting, National Harbor, MD, July 27-31, 2014.
22. R. T. Elliott, R. H. Byrne, A. Ellis, and L. Grant, "Impact of increased photovoltaic generation on inter-area oscillations in the western north american power system," IEEE Power & Energy Society General Meeting, National Harbor, MD, July 27-31, 2014.
23. D. Trudnowski, D. Kosterev, J. Wold, "Open-Loop PDCI Probing Tests for the Western North American Power System," IEEE Power & Energy Society General Meeting, National Harbor, MD, July 27-31, 2014.
24. J. C. Neely, R. T. Elliott, R. H. Byrne, D. A. Schoenwald, and D. J. Trudnowski, "The Benefits of Energy Storage Combined with HVDC Transmission Power Modulation for Mitigating Inter-Area Oscillations," Proceedings of the 2013 Biennial International Conference on Electrical Energy Storage Applications and Technologies (EESAT 2013), San Diego, CA, October 20-23, 2013.
25. D. J. Trudnowski, D. N. Kosterev, and J. Undrill, "PDCI Damping Control Analysis for the western North American Power System," IEEE Power & Energy Soc. General Meeting, Vancouver, Canada, July 21-25, 2013.
26. J. C. Neely, R. H. Byrne, C. A. Silva Monroy, R. T. Elliott, D. A. Schoenwald, D. Trudnowski, and M. Donnelly, "Damping of Inter-Area Oscillations using Energy Storage", IEEE Power & Energy Society General Meeting, Vancouver, Canada, July 21-25, 2013.
27. C. A. Silva Monroy, J. C. Neely, R. H. Byrne, R. T. Elliott, D. A. Schoenwald, "Wind Generation Controls for Damping of Inter-Area Oscillations", IEEE Power & Energy Society General Meeting, Vancouver, Canada, July 21-25, 2013.
28. R. H. Byrne, J. C. Neely, C. A. Silva Monroy, D. A. Schoenwald, D. Trudnowski, and M. Donnelly, "Energy Storage Controls for Grid Stability", ECI Conference on Modeling, Simulation, and Optimization for the 21st Century Electric Power Grid Conference, Lake Geneva, WI, October 21-25, 2012.

D.7. Project Reports

The following list provides the citations for formal SAND reports whose content was entirely derived from this project.

1. David A. Schoenwald, Daniel J. Trudnowski, Brian J. Pierre, Felipe Wilches-Bernal, Ryan T. Elliott, Raymond H. Byrne, and Jason C. Neely, "PDCI Damping Controller Test Results and Project Summary," Sandia National Laboratories Technical Report, SAND2019-XXXX, Albuquerque, NM, May 2019.
2. D. Schoenwald, C. Rawlins, B. Pierre, F. Wilches-Bernal, and R. Elliott, "Executive Summary to PDCI Oscillation Damping Controller Software Documentation," Sandia National Laboratories Tech. Report, SAND2018-10049, Albuquerque, NM, Sept 2018.
3. C. Rawlins, D. Schoenwald, B. Pierre, F. Wilches-Bernal, and R. Elliott, "PDCI Oscillation Damping Controller Software Documentation," Sandia National Laboratories Technical Report, SAND2018-10048, Albuquerque, NM, September 2018.
4. D. Schoenwald, B. Pierre, F. Wilches-Bernal, R. Elliott, R. Byrne, J. Neely, and D. Trudnowski, "PDCI Oscillation Damping Controller Documentation and Specifications," Sandia National Laboratories Technical Report, SAND2018-2389, Albuquerque, NM, March 2018.
5. F. Wilches-Bernal, B. Pierre, R. Elliott, D. Schoenwald, R. Byrne, J. Neely, D. Trudnowski, and M. Donnelly, "PDCI Wide-Area Damping Control: PSLF Simulations of the 2017 Test Plan - Dual Export Case," Sandia National Laboratories Technical Report, SAND2017-6196, Albuquerque, NM, June 2017.
6. F. Wilches-Bernal, B. Pierre, R. Elliott, D. Schoenwald, R. Byrne, J. Neely, D. Trudnowski, and M. Donnelly, "PDCI Wide-Area Damping Control: PSLF Simulations of the 2017 Test Plan - Heavy Summer Case," Sandia National Laboratories Technical Report, SAND2017-6195, Albuquerque, NM, June 2017.
7. F. Wilches-Bernal, B. Pierre, R. Elliott, D. Schoenwald, R. Byrne, J. Neely, D. Trudnowski, and M. Donnelly, "PDCI Wide-Area Damping Control: PSLF Simulations of the 2017 Test Plan - Light Summer Case," Sandia National Laboratories Technical Report, SAND2017-6194, Albuquerque, NM, June 2017.
8. F. Wilches-Bernal, B. Pierre, R. Elliott, D. Schoenwald, R. Byrne, J. Neely, D. Trudnowski, and M. Donnelly, "PDCI Wide-Area Damping Control: PSLF Simulations of the 2016 Open and Closed Loop Test Plan," Sandia National Laboratories Technical Report, SAND2017-2755, Albuquerque, NM, March 2017.
9. B. Pierre, F. Wilches-Bernal, R. Elliott, D. Schoenwald, J. Neely, R. Byrne, and D. Trudnowski, "PDCI Wide Area Damping Control - Open Loop Data Analysis," Sandia National Laboratories Technical Report, SAND2017-2211, Albuquerque, NM, Feb 2017.
10. B. Pierre, R. Elliott, and D. Schoenwald, "Telecom Requirements at Celilo for BPA Damping Controller Prototype," Sandia National Laboratories Technical Report, SAND2015-7523, Albuquerque, NM, September 2015.
11. B. Pierre, R. Elliott, and D. Schoenwald, "Quick Start Guide for BPA Damping Controller Prototype," Sandia National Laboratories Technical Report, SAND2015-5885, Albuquerque, NM, July 2015.

12. D. Schoenwald, R. Elliott, J. Neely, and R. Byrne, "Input-Output Data Specifications for BPA Project TIP 289," Sandia National Laboratories Technical Report, SAND2014-16309, Albuquerque, NM, July 2014.

D.8. Project Presentations

The following list provides the presenter name(s), title, location, and date for oral presentations delivered by project staff whose content was primarily derived from this project.

1. D. Schoenwald, "Challenges in the Use of PMU Data for Real-Time Feedback Control," PNNL PMU Metrology Meeting, Richland, WA, April 16, 2019, SAND2019-4532PE.
2. D. Schoenwald, "Data Considerations in Real-Time PMU Feedback Control Systems," NASPI Spring Meeting, San Diego, CA, April 9, 2019, SAND2019-4119C.
3. D. Schoenwald, "Real-Time Damping of Power Grid Oscillations Using Synchrophasor Feedback," CURENT Industry Seminar, Knoxville, TN, March 1, 2019, SAND2019-2114PE.
4. D. Schoenwald, "Lecture on Technology Transfer at Sandia National Labs," Invited lecture to Portland State University Technology Transfer class, Invited by Dr. Judith Estep, Webinar-based lecture, February 19, 2019, SAND2019-1800PE.
5. D. Schoenwald and F. Wilches-Bernal, "Real-Time Damping Control Using PMU Feedback," JSIS Meeting, Portland, OR, November 9, 2019, SAND2018-12843PE.
6. D. Schoenwald, "Grid Stability Using Distributed Energy Storage – Presentation," DOE Energy Storage Program Peer Review Meeting, Santa Fe, NM, September 26, 2019, SAND2018-10860C.
7. F. Wilches-Bernal, "Stability Criteria for Power Systems with Damping Control and Asymmetric Feedback Delays – presentation," 2018 North American Power Symposium (NAPS), Fargo, ND, September 10, 2019, SAND2018-10312C.
8. D. Schoenwald, "Time Synchronization in Wide Area Damping Control of Power Systems – Presentation," 2018 Probabilistic Methods Applied to Power Systems Conference, Boise, ID, June 26, 2018, SAND2018-7657C.
9. D. Schoenwald, "Wide-Area Damping Control Using PMU Feedback," Oscillation Analysis Work Group Webinar, Webinar presentation invited by Dr. James Follum, July 17, 2018, SAND2018-7416PE.
10. D. Schoenwald and B. Pierre, "Wide-Area Damping Control Using PMU Feedback," DOE Transmission Reliability Peer Review Meeting, Washington, DC, June 6, 2018, SAND2018-5913PE.
11. B. Pierre, "The Pacific DC Intertie Wide Area Damping Controller," NASPI Spring Meeting, Albuquerque, NM, April 24, 2018, SAND2018-5252C.
12. D. Schoenwald, B. Pierre, and F. Wilches-Bernal, "Damping Control Using PMU Feedback," JSIS Meeting, Salt Lake City, UT, May 17, 2018, SAND2018-5248PE.
13. F. Wilches-Bernal, "Analysis of the Effect of Communication Latencies on HVDC-Based Damping Control," IEEE T&D Conference, Denver, CO, April 17, 2018, SAND2018-3770C.

14. D. Schoenwald, "2017 R&D 100 Award Winner: Control System for Active Damping of Inter-Area Oscillations," Briefing on R&D 100 Award Winning Project to DOE-OE Leadership, Washington, DC, March 14, 2018, SAND2018-2963PE.
15. D. Schoenwald, "Control System Design for Active Damping of Large-Scale Power Grids," Invited seminar in ECE Department at The Ohio State University, Columbus, OH, December 4, 2017, SAND2017-13155PE.
16. D. Schoenwald, "Wide Area Transmission Controls R&D," Sandia Controls Focus Group Meeting, Albuquerque, NM, September 6, 2017, SAND2017-9563PE.
17. F. Wilches-Bernal, "Effect of Time Delay Asymmetries in Power System Damping Control," 2017 IEEE PES General Meeting, Chicago, IL, July 17, 2017, SAND2017-7356C.
18. F. Wilches-Bernal, "Time Delay Definitions and Characterization in the Pacific DC Intertie Wide Area Damping Controller," 2017 IEEE PES General Meeting, Chicago, IL, July 17, 2017, SAND2017-7346C.
19. D. Schoenwald, "Wide-Area Damping Control Proof of Concept Demonstration," DOE Transmission Reliability Program Review Meeting, Washington, DC, June 13, 2017.
20. D. Schoenwald and D. Trudnowski, "TIP 289: Wide Area Damping Control Proof-of-Concept Demonstration," 2017 BPA Technology Innovation Summit, Portland, OR, January 30, 2017.
21. D. Schoenwald, "WECC-BPA Project Using PMU Data to Damp Inter-Area Oscillations," CURENT Industry Meeting & NSF/DOE Annual Site Visit, Knoxville, TN, November 15, 2016, SAND2016-11535PE.
22. D. Schoenwald, "Damping of Power Grid Oscillations Using Energy Storage and PMU Feedback," DOE Energy Storage Program Peer Review, Washington, DC, September 26, 2016, SAND2016-9534PE.
23. B. Pierre, "Supervisory System for a Wide Area Damping Controller Using PDCI Modulation and Real-Time PMU Feedback," 2016 IEEE PES General Meeting, Boston, MA, July 18, 2016, SAND2016-6872C.
24. D. Schoenwald, "Wide-Area Damping Control," DOE Transmission Reliability Program Review Meeting, Washington, DC, June 8, 2016, SAND2016-5869PE.
25. D. Schoenwald, "BPA Project Briefing: Active Damping using PMU Feedback," JSIS Meeting, Salt Lake City, UT, April 27, 2016, SAND2016-4275PE.
26. D. Schoenwald and D. Trudnowski, "TIP 289: Wide Area Damping Control Proof-of-Concept Demonstration," 2016 BPA Technology Innovation Summit, Portland, OR, January 27, 2016, SAND2016-0472C.
27. D. Schoenwald, "Active Damping of Power Grid Oscillations Using Distributed Energy Storage," DOE Energy Storage Program Peer Review, Portland, OR, September 23, 2015, SAND2015-7854C.
28. D. Schoenwald, "Wide-Area Damping Control," DOE Transmission Reliability Program Review Meeting, Washington, DC, June 10, 2015.
29. D. Schoenwald and D. Trudnowski, "TIP 289: Wide Area Damping Control Proof-of-Concept Demonstration," 2015 BPA Technology Innovation Summit, Portland, OR, January 27, 2015, SAND2015-0400C.

30. D. Schoenwald, "Wide-Area Damping Control Proof of Concept," DOE Energy Storage Program Review Meeting, Washington, DC, September 19, 2014.

31. D. Schoenwald, "Wide-Area Damping Control Proof of Concept," DOE Transmission Reliability Program Review Meeting, Washington, DC, June 4, 2014.

32. D. Schoenwald and D. Trudnowski, "TIP 289: Wide Area Damping Control Proof-of-Concept Demonstration," 2014 BPA Technology Innovation Summit, Portland, OR, January 28, 2014, SAND2014-0390C.

33. D. Schoenwald, "Update on BPA Wide Area Damping Control Project," 2013 CERTS Industry Leadership Council Meeting, Presented via webinar, October 16, 2013, SAND2013-10061C.

34. R. Byrne and D. Trudnowski, "TIP 289: Wide Area Damping Control Proof-of-Concept Demonstration," 2013 BPA Technology Innovation Summit, Portland, OR, January 30, 2013, SAND2013-0350P.

This page left blank

DISTRIBUTION

Email—External (encrypt for OUO)

Name	Company Email Address	Company Name
Jeff Barton	jgbarton@bpa.gov	Bonneville Power Administration
Gilbert Bindewald	gilbert.bindewald@hq.doe.gov	U. S. Department of Energy
Lori Bonn	labonn@bpa.gov	Bonneville Power Administration
Cain Bloomer	mcbloomer@bpa.gov	Bonneville Power Administration
Amilcar Chavez	axchavez@bpa.gov	Bonneville Power Administration
Kerry Cheung	kerry.cheung@hq.doe.gov	U. S. Department of Energy
Matt Donnelly	mdonnelly@mtech.edu	Montana Technological University
Judith Estep	jaestep@bpa.gov	Bonneville Power Administration
Anthony Faris	ajfaris@bpa.gov	Bonneville Power Administration
Rhett Fulwider	rtfulwider@bpa.gov	Bonneville Power Administration
Alireza Ghassemian	alireza.ghassemian@hq.doe.gov	U. S. Department of Energy
Dan Goodrich	dagoodrich@bpa.gov	Bonneville Power Administration
Imre Gyuk	imre.gyuk@hq.doe.gov	U. S. Department of Energy
Debbie Haught	deborah.haught@hq.doe.gov	U. S. Department of Energy
James Hillegas-Elting	jvhillegas@bpa.gov	Bonneville Power Administration
Dmitry Kosterev	dnkosterev@bpa.gov	Bonneville Power Administration
Gordon Matthews	ghmatthews@bpa.gov	Bonneville Power Administration
Michael Overeem	mlovereem@bpa.gov	Bonneville Power Administration
Phil Overholt	philip.overholt@hq.doe.gov	U. S. Department of Energy
Shawn Patterson	smpatterson@bpa.gov	Bonneville Power Administration
Greg Stults	ggstults@bpa.gov	Bonneville Power Administration
Dan Trudnowski	dtrudnowski@mtech.edu	Montana Technological University

Email—Internal

Name	Org.	Sandia Email Address
Steven F. Glover	01353	sfglove@sandia.gov
Jason C. Neely	01353	jneely@sandia.gov
David G. Wilson	01353	dwilso@sandia.gov
Carol L. J. Adkins	08800	cladkin@sandia.gov
Charles J. Hanley	08810	cjhanle@sandia.gov
Babu Chalamala	08811	bchalam@sandia.gov

Name	Org.	Sandia Email Address
David Copp	08811	dcopp@sandia.gov
Abraham Ellis	08812	aellis@sandia.gov
Ross Guttromson	08812	rguttro@sandia.gov
Michael J. Baca	08813	mbaca2@sandia.gov
Raymond H. Byrne	08813	rhbyrne@sandia.gov
Ricky J. Concepcion	08813	rconcep@sandia.gov
Ryan T. Elliott	08813	rtellio@sandia.gov
Brian J. Pierre	08813	bjpierr@sandia.gov
David A. Schoenwald	08813	daschoe@sandia.gov
Felipe Wilches-Bernal	08813	fwilche@sandia.gov
Daniel J. Jenkins	11500	djjenk@sandia.gov
Technical Library	9536	libref@sandia.gov

This page left blank

Sandia National Laboratories

Sandia National Laboratories is a multimission laboratory managed and operated by National Technology & Engineering Solutions of Sandia LLC, a wholly owned subsidiary of Honeywell International Inc. for the U.S. Department of Energy's National Nuclear Security Administration under contract DE-NA0003525.